Investigation of a carbohydrate and cholesterol-responsive transcriptional switch in the liver

Master's thesis by Cecilie Maria Ness

Supervisors:
Thomas Sæther and Kirsten Holven

Department of Nutrition
Institute of Basic Medical Sciences
Faculty of Medicine

UNIVERSITY OF OSLO

May 2018

2018

Investigation of a carbohydrate and cholesterol-responsive transcriptional switch in the liver

Cecilie Maria Ness

http://www.duo.uio.no/

Print: Reprosentralen, University of Oslo

Abstract

Obesity-related metabolic diseases, including type 2 diabetes and non-alcoholic fatty liver disease, are associated with dysregulation of metabolic pathways, including lipogenesis. The transcription factors LXRα, SREBP-1c and ChREBP are activated by cholesterol metabolites, insulin and glucose metabolites, and together regulate the network of lipogenic genes. The activation of ChREBP by glucose has been suggested to occur via an intramolecular mechanism involving a low-glucose inhibitory domain (LID) and a glucose-response activation conserved element (GRACE). Under low glucose concentrations, LID inhibits ChREBP's transactivity controlled by GRACE, while elevated glucose concentration causes this inhibition to be lifted. This leads to the transcription of a shorter, constitutively active ChREBP isoform, termed ChREBPβ. In contrast with the full-length ChREBPα isoform, ChREBPβ show increased expression in response to glucose.

Preliminary data indicated that LXRα and ChREBPα interact and may constitute a sugar and cholesterol-responsive transcriptional switch. We could show through gene reporter assays in HuH-7 cells, that a Carbohydrate Response Element (ChoRE)-like E-box/E-box-like motif upstream of the canonical ChoRE is the functional site of ChREBPα, with greater ability to activate the *Chrebpb* promoter. Treatment with GW3965 led to an increase in *Chrebpb* promoter activity, suggesting a regulatory role for LXRα on this promoter. A putative LXRE was deleted, with no appreciable effect on *Chrebpb* activity, suggesting that LXR must bind elsewhere. Co-immunoprecipitation experiments revealed that LXRα is able to interact with the ChREBPα LID. We suggest a model in which LXRα binds to a more distal site on DNA and transrepresses ChREBPα through DNA looping.

We also investigated the possibility of using peripheral blood mononuclear cells (PBMCs) as a relevant model for liver biology, to be able to study our hypotheses *in vivo*. Gene expression analysis in PBMCs from diabetic and pre-diabetic patients revealed that both isoforms of ChREBP are negligibly expressed in these cells, which may have implications for their future use as a proxy for liver tissue.

Acknowledgements

This thesis describes work undertaken from August 2017 to May 2018 at the Department of Nutrition, University of Oslo, under the supervision of Thomas Sæther.

First and foremost I would like to thank Thomas Sæther for patiently guiding me during the lab work and writing process. Thank you for always being encouraging and for inspiring me to explore the world of molecular biology. I could not have asked for a better supervisor.

I would also like to thank Qiong Fan and Christin Lucas for guiding me in the lab and sharing your knowledge with me. Your guidance has been invaluable. I would also like to thank the whole Nuclear Receptor group for including me in the group and for all the delicious cakes!

I would also like to thank Kirsten Holven for giving us access to the PBMCs and related data that were used in this project.

Last but not least I would like to thank my friends and family for supporting me over the years.

Oslo, May 2018

Cecilie Maria Ness

List of abbreviations

ACC	Acetyl-CoA carboxylase
AF	Activation function
β-ME	2-mercaptoethanol
bHLH-LZ	Basic helix loop helix leucine zipper
bp	Base pairs
BSA	Bovine serum albumin
CETP	Cholesteryl ester transfer protein
ChIP	Chromatin immunoprecipitation
ChoRE	Carbohydrate response element
ChREBP	Carbohydrate response element binding protein
CoIP	Co-immunoprecipitation
CPB	CREB binding protein
C_T	Threshold cycle
d/ddH_2O	Distilled/double-distilled H_2O
DBD	DNA binding domain
DMEM	Dulbecco's modified eagle's medium
DMSO	Dimethyl sulfoxide
DNL	*de novo* lipogenesis
dNTP	Deoxynucleotide triphosphate
DR	Direct repeat
ELOVL	Elongation of very long chain fatty acids protein
ER	Endoplasmic reticulum
F-2,6-bP	Fructose-2,6-bisphosphate
FASN	Fatty acid synthase
FBS	Foetal bovine serum
FXR	Farnesoid X receptor
G6P	Glucose-6-phosphate
G6PC	Glucose-6 phosphatase, catalytic subunit
GRACE	Glucose-response activation conserved element
GSM	Glucose sensing module
HDL	High-density lipoprotein
HNF-4α	Hepatocyte nuclear factor 4 alpha
HOMA-IR	Homeostasis model assessment for insulin resistance
HRP	Horseradish peroxidase
IFG	Impaired fasting glucose

IGT	Impaired glucose tolerance
LBD	Ligand binding domain
LDL	Low-density lipoprotein
LDL-R	Low-density lipoprotein receptor
LID	Low glucose inhibitory domain
L-PK	Liver pyruvate kinase
LPL	Lipoprotein lipase
LXR	Liver X receptor
LXRE	Liver X response element
MCR	Mondo conserved region
Mlx	Max-like factor X
MLXIPL	MLX-interacting protein-like (ChREBP)
NAFLD	Non-alcoholic fatty liver disease
NASH	Non-alcoholic steatohepatitis
NES	Nuclear export signal
NLS	Nuclear localization signal
NR	Nuclear receptor
OGA	O-GlcNAcase
O-GlcNAc	O-linked β-*N*-acetylglucosamine
OGT	O-GlcNAc transferase
PBMC	Peripheral blood mononuclear cells
PBS	Phosphate-buffered saline
PEPCK	Phosphoenolpyruvate carboxykinase
PFK-1	Phosphofructokinase 1
PP2A	Protein phosphorylase 2A
PPAR	Peroxisome proliferator-activated receptor
PTM	Post-translational modification
PUFA	Polyunsaturated fatty acids
PVDF	Polyvinylidene fluoride
qPCR	Quantitative polymerase chain reaction
rcp	Relative centrifugal force
RCT	Reverse cholesterol transport
RIN	RNA integrity number
RLU	Relative light units
rpm	Revolutions per minute
RSD	Relative standard deviation
RT	Reverse transcriptase
RXR	Retinoid X receptor
SCAP	SREBP cleavage-activating protein
SCD	Stearoyl CoA desaturase

SDS	Sodium dodecyl sulphate
SR-BI	Scavenger receptor class B type 1
SREBP	Sterol regulatory element-binding protein
T2DM	Type 2 diabetes mellitus
TAD	Transactivation domain
TAE	Tris acid EDTA
TAG	Triacylglycerol
TBP	TATA-binding protein
TCA	Tricarboxylic acid
TF	Transcription factor
T_M	Melting temperature
VLDL	Very low-density lipoprotein
WAT	White adipose tissue
X5P	Xylulose-5-phosphate

Table of contents

List of tables

Pages

List of figures

List of appendices

1 Introduction

1.1 Obesity-related metabolic disorders

The increasing prevalence obesity is a public health concern worldwide. Physical inactivity and unhealthy diets high in simple sugars have been linked to the increasing risk of non-communicable diseases such as type 2 diabetes, metabolic syndrome, non-alcoholic fatty liver disease and cardiovascular disease (1-4). Many of these diseases are associated with dysregulation of metabolic pathways, but the exact mechanisms for how environmental factors lead to this dysregulation are still largely uncertain. However, the understanding of how nutrients and their metabolites affect health is paramount for effective prevention, as well as for the discovery of new therapeutic targets.

1.1.1 Type 2 diabetes mellitus

Type 2 diabetes mellitus (T2DM) is characterized by the failure of pancreatic β cells to secrete sufficient amounts of insulin, as well as insulin resistance in liver, adipose tissue and skeletal muscle (5). The lack of insulin action results in a variety of metabolic disturbances, affecting carbohydrate and lipid, as well as protein metabolism. Because of hyperglycaemia and lipid disturbances, individuals with T2DM are at high risk of developing microvascular complications, such as neuropathy, nephropathy, retinopathy, as well as macrovascular complications such as atherosclerosis and cardiovascular disease.

Prediabetes is a high-risk condition that precedes overt hyperglycemia and patients with prediabetes have a strong predisposition for developing T2DM. Prediabetes is characterized by impaired fasting glucose (IFG), impaired glucose tolerance (IGT) or increased HbA1c (5). In IFG, fasting plasma glucose is higher than normal, but does not meet the criteria for diabetes. IGT is characterized by increased plasma glucose following an oral glucose tolerance test (OGTT), but not to the same degree as in diabetes.

Table 1 gives an overview of the diagnostic criteria for diabetes and prediabetes by the World Health Organization (6), which are in concordance with Norwegian guidelines (7).

Table 1: Diagnostic criteria for diabetes and prediabetes

Parameters	Normal	Prediabetes	T2DM
HbA1c	<6.0 %	5.7-6.4 %	≥6.5 %
Fasting plasma glucose	<6.1 mmol/L	6.1-6.9 mmol/L	≥7.0 mmol/L
Two-hour plasma OGTT	<7.8 mmol/L	7.8-11.1 mmol/L	≥11.1 mmol/L

OGTT: oral glucose tolerance test; T2DM: type 2 diabetes mellitus.

1.1.2 Non-alcoholic fatty liver disease

Non-alcoholic fatty liver disease (NAFLD) is defined as the presence of hepatic steatosis in the absence of excess alcohol consumption (8). The term NAFLD refers to a spectrum of liver diseases, ranging from simple hepatic steatosis to non-alcoholic steatohepatitis (NASH), fibrosis and cirrhosis. Steatosis can be defined as the presence of visible fat in >5 % of hepatocytes (9). About 20 % of patients with simple steatosis develop NASH, and out of these cases, about 20 % will progress to fibrosis and ultimately cirrhosis (10).

NAFLD is associated with features of metabolic syndrome such as obesity, insulin resistance, type 2 diabetes and dyslipidemia (8). It is also an independent risk factor for cardiovascular disease (11). The prevalence of NAFLD in a normal weight population has been estimated to be ~16 % (12), but may be as high as 90 % in obese individuals undergoing bariatric surgery (13). The pathogenesis of NAFLD is complex and not well understood, but both increased *de novo* lipogenesis and decreased β-oxidation have been implicated (14, 15). Using labelled isotopes, Donnelly *et al*. revealed that *de novo* fatty acid synthesis accounted for ~25 % of the TAG in the livers of NAFLD patients, while 60 % came from non-esterified fatty acids in the circulation and 15 % from the diet (14).

1.2 Metabolic regulation

Glucose is used at a high rate by organs such as the brain, the renal medulla, and red blood cells. It is therefore important to keep a steady-state supply of glucose to these tissues. At the same time, persisting high glucose concentrations in the blood can have detrimental effects on the organism. Therefore, a number of regulatory mechanisms ensure that the concentration of glucose in the blood is kept within certain limits when nutrient availability changes, such as in the transition from fasting to feeding.

The liver plays an integral part in maintaining glucose and lipid homeostasis. In fasting conditions, the liver maintains glucose homeostasis by breaking down glycogen to glucose, and through the production of glucose from non-carbohydrate sources such as proteins, a process known as gluconeogenesis. During feeding, the liver ensures efficient storage of excess glucose as glycogen and fat. Since mammals have a limited capacity of storing energy as carbohydrates, excess carbohydrate and protein are ultimately converted to fat in adipose tissue and the liver in a process known as *de novo* lipogenesis (DNL). Newly synthesized fatty acids are esterified with glycerol-3-phosphate to form triacylglycerol (TAG), which is stored primarily in adipose tissue.

In the short term, these metabolic pathways are regulated by allosteric regulation and hormonal cues, which modulate the activity of key enzymes. The integration of energy metabolism is controlled primarily by glucagon and insulin, which are secreted from pancreatic α and β ells respectively, in response to changing substrate availability in the blood. They regulate cellular metabolism by activating signalling pathways that lead to changes in the phosphorylation status of key enzymes. Effects of insulin include increased glucose uptake in muscle and adipose tissue, increased glycogen synthesis and decreased lipolysis and gluconeogenesis, while glucagon has opposing effects.

Long-term adaptation to reduced or increased food intake occurs through changes in the rate of transcription of genes encoding metabolic enzymes. Gene expression includes multiple processes, including transcription from DNA to RNA, RNA splicing, translation, post-translational modification of a protein, and protein degradation. The expression of a gene product can be regulated on all these levels but is most often regulated at the transcriptional level (16).

1.2.1 Glucose metabolism

Glucose is transported into cells by a family of glucose transporters designated GLUT-1 to GLUT-14 (17). When extracellular glucose binds to the transporter, its conformation is altered, and glucose is transported across the cell membrane down a concentration gradient. Expression of the different GLUTs is tissue specific. GLUT-1 is abundant in erythrocytes and the blood-brain barrier. GLUT-3 is the primary glucose transporter in neurons, while GLUT-4 is abundant in striated muscle and adipose tissue. Unlike other glucose transporters, the

number of active GLUT-4 transporters in the cell membrane is regulated by insulin. The abovementioned GLUTs are primarily involved in glucose uptake from the blood. GLUT-2 however, abundant in liver, kidney, and the pancreatic β cells, is able to transport glucose into the cells when blood glucose is high, or out of cells when blood glucose is low. This is due to its exceptionally high K_m for glucose, ~17 mM, which ensures fast equilibration of glucose concentrations between the cytosol and the extracellular space (18). This allows for appropriate regulation of glucose sensitive genes during the transition from fed to fasting conditions.

Within the cell, glucose is phosphorylated to form glucose 6-phosphate. In the liver, this is effectuated by glucokinase (GK), the first rate-limiting enzyme in glycolysis. Like GLUT-2, GK has a high K_m for glucose, enabling the liver to take up unlimited quantities of glucose (19). Glucose 6-phosphate may then enter glycolysis or the glycogenic pathway. Glycolysis, the oxidation of glucose, provides energy and intermediates for other metabolic pathways (17). Apart from GK, glycolysis is regulated on two additional steps: phosphofructokinase-1 (PFK-1) and pyruvate kinase (PK). In cells with mitochondria and with an adequate supply of oxygen, pyruvate is the end product of glycolysis. Pyruvate can be converted to acetyl-CoA by pyruvate dehydrogenase, and then enter the tricarboxylic acid (TCA) cycle, or serve as a building block for the synthesis of fatty acids. An alternative fate for glucose is through the pentose phosphate pathway. Activated glycolysis and TCA cycle lead to the production of citrate and ATP, which allosterically inhibit PFK-1. This reduces the rate of glycolysis and redirects glucose metabolites into this alternative pathway, which provides the cells with pentose sugars utilized in RNA and DNA synthesis. Moreover, NADPH is produced, which acts as a reductant in the biosynthesis of fatty acids and cholesterol.

Glycolysis is regulated in the short term by allosteric activation or inhibition by metabolites, or by covalent phosphorylation and dephosphorylation of the rate-limiting enzymes PFK1 and PK. During fasting, low levels of glucose stimulate glucagon secretion, which increases hepatic glucose production, glycogenolysis, and gluconeogenesis. In the long term, the glycolysis can be regulated by modulating the levels of the enzymes involved. Regular meals containing carbohydrates stimulate secretion of insulin. Insulin will, when binding to the insulin receptor on target cells activate signalling cascades, e.g. Ras/Raf/MEK/ERK, which converge on chromatin and increase gene expression of several rate-limiting enzymes in the

liver (17). Conversely, transcription and synthesis of these enzymes are low when glucagon is high.

1.2.2 *de novo* lipogenesis

De novo lipogenesis (DNL) is the synthesis of fatty acids from simple precursors such as glucose, and the process of elongation and desaturation of these fatty acids. The main sites of DNL are considered to be the liver, adipose tissue, and lactating mammary gland. However, the liver is thought to be quantitatively more important in humans (20). The newly synthesised fatty acids can be incorporated into triacylglycerol (TAG), which can be stored as protein-coated lipid droplets in the hepatocytes, or exported as very low-density protein (VLDL) to provide fatty acids to other tissues.

After glucose has been converted to pyruvate, the end product of glycolysis, it is transported into the mitochondrion and converted to citrate in the TCA cycle. Citrate is transported into the cytosol and converted into acetyl-CoA by ATP-citrate lyase (*ACLY*). Acetyl-CoA carboxylase (*ACC*), the rate-limiting and regulated step in fatty acid synthesis, then converts acetyl-CoA to malonyl-CoA (17). Malonyl-CoA undergoes a number of condensation reactions with acetyl-CoA to form palmitate, a 16-carbon saturated fatty acid in a process that is catalyzed by fatty acid synthase (*FASN*). Palmitate can later be elongated by enzymes in the Elongation of very long chain fatty acids protein (*ELOVL*) family, bound to the membrane of the endoplasmic reticulum (ER), and desaturated by stearoyl-CoA desaturase (*SCD*), which introduces a double bond at the ω9 position (21).

Following a carbohydrate-rich meal, insulin signalling results in dephosphorylation and activation of ACC, which leads to increasing concentrations of malonyl-CoA, causing inhibition of β-oxidation. Moreover, insulin leads to increased activity of lipoprotein lipase (LPL) in adipose tissue, which results in increased uptake of fatty acids from VLDL and chylomicrons, as well as increased production of glycerol-3-phosphate by stimulating glycolysis. Together, this facilitates fatty acid esterification to form triacylglycerol.

1.2.3 Transcriptional regulation *de novo* lipogenesis

Transcriptional regulation of lipogenic genes is complex and involves multiple transcription factors and nuclear receptors. Three transcription factors have been identified as particularly important for regulation of lipogenesis: liver X receptor (LXR), sterol regulatory element-binding protein 1c (SREBP-1c), and carbohydrate response element-binding protein (ChREBP) (22).

SREBP-1c is synthesized as an inactive precursor, which is bound to the ER membrane. To become active, the precursor must undergo proteolytic cleavage, which liberates the N-terminal domain. This part of SREBP-1c can then translocate to the nucleus and act as a transcription factor. Insulin mediates its long-term effects by upregulating the expression of the inactive precursor, as well as the proteolytic maturation of SREBP-1c (23). SREBP-1c is primarily responsible for expression of lipogenic genes by binding to sterol response elements (SREs) in the promoter of its target genes (24). Glucose itself also acts as an activator of transcription of glycolytic and lipogenic enzymes in the liver and fat cells via ChREBP (25-27). Target genes of ChREBP include enzymes in glucose metabolism such as *PKLR* and *GLUT-4*, as well as lipogenic enzymes such as *ACLY*, *FASN*, *ACC*, and *SCD1*.

LXR plays a role in regulating lipogenic genes in response to feeding, indirectly by inducing the expression of ChREBP (28) and SREBP-1c (29), but also directly by activation of *FASN* (30) and *SCD1* expression (31). LXR, ChREBP, and SREBP-1c thus work in concert to control gene expression of lipogenic and glycolytic enzymes (32), as shown in **Figure 1**.

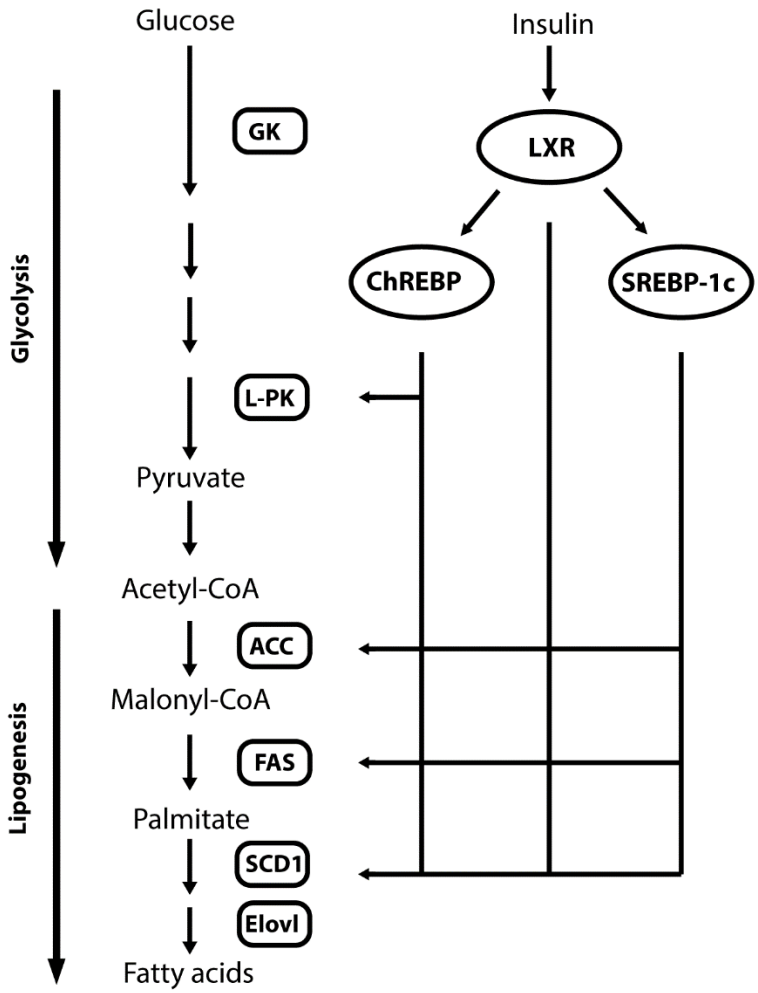

Figure 1: *de novo* lipogenic pathway

LXR regulates SREBP-1c and ChREBP to enhance hepatic fatty acid synthesis, as well as key enzymes in *de novo* lipogenesis. ACC: Acetyl CoA carboxylase; ELOVL: Elongation of very long chain fatty acids protein; FAS: fatty acid synthase; GK: Glucokinase; L-PK: Liver pyruvate kinase; SCD1: stearoyl CoA desaturase 1.

1.2.4 Lipoprotein and cholesterol metabolism

Neutral lipids such as TAG and cholesterol are not water soluble, and must therefore be incorporated into lipoprotein particles to be able to circulate in the blood. Lipoprotein particles consist of a TAG-rich hydrophobic lipid core and a surface monolayer of amphipathic phospholipids, associated with special lipid-binding proteins called apolipoproteins.

Dietary fatty acids are absorbed and re-esterified in the enterocytes and secreted as large lipoprotein particles, called chylomicrons, into the circulation via the lymphatic system.

Chylomicrons deliver TAG to, e.g. adipose tissue and skeletal muscle, and the remnant particle is taken up and metabolized by the liver. Lipids are transported from the liver to other tissues in the form of VLDL particles. Peripheral tissues take up fatty acids from VLDL via LPL, and the lipid-depleted particles are then removed by receptors in the liver, or they remain in circulation until they shrink and become low-density lipoprotein (LDL) particles. Cholesterol from LDL particles is taken up in tissues via the LDL receptor (LDL-R). The cellular cholesterol content is regulated by the SCAP-SREBP2 system (19). Like SREBP-1c, SREBP-2 is an integral part of the ER membrane and associated with SREBP cleavage-activating protein (SCAP). When sterols are abundant, SCAP is bound to an INSIG protein which keeps the SREBP-SCAP complex inactive. At low cholesterol concentrations, the SREBP-SCAP complex moves from ER to the Golgi, where SREBP-2 is proteolytically cleaved by SCAP. Proteolytic cleavage generates an SREBP fragment that acts as a transcription factor that can translocate to the nucleus and enhance expression of LDL receptors. In addition, SREBP-2 increases expression of enzymes involved in cholesterol biosynthesis, such as HMG CoA reductase (17).

Non-hepatic cells acquire cholesterol via uptake of cholesterol from LDL particles and through *de novo* synthesis, but they are unable to catabolize it. Excess cholesterol must therefore be transported from peripheral tissues to the liver for faecal and biliary excretion in a process called reverse cholesterol transport (RCT). The RCT system consists of various steps, the first and most critical step being the efflux of cholesterol from peripheral cells. Macrophages are responsible for a tiny fraction of total body RCT. However, their activity is directly relevant to the development of atherosclerosis. Macrophages are “professional phagocytes” and are able to take up modified cholesterol and other debris via their scavenger receptors, and cholesterol is esterified to protect the cell against cholesterol toxicity. As they accumulate cholesteryl ester, they form foam cells, which is the first step in the development of atherosclerosis.

Efflux of cholesterol from peripheral cells is mediated by the ATP-binding cassette transporters ABCA1 and ABCG1. Free cholesterol is transferred via ABCA1 to lipid-poor apolipoprotein A-I, resulting in the formation of nascent high-density lipoprotein (HDL) particles, also called pre-β-HDL. Further uptake of cholesterol by HDL is mediated by ABCG1 and the scavenger receptor class B type I (SR-BI) (33). In the HDL particle, the

cholesterol is immediately esterified by Lecithin cholesterol acyltransferase (LCAT) to form cholesteryl ester, which allows HDL to take up additional free cholesterol. Cholesterol is then transported in HDL particles via the systemic circulation and taken up by the liver through SR-BI, and can then be excreted into the bile as free cholesterol or bile salts. An alternative route for cholesterol in HDL particles is transfer via cholesteryl ester transfer protein (CETP) to TAG-rich particles, whose remnants become cholesterol-enriched and can be taken up into the liver. While some species, e.g. rats, don't have CETP, this might be the major pathway in humans (19).

1.3 Transcription factors

Transcription factors (TFs) are proteins that control gene regulation and determine where, when and how efficiently the RNA polymerase II functions. The term TF covers several functionally different groups of transcription regulators, including general transcription factors and sequence-specific DNA-binding transcription factors.

General transcription factors, such as TATA-binding protein (TBP) and polymerase II-associated transcription factors (TFIIA and TFIIB, etc.) are accessory proteins that assemble on the promoter to form a transcription initiation complex. These TFs are necessary for the initiation of transcription, as they position the RNA polymerase II and pull apart the double helix to expose the template strand. Additionally, the transcription factor TFIIH is involved in releasing the other TFs from the RNA polymerase so that that transcription can take place.

Sequence-specific DNA-binding TFs bind to short DNA sequences called response elements to regulate the rate of gene transcription. They work as transcriptional activators by aiding the assembly of the RNA polymerase and general TFs at the promoter, or they work as repressors to prevent the assembly of the protein complex. TFs can also modulate chromatin structure to affect the accessibility of the promoter to the general transcription factors and RNA polymerase. The sequence-specific DNA-binding transcription factors do not have enzymatic activity of their own but require co-regulators such as histone modifying enzymes or nucleosome remodelers to function.

As a minimal requirement, DNA-binding TFs always have two functional domains; a DNA-binding domain (DBD) and a transactivation domain (TAD). TFs are often classified based on their DBD. Common DBD structural motifs include the homeodomain, zinc fingers, helix-loop-helix and leucine zippers (34). The DBD often contains one or more α helices which dock into the major groove of DNA wherever it recognizes its binding site, so-called responsive element. The TAD interacts with other co-regulatory proteins to activate transcription from a nearby promoter. Transcription factors frequently bind to DNA as dimers, which increase the strength and specificity of the protein-DNA interaction. Two different proteins can pair in different combinations, which allows for many different DNA sequences to be recognized by a limited number of proteins.

1.3.1 bHLH-LZ transcription factors

Basic helix-loop-helix (bHLH) proteins make up a superfamily of dimeric transcription factors that play a crucial role in several developmental processes. The bHLH TFs have two highly conserved and functionally distinct domains. The N-terminal contains a basic domain, which binds to DNA at consensus sequences known as enhancer boxes (E-box). The canonical E-box sequence is CANNTG, where N is any nucleotide. However, non-canonical E-boxes also exist, and different families of bHLH proteins recognize different E-box consensus sequences. The central HLH domain facilitates interactions with other proteins to form homo- and heterodimeric complexes. Some bHLH protein family members also have a leucine-zipper domain C-terminal to the bHLH region. A leucine zipper motif consists of an α-helix with repeating leucine residues at every 7^{th} position. These residues stabilize leucine zipper dimers through hydrophobic leucine-leucine interactions (**Figure 2**). Members of the basic helix-loop-helix leucine zipper (bHLH-LZ) family include transcription factors such as Myc, Mad, Max, Mondo, ChREBPs, SREBPs, and Mlx.

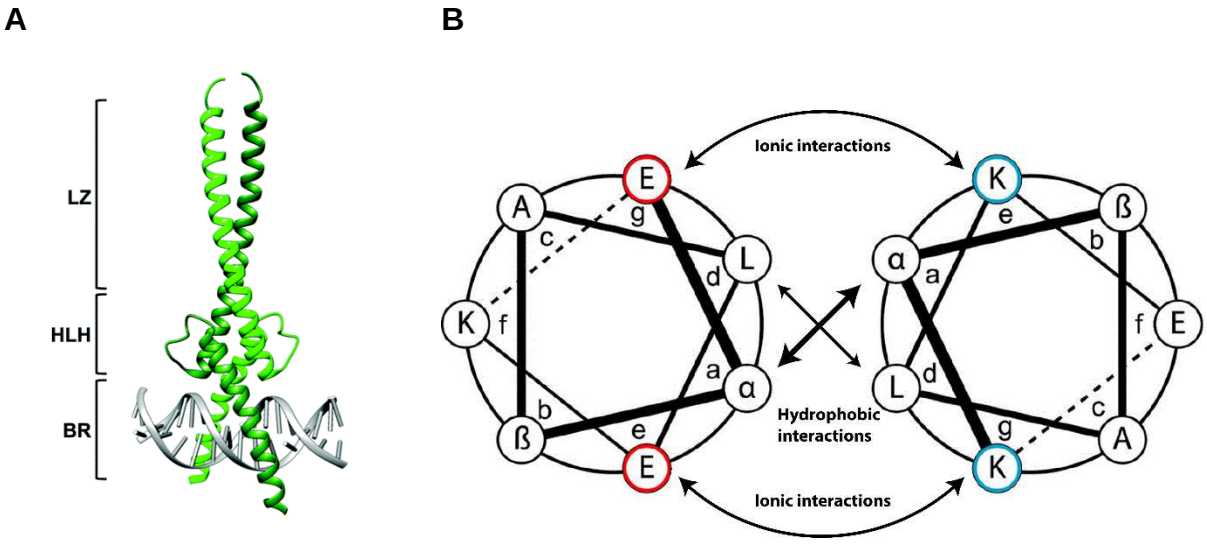

Figure 2: Leucine zipper domain

A: Protein structure showing essential domains of the bHLH transcription factor Max homodimer. Reproduced from (35) by permission of The Royal Society of Chemistry. BR: basic region; HLH: helix loop helix; LZ: Leucine zipper. **B:** Illustration of how a leucine zipper domain is stabilized through hydrophobic leucine-leucine interactions and ionic interactions. Modified from (36).

1.3.2 Nuclear receptors

The nuclear receptors (NRs) are a family of ligand-regulated transcription factors that are activated by steroid hormones, such as estrogen and progesterone, or other lipid-soluble molecules, such as retinoic acid, oxysterols, and thyroid hormone. NRs regulate the transcription of genes that are essential for a variety of biological processes, including embryonic development, cell proliferation and metabolism (37). Since NRs play a key role in many diseases, such as diabetes, and cancer, they are also major targets for drug design and discovery.

The NRs are modular proteins and share a common structure of four domains (38), as shown in **Figure 3**. The N-terminal domain contains a ligand-independent transactivation function, known as activation function 1 (AF-1). It is recognized by coactivators and other transcription factors and its length and sequence varies in different members of the NR family. The central DNA-binding domain (DBD) consists of two Zinc-finger motifs, which are common to the NR family. Following the DBD is a hinge domain, which confers spatial flexibility to the receptor. The C-terminal contains the ligand-binding domain (LBD) that is fairly well

conserved. It engages in the binding of agonistic and antagonistic ligands but also contributes to dimerization with other NRs. The LBD also has a ligand-induced activation function 2 (AF-2) which is involved in interactions with co-regulators.

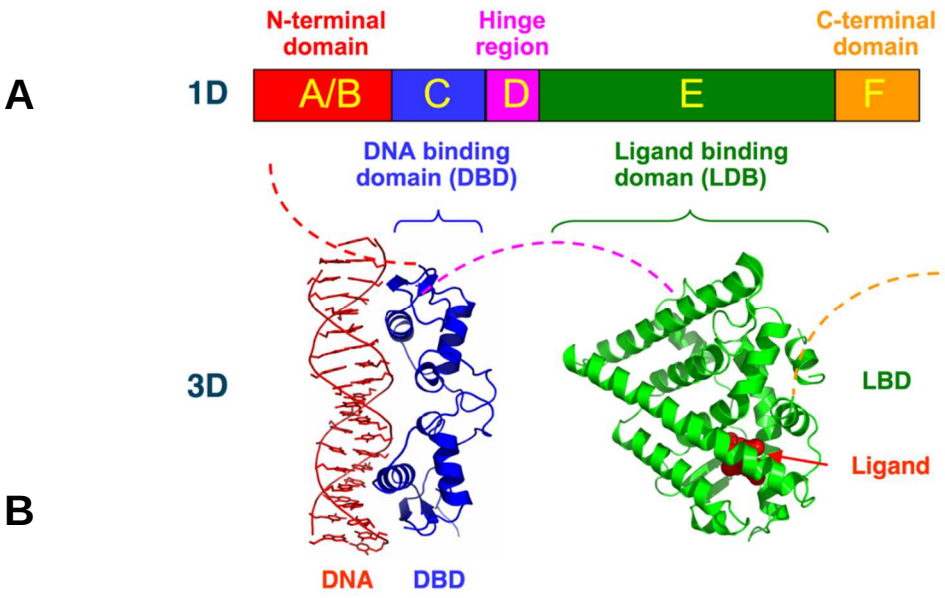

Figure 3: Structural organization of nuclear receptors

A: Schematic 1D amino acid sequence of a nuclear receptor. **B:** 3D structures of estrogen receptor domains: DBD (bound to DNA) and LBD (bound to ligand). Reproduced from Wikimedia Commons.

Nuclear receptors can form homodimers or heterodimers, or as for certain receptors; function as monomers. As an example, steroidogenic factor-1 acts as a monomer, while steroid receptors such as androgen receptor and estrogen receptor act as homodimers. A number of NRs form heterodimers with retinoid X receptor (RXR), for example, retinoic acid receptor (RAR), thyroid hormone receptor (THR) and the metabolic nuclear receptors LXR, farnesoid X receptor (FXR), and peroxisome proliferator-activated receptor (PPAR). The NRs bind to hormone response elements (HREs), which are derivatives of the canonical sequence RGGTCA, in which R is a purine. This sequence can be modified, extended and repeated, and the repeat can be direct, inverted or everted. The repeated sequences can also be separated by a different number of nucleotides, which ensures that the response elements are selective for a given receptor or group of receptors.

1.3.3 Carbohydrate response element binding protein

Carbohydrate response element binding protein (ChREBP), also known as MLX-interacting protein-like (MLXIPL) or MondoB, is a large transcription factor of ~95 kDa (864 amino acids) and belongs to the bHLH-LZ family of transcription factors. ChREBP contains several functional domains (**Figure 4**), including an N-terminal glucose-sensing module (GSM), which is evolutionally conserved in Mondo proteins, also known as Mondo conserved region (MCRI-IV). The MCR/GSM contains two nuclear export signals (NESs) and a nuclear localization signal (NLS), important for the cellular localization of ChREBP. The glucose-responsiveness of ChREBP has been mapped to the GSM/MCR region, which consists of a glucose-response activation conserved element (GRACE), and a low-glucose inhibitory domain (LID), which inhibits ChREBP's transactivational activity, conferred by GRACE in conditions of low glucose concentrations (39). This inhibition is lifted in conditions of high glucose concentrations. The C-terminal region contains a basic helix-loop-helix/Zip domain that is responsible for DNA-binding and regulation of transcriptional activity through heterodimerization with Max-like factor X (Mlx) (40).

The human *MLXIPL* gene consists of 17 exons spanning position 73,624,540-73,593,194 on the minus strand on chromosome 7. In 2012, Herman and collaborators discovered a shorter and more potent isoform, which they named ChREBPβ to separate it from the canonical, full-length isoform ChREBPα (41). The ChREBPβ isoform is transcribed from an alternative promoter 24 kb upstream of the *MLXIPL* exon 1A. When transcribed, the alternative exon 1B is spliced to exon 2, losing exon 1A and the canonical ChREBPα translational start site. Instead, translation begins at codon 177 (AUG) in exon 4, leading to a shorter protein of 687 amino acids (**Figure 4**). Since ChREBPβ lacks most of the LID, it is constitutively active regardless of glucose concentrations.

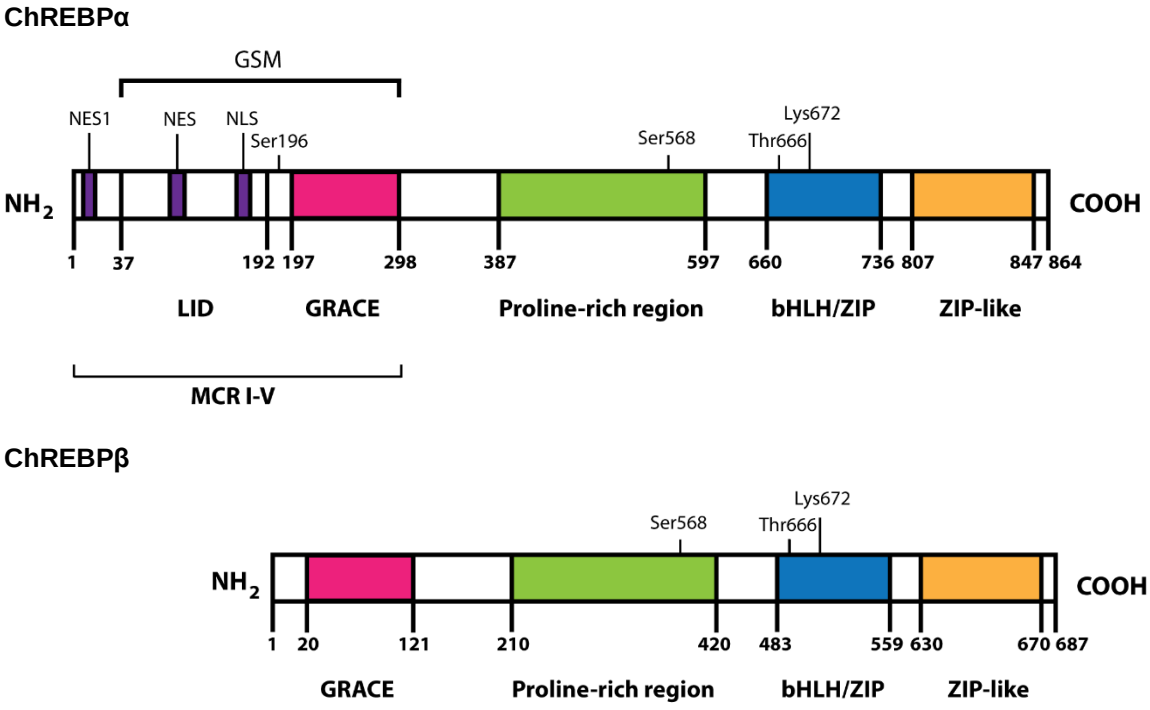

Figure 4: Schematic representation of the ChREBPα and ChREBPβ proteins.

Schematic protein structure of the murine ChREBPα and its shorter isoform ChREBPβ. Recognized domains and sites for post-translational modification are indicated. bHLH: Basic helix-loop-helix domain; LID: Low-glucose inhibitory domain; GRACE: Glucose response activation conserved element; GSM: Glucose sensing module: MCR: Mondo conserved region; NES: Nuclear export signal; NLS: Nuclear import signal; ZIP-like: Leucine zipper-like domain.

ChREBP is most abundantly expressed in tissues active in de novo lipogenesis; the liver, white adipose tissue, brown adipose tissue and the mammary gland (42, 43). It is also highly expressed in pancreatic islets, small intestine, skeletal muscle, and to a lesser extent in the kidney and the brain (42). ChREBPβ shows lower expression than ChREBPα in the liver, WAT, and pancreatic islets, and also respond differently with respect to expression levels following fasting and refeeding. Herman *et al*. proposed a model in which ChREBPα potently induces the expression of the ChREBPβ isoform through an identified carbohydrate response element (ChoRE) in exon 1B upon glucose activation (41). ChREBPβ has a transcriptional activity 20-fold higher than ChREBPα, but also a much higher turn-over (41). Thus, while changes in dietary carbohydrate availability primarily regulate ChREBPα activity, this feed-forward loop ensures that ChREBPβ expression, and thereby the total ChREBP transcriptional

activity, is upregulated concomitantly (44). Moreover, in pancreatic β-cells, ChREBPβ has been shown to inhibit the expression of ChREBPα through a negative feedback loop (45).

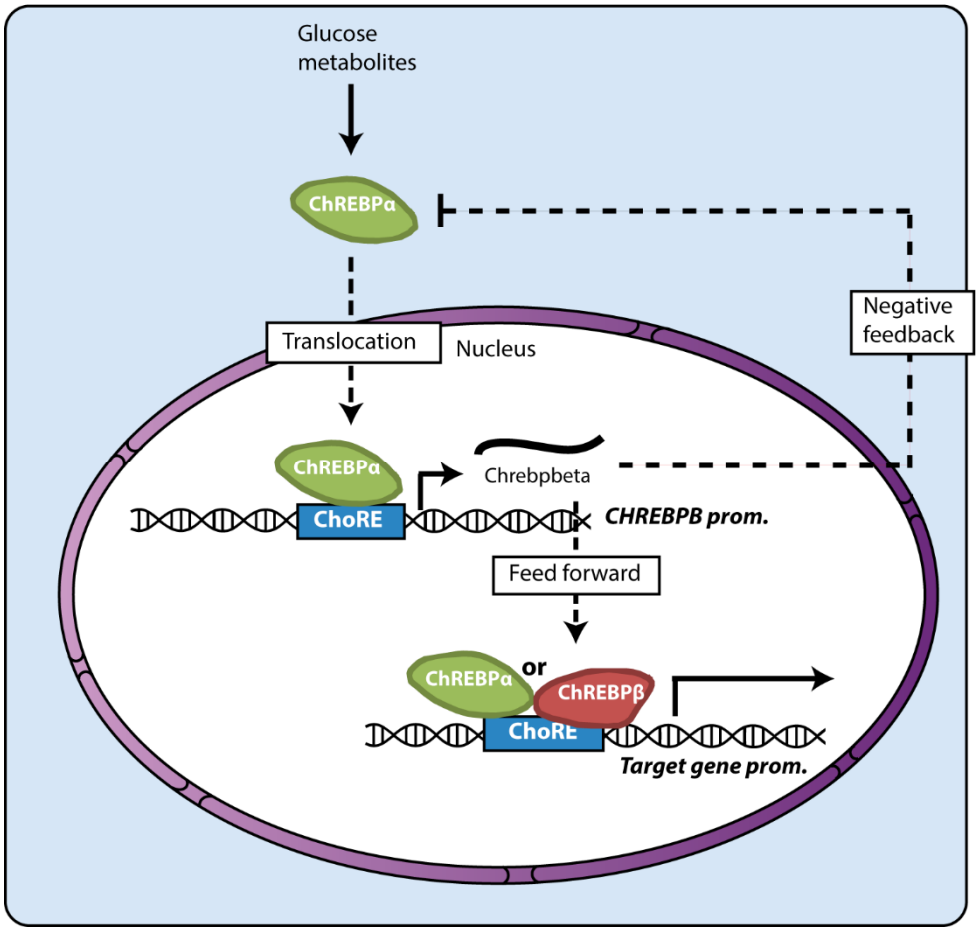

Figure 5: A proposed feed-forward and feedback mechanism

Activation of ChREBPα by glucose metabolites leads to translocation to the nucleus, and binding to ChoRE in the ChREBPβ promoter. As a result of this feed-forward mechanism, ChREBPβ induces transcription of lipogenic genes by binding to ChoREs in the target gene promoters. In pancreatic β-cells, ChREBPβ has also been shown to inhibit ChREBPα in a negative feedback loop. This mechanism has not been reported in other tissues, such as liver and adipose tissue. ChoRE: Carbohydrate response element.

Several nutritional and hormonal signals have been shown to regulate ChREBP activity, and regulation occurs at the level of subcellular localization, DNA-binding, and transcriptional activity. ChREBP is activated in response to carbohydrate feeding (fructose and glucose) and inhibited by signals pertinent to fasting, including glucagon/PKA, AMPK and ketone bodies (46). Interestingly, polyunsaturated fatty acids have also been shown to inhibit ChREBP

activity (47), suggesting that ChREBP has a role in regulating metabolic signals beyond being a glucose sensor.

Activators of ChREBP regulate its entry from the cytosol to the nucleus, where it forms heterodimers with Mlx and binds to ChoREs in regulatory regions of genes involved in metabolism, particularly lipogenesis, glycolysis, gluconeogenesis, insulin signalling and tumorigenesis. The ChoRE is a conserved consensus sequence, which is composed of two canonical CACGTG E-box sequences separated by five base pairs (48). Mlx is a member of the Myc/Max family of basic helix-loop-helix leucine zipper transcription factors and is an obligate binding partner of ChREBP (40, 49). Two ChREBP/Mlx dimers form a tetramer that binds to the two E-boxes of the ChoRE motif to form a transcriptional complex regulated by glucose (50).

It is thought that nuclear-shuttling factors such as 14-3-3 proteins, CRM1, and importins bind to NES1, NES2 and NLS in ChREBP to affect its subcellular localization in response to variations in glucose concentrations. Deletion or mutation of the MCRII (containing NES1) or MCRIII (containing the 14-3-3 binding site) leads to increased ChREBP nuclear localization (51). However, trapping the full-length ChREBP in the nucleus does not lead to constitutive activation, suggesting that mechanisms other than nuclear shuttling are important for the regulation of ChREBP activity (52). Individually deleting or mutating MCRI-IV abolishes ChREBP transactivation in response to glucose (53, 54). Moreover, the distances between the MCRII, MCRIII and MCRIV are conserved across species, which suggests that they act as one functional module (55). Davies *et al.* proposed a model where a dynamic intramolecular interaction between LID and GRACE prevents binding to DNA, recruitment of co-activators, and stimulation of transcription (53). In this model, an active metabolism leads to the production of a glucose metabolite which might bind to the MCRI-IV region and lift the inhibition by LID, thus increasing the transactivation activity conferred by GRACE. Exactly how glucose metabolites cause this conformational change is uncertain, but it may involve allosteric activation, which is the case for glycogen synthase, a key enzyme of glycogen synthesis in the liver (56).

It is still a matter of debate precisely which glucose metabolite that induces ChREBP activity. At least three metabolites have been suggested; xylulose-5-phosphate (X5P) (57), glucose-6-

phosphate (G6P) (58) and fructose-2,6-bisphosphate (F2,6bP) (59). In low glucose concentrations, ChREBP is phosphorylated on Ser-196 and Thr-666, which sequesters ChREBP in the cytosol in association with the 14-3-3 protein, thus hindering transcription of target genes (57). High glucose concentrations result in elevated concentrations of X5P, a product of the pentose phosphate pathway, which activates protein phosphorylase 2A (PP2A). PP2A will, in turn, lead to the dephosphorylation of ChREBP, which allows for its translocation into the nucleus (57). However, this model was challenged by Dentin *et al*., who reported that G6P, but not X5P was necessary for ChREBP activation. Their data showed that dephosphorylation by PP2A is not enough to activate ChREBP. Phosphorylation may, however, play a part in the transition from fasting to feeding. Glucagon treatment leads to significant rise in Ser-196 phosphorylation and to the subsequent export of ChREBP from the nucleus both *in vivo* and *in vitro* (58, 60). Other post-translational modifications, such as acetylation and O-GlcNAcylation, do not influence ChREBP nuclear shuttling but increase its transcriptional activity within the nucleus by favouring its recruitment to its target gene promoters (61, 62).

1.3.4 Liver X receptor

The two Liver X receptors LXRα (NR1H3) and LXRβ (NR1H2), are members of the NR family of transcription factors. They function as physiological regulators of lipid and cholesterol metabolism and control diverse pathways in development, reproduction, metabolism, immunity, and inflammation. Structural studies of the LXR LBDs have revealed that they are canonical NR structures. LXRα and LXRβ are closely related and share >75 % amino acid identity in both DBD and LBD. LXRα is highly expressed in the liver, but also in the kidney, intestine and macrophages, while LXRβ is ubiquitously expressed (63-65)

A schematic structure of the LXR proteins is shown in **Figure 6**.

Figure 6: Schematic structure of human LXRα and β proteins

NTD: N-terminal domain; DBD: DNA-binding domain; LBD: Ligand-binding domain. The numbers represent the amino acid positions that demarcate the domain borders in LXRα and LXRβ, respectively.

Activation of LXR leads to heterodimerization with RXR and binding to LXR response element (LXRE) to induce the expression of its target genes. The LXRE consists of two 5′-AGGTCA-3′ consensus half-sites spaced by four nucleotides (DR-4 motif). The LXRs were initially discovered as orphan receptors (66), and oxysterols were later suggested to be their endogenous ligands. Oxysterols are 27-carbon derivatives of cholesterol or by-products of cholesterol biosynthesis and contain hydroxyl, carbonyl or epoxide groups (67). Physiologically important endogenous LXR ligands include 24(*S*)-hydroxycholesterol, present in the brain and plasma, 22(*R*)-hydroxycholesterol, a metabolite of steroid hormones, 24(*S*),25-epoxycholesterol in the liver, and 27-hydroxycholesterol in macrophages and plasma (68). The LXR ligand binding pocket (LBP) is relatively flexible and allows for compounds of very different structures to bind (69), including the synthetic ligands Tularik (T0901317) and GW3965 (

Figure 7). While Tularik also activates other NRs, namely FXR and pregnane X receptor (PXR) (70), GW3965 is a more selective agonist for LXR (71).

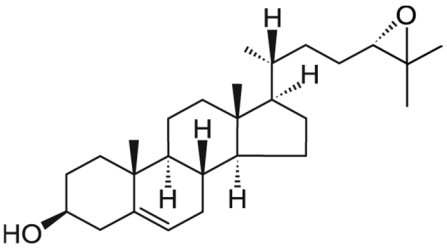

24(*S*),25-epoxycholesterol

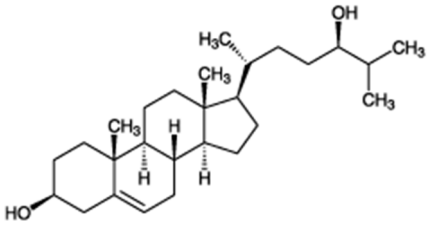

24(*S*)-hydroxycholesterol

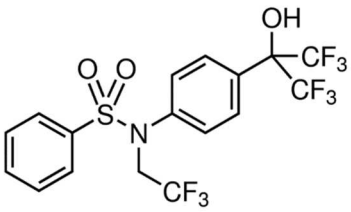

Tularik (T0901317)

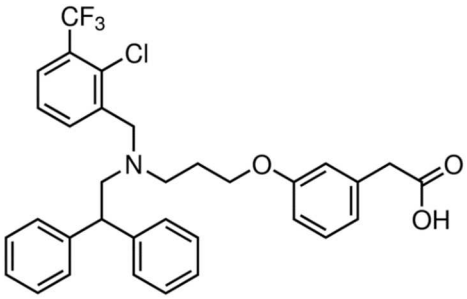

GW3965

Figure 7: Natural and synthetic ligands for LXR

The classical model of LXR activation assumes that the LXR and RXR heterodimer is constitutively bound to LXREs in the nucleus. Transcription is suppressed by corepressors such as nuclear receptor co-repressor (NCoR) and silencing mediator for retinoic acid and thyroid hormone receptor (SMRT). Upon ligand activation, the corepressor complex disassociates, and coactivators such as p300, CPB and ASC2/NCOA6, are recruited and activate transcription (72). An alternative model suggests that ligands, pioneer factors, co-regulators and post-translational modifications (PTMs) play important roles in determining LXR binding sites (68). In this model, histone H3K4 monomethylation signals for LXR recruitment. Upon ligand treatment LXR recruits demethylases, and the histones are demethylated, causing a more open chromatin structure, allowing for LXR to bind to the LXRE.

LXRs are subjected to a variety of PTMs, including phosphorylation (73), ubiquitination (74), SUMOylation (75) and O-GlcNacylation (76, 77). These PTMs can function cooperatively or competitively, and have been shown to cross-talk with and affect the action of co-regulatory proteins. LXRs are modified by O-linked β-*N*-acetylglucosamine (O-GlcNAc), a product of the hexosamine biosynthetic pathway, in response to high glucose conditions. This potentiates their transactivational activity and increases the expression target genes like SREBP-1c (76). Interestingly, it has been suggested that SUMOylation of LXRs leads to anti-inflammatory effects, by inhibiting gene expression of pro-inflammatory cytokines such as TNFα and IL-6 (78). These genes that are induced by pro-inflammatory TFs such as NF-κB, STATs, and AP1 family members, can be transrepressed by SUMOylated LXR: When LXR bind agonists this can trigger modification by SUMO, allowing LXR to enter the transrepression pathway (75). SUMOylated LXR docks to the NCoR-SMRT co-repressor complex at the promoters of inflammatory response genes, thereby preventing co-repressor complex disassembly and gene activation (78).

In addition to playing a role in lipogenesis, LXR also regulates several proteins involved in cholesterol homeostasis and bile acid metabolism. LXR increases the expression of the cholesterol transporters *ABCA1* and *ABCG1* in macrophages, thus increasing the rate of reverse cholesterol transport (79, 80). In the liver, LXR induces the expression of *ABCG5 and ABCG8*, which are involved in the excretion of bile acids. Upregulation of *ABCG5 and ABCG8* also limits the uptake of cholesterol in the intestine (81). LXR increases expression of

IDOL, a negative regulator of LDL-R, which leads to reduced uptake of LDL-cholesterol in macrophages (82). In mice, LXR has been shown to upregulate *Cyp7a1*, which is involved in the conversion of cholesterol to bile acids. However, the human *CYPA1* promoter is unresponsive to LXR (83). Because of the role of LXR in regulating cholesterol homeostasis, they have been evaluated as potential therapeutic targets for diseases related to hypercholesterolemia, i.e. atherosclerosis. Indeed, the administration of LXR agonists in mice led to reduced aortic lesion formation (84) and even lesion regression (85). However, these mice also displayed hepatic steatosis and hypertriglyceridemia due to increased hepatic lipogenesis and VLDL secretion, which has hampered the development of pharmacological therapies targeting LXRs.

1.4 Role of ChREBP and LXR in metabolic pathophysiology

Dysregulation of lipogenesis can contribute to hepatic steatosis, which is associated with obesity and insulin resistance. Both ChREBP and LXR stimulate the lipogenic pathway in the liver, and it is reasonable to believe that they play a role in the development of metabolic diseases such as hepatic steatosis and T2DM.

1.4.1 NAFLD

Increased expression of ChREBP in the liver has been shown to correlate with obesity and hepatic steatosis in humans (86). Genetic models of obesity in mice and rats have established ChREBP as a key mediator of hepatic steatosis. Steatosis is worsened by ChREBP overexpression in liver (87, 88), while ChREBP deficiency improves hepatic steatosis and other metabolic anomalies, including insulin resistance (88, 89). However, a recent study associated decreased hepatic ChREBP expression with the development of NASH, while treatment of NASH decreased inflammatory markers and increased ChREBP expression (90). The authors then speculated if the decrease in ChREBP expression is associated with the progression of NASH.

Similarly, it has been proposed that LXR play a dual role in NAFLD. On the one hand, hepatic LXR expression is associated with increasing severity of NAFLD (91). On the other, LXR also has anti-inflammatory effects which may decrease the progression from steatosis to

steatohepatitis. The anti-inflammatory effects of LXR have been suggested to occur via a direct and an indirect mechanism. The direct mechanism involves SUMOylated LXR, which as described above is capable of transrepressing NF-κB by a tethering mechanism. Transrepression inhibits production of inflammatory cytokines, including tumour necrosis factor α, interleukin-6, and interleukin-1β (78). The indirect mechanism involves ABCA1, which reduces the amount of cholesterol in the plasma membrane of peripheral cells. Cholesterol in the plasma membrane affects the function of Toll-like receptors such as TLR4, and thus higher levels of ABCA1 reduces the activation of TLRs (92)

1.4.2 Insulin resistance

The evidence for the role of hepatic ChREBP in insulin resistance is contradictory. Both global and liver-specific ChREBP deficiency leads to impaired glucose tolerance and insulin resistance in mice (42, 93). However, RNAi-mediated downregulation of ChREBP in obese *ob/ob* mice improved hepatic steatosis and metabolic alterations, including insulin resistance (88, 89), suggesting different effects of ChREBP in a context of lipid overload. In another study, ChREBP overexpression in the liver led to improved insulin sensitivity, despite exacerbated steatosis, which may suggest that hepatic steatosis is disassociated from insulin resistance (86). This seemingly contradictory finding may be linked to ChREBP's role in upregulating SCD-1, which converts saturated fatty acids (SFA) into monounsaturated fatty acids (MUFA), as steatosis was associated with an increased MUFA:SFA ratio in the liver of these mice.

As DNL in adipose tissue helps sink excess energy intake, it is associated with a favourable effect on glycaemic control (94, 95). In obese humans, expression of ChREBPβ, but not ChREBPα, in adipose tissue correlates with improved insulin sensitivity (41, 96, 97). This suggests that ChREBP protects against obesity-associated insulin resistance, possibly by inducing DNL. Also, decreased ChREBP expression in adipocytes may exacerbate the state of insulin resistance by directly affecting the release of specific adipokines and lipid species such as diacylglycerol and ceramides (98, 99).

Activation of LXR has been shown to have potent serum glucose-lowering effects (70, 100). This has been attributed to the ability of LXR to inhibit hepatic gluconeogenesis and promote glucose uptake in white adipose tissue (WAT), as treatment with synthetic LXR agonists has

been demonstrated to downregulate the gluconeogenic enzymes *PEPCK* and *G6PC* (100, 101). In addition, LXR activation induces expression of hepatic glucokinase, increasing glucose flux into the liver and enhancing glucose utilization (100). In murine WAT, LXR has been shown to promote glucose uptake via the upregulation of GLUT-4 (71, 100). However, treatment with LXR agonist impaired glucose uptake in adipocytes derived from overweight individuals, suggesting possible species selective effects of LXR or dysfunctional signalling in obesity (102).

1.5 The rationale behind the current project

While DNL in WAT is associated with increased insulin sensitivity, DNL in the liver is linked to hepatic steatosis, insulin resistance and metabolic syndrome. The current model of transcriptional regulation of hepatic DNL involves LXR, which regulate expression of SREBP-1c and ChREBPα. ChREBPα, in turn, regulates ChREBPβ expression. Preliminary data from our group indicate that LXRα also has the ability to regulate the ChREBPβ promoter, indicating that LXR and ChREBP engage in transcriptional cross-talk. The molecular mechanisms involved in this cross-talk are largely unknown but may involve some kind of protein-protein interaction. Interestingly, it has been shown that LXRα interacts with ChREBPα, but not ChREBPβ (Nørgaard, unpublished data). Further data indicated that when LXRα and ChREBPα are exposed to LXRα ligands such as GW3965, the activity of the ChREBPβ promoter is reduced. This apparent contradiction led to the hypothesis that ChREBP and LXR are part of a carbohydrate and cholesterol-responsive transcriptional switch. In this model, oxysterols would drive the expression of ChREBPα, while glucose would drive the expression of ChREBPβ.

Expression of ChREBPβ in adipose tissue has been shown to correlate with increased insulin sensitivity, while an inverse correlation has been observed in the liver, suggesting opposite roles for ChREBP in WAT and liver. While adipose tissue samples are fairly accessible, it is generally not possible to obtain liver tissue samples from healthy volunteers. Therefore, any accessible cell type or tissue that could be used as a proxy to study liver biology is of interest. Peripheral blood mononuclear cells (PBMCs) are blood cells with round nuclei and include lymphocytes (T cells, B cells, and NK cells), monocytes and dendritic cells. These cells are part of the innate and adaptive immune system, whose main function is to prevent and limit

infections from pathogens such as viruses and bacteria (103). The innate immune system is the first line of defence against pathogens. Cells of the innate immune system, such as monocytes and macrophages, secrete cytokines which lead to inflammation and activation of cells in the adaptive immune system. The cells of the adaptive immune system, i.e. lymphocytes, recognize specific pathogens and protect against recurring infections. Lymphocytes are the largest cell population covered by the term PBMC (104).

PBMCs are fairly easy to obtain from humans, and since blood cells are part of the transport system in the body, they interact with most tissues and are exposed to an array of nutrients, metabolites, excreted factors, and waste products. PBMCs share more than 80 % of the transcriptome with other tissues like kidney and liver, and also express organ-specific genes (105). PBMCs also express genes that are responsive to physiological stimuli such as fasting and feeding, or different levels of fatty acids (106, 107). Furthermore, PBMCs seem to reflect the liver environment and compliment adipose tissue findings in transcriptomics (104). Therefore, they have been used for studying the response of certain genes related to fatty acid and cholesterol metabolism, such as *HMGCR* and *LDLR* (108, 109). We were interested in finding out whether these cells could serve as an *in vivo* model for investigating our hypothesis.

1.6 Aims of the project

The main objective was to attain a deeper understanding of the putative carbohydrate and cholesterol-responsive transcriptional switch in the liver. By using a combination of *in vitro* assays and patient material, we wished to investigate:

1. How LXR and ChREBP work individually, and together, to regulate the ChREBPβ expression.
2. How LXR and ChREBP bind to each other in the cell, and how this binding is regulated.
3. How expression of ChREBPα and ChREBPβ and the ratio between the isoforms changes under different physiological and pathophysiological conditions, like hypercholesterolemia, hyperglycemia or high levels of polyunsaturated fatty acids.

2 Methods

This section describes the laboratory techniques and procedures carried out in this project. Details about reagents, kits, equipment, and software are listed in **Appendix I**, antibodies are listed in **Appendix II**, preparation of buffers and reagents is outlined in **Appendix III**, plasmids are listed in **Appendix IV**, and finally, primer sequences are given in **Appendix V**.

2.1 Peripheral blood mononuclear cells

A pilot study had been conducted by Prof. KB Holven, in which blood samples were collected from diabetic and pre-diabetic patients. Serum biomarkers were analyzed at Department of Medical Biochemistry, Oslo University Hospital. Biomarkers included fasting serum concentrations of glucose, insulin, C-peptide, LDL, HDL and total cholesterol, triglycerides, free fatty acids, C reactive protein (CRP), aspartate aminotransferase (ASAT), alanine aminotransferase (ALAT), vitamin B12, folate, creatinine and plasma homocysteine. Additionally, PMBCs were isolated from whole blood and frozen at -80°C as described previously (110). The study was approved by the Regional Committees for Medical and Health Research Ethics (REC) South-East Norway.

2.1.1 Homeostatic Model Assessment for Insulin Resistance

Homeostatic Model Assessment for Insulin Resistance (HOMA-IR) is a method which provides a score for estimating insulin resistance, based on measurements of fasting serum glucose and insulin levels. There has been demonstrated a reasonable correlation between HOMA-IR and euglycemic and hyperglycemic clamp studies, which are considered the gold standard for assessing insulin sensitivity (111). In this project, HOMA-IR was calculated using the formula (insulin, μU/mL × glucose mmol/L)/22.5. Common cut-off levels range from 1.6-3.0, depending on the study population (112, 113).

2.1.2 Gene expression analysis

In this project, total RNA was isolated from the PBMCs, cDNA was synthesized, and gene expression of *LXRA*, *MLXIPL* (ChREBPα/β), *FASN* and *SREBF1* was analyzed by qPCR, as described in **Section 2.4**.

2.2 Culturing of mammalian cells

Cell culturing is the process where animal or plant cells are removed from the tissue and grown in a favourable artificial environment. These cells can be derived from multicellular eukaryotes or an established cell line or cell strain. As such, the cell culture represents a simplified model system for studying basic cell biology, perform toxicity testing, develop gene therapy etcetera (114). When cells are isolated from tissue and allowed to proliferate, this is known as a primary culture. When the primary culture occupies all of the available substrate, they have to be sub-cultured by transferring them to a new vessel with fresh growth medium to provide more room for continued growth. After the first sub-culture, the primary culture becomes what is known as a cell line. Cell lines derived from primary cultures have a limited lifespan. As they are passaged, cells with the highest growth capacity will start predominating the culture, resulting in genotypic and phenotypic uniformity in the population. If a subpopulation of the cells is positively selected from the culture by, e.g. cloning, the culture is known as a cell strain. Normal cells usually lose their ability to proliferate after a limited number of cell cycles. These cell lines are known as finite. However, some cell lines become immortal through a process called transformation, which can occur through stable transfection or naturally occurring mutations.

Three different mammalian cell lines were used for the *in vitro* experiments of this project; COS-1, HuH-7 and HepG2. These cell lines are further described in the following chapters: **2.2.1-2.2.3**. HuH-7 cells were used for reporter gene assays described in **Section 2.7**. HepG2 cells were used for gene expression studies, described in **Section 2.4**. COS-1 cells were used for co-immunoprecipitation assays, described in **Section 2.8**. All cells were cultured in single-use sterile polystyrene culture flasks (Corning Inc., Falcon™). For downstream applications, the cells were seeded in single-use sterile polystyrene culture plates (Corning Inc., Falcon™). All cell line work was performed in biological safety cabinets in a designated cell lab, where the working area was washed with ddH_2O and 70 % ethanol before use.

The regrowth of cells follows a standard pattern with a lag phase, log phase and plateau phase in which the cell concentration exceeds the capacity of the medium. If the cells are left in this phase, the cells will withdraw from the replication cycle, the medium will become exhausted and eventually the cells will die. It is therefore important to routinely sub-culture the cells to avoid the senescence associated with prolonged high cell density and to ensure reproducible behaviour of the cells. Sub-culturing, or passaging, of cells involves detaching adherent cell cultures from the surface of the culture flasks by using the proteolytic enzyme trypsin and transferring a small number of cells into a new vessel with fresh culture medium. The procedure for sub-culturing of cells is described in **Section 2.2.4**.

2.2.1 HuH-7

The HuH-7 cell line is a well-differentiated hepatocyte-derived carcinoma cell line. The cell line was established by Nakabayashi *et al*. from cells derived from liver tissue from a 57-year-old Japanese male with well-differentiated hepatocellular carcinoma (115). HuH-7 cells are epithelial-like cells, adhere to the surface of flasks and plates and grow in a 2D monolayer. HuH-7 cells have a number of mutations, e.g. a point mutation in the p53 gene.

In the current project, culture medium for HuH-7 cells was composed of high (25 mM) glucose Dulbecco's modified Eagle's medium (DMEM) with L-Gln (Lonza, #12-604F), 10 % heat-inactivated FBS (Sigma-Aldrich, #F7524), and 50 U/mL penicillin/50 µg/mL streptomycin (Sigma-Aldrich, #P4458).

2.2.2 HepG2

The HepG2 cell line, established by Knowles *et al.,* is an immortalized cell line derived from liver tissue from a 15-year-old Caucasian male. The cell line was originally reported to be a hepatocellular carcinoma cell line, however, more recently it has been reported that HepG2 may, in fact, is a hepatoblastoma-derived cell line (116). HepG2 cells are epithelial-like, adherent and grow in a 2D monolayer and in small aggregates. The cells perform many differentiated hepatic functions, such as triglyceride and cholesterol metabolism, lipoprotein metabolism, glycogen synthesis and insulin signalling (117).

HepG2 cells were cultured in low (5mM) glucose DMEM with L-Gln (Lonza, #BE12-707F), 10 % heat-inactivated FBS (Sigma-Aldrich, #F7524), 4 mM L-glutamine (Sigma-Aldrich, #G7513) and 50 U/mL penicillin/50 µg/mL streptomycin (Sigma-Aldrich, #P4458).

2.2.3 COS-1

COS-1 is an African green monkey kidney fibroblast-like cell line suitable for transfection by vectors requiring expression of SV40 T antigen. The line was derived from the CV-1 cell line (ATCC CCL-70) by transformation with an origin defective mutant of SV40 which codes for wild-type T antigen. The cells contain a single integrated copy of the complete early region of the SV40 genome.

COS-1 cells were cultured in culture medium composed of high (25 mM) glucose DMEM with L-Gln (Lonza, #12-604F), 10 % heat-inactivated FBS (Sigma-Aldrich, #F7524), and 50 U/mL penicillin/50 µg/mL streptomycin (Sigma-Aldrich, #P4458).

2.2.4 Cell cultivation procedures

All cells used in this project were cultivated at 37 ° C in a humidified atmosphere of 5 % CO_2 in the air.

Procedure for sub-culturing of cells

The volumes and concentrations detailed in this procedure are adapted to culturing in 75 cm^2 (T-75) flasks. For larger culture flasks, adjust volumes accordingly. First, remove the old medium and wash twice with 5 mL PBS. Add 2.5 mL trypsin and incubate at 37 ° C until the cells detach. HuH-7 and COS-1 cells are incubated for 3-4 minutes, while HepG2 cells are incubated for 5-6 minutes. After incubation, gently shake the flask so that the cells detach. Add 5 mL culture medium with FBS to inactivate the trypsin. Count the cells as described in **Section 2.2.5**. Transfer 1:5 or 1:10 of cells to a new flask, depending on the number of days until next sub-culturing. Adjust the final volume to 12 mL. Sub-culture or renew the medium of the cells three times per week, and ensure that the total cell concentration does not exceed 8×10^6 cells/T-75.

Procedure for freezing cells

Wash the cells with PBS and add trypsin to detach the cells, as previously described. Count the cells as described in **Section 2.2.5**, and calculate how many aliquots to freeze. The concentration of cells should be approximately 1×10^6 in 1 mL freezing medium per ampulla. Spin down the cells at 1300 rpm for three minutes, and discard the medium. Re-suspend the cells in freezing medium to a concentration of 1×10^6/mL. For the cell lines used in this project, the freezing medium consisted of 5 % DMSO and 95 % heat-inactivated FBS v/v. Freeze the cells at -80ºC using a cryogenic freezing container, which lowers the temperature 1ºC/min. Do not move or disturb the cells during the freezing. After 24 hours, transfer the cell ampullas to a liquid nitrogen (N_2) tank for long-term storage.

Procedure for thawing cells

The cell line ampullas are kept in liquid N_2 tanks at -196°C. Equilibrate 15 mL culture medium in a T-75 culture flask at 37°C and 5 % CO_2 for 30 minutes. Thaw tubes of cell in a water bath at 37°C. Transfer the cells to the cell culture flask. Change the medium after approximately 24 hours to remove the DMSO.

2.2.5 Cell counting

In order to be able to sub-culture or seed cells at an appropriate concentration, it is necessary to count the cells. This can be done using the Invitrogen™ Countess™ Automated Cell Counter. The Trypan Blue Stain is mixed 1:1 with the cell suspension. Live cells will actively transport the stain out of the cell, while the dead cells will absorb the staining. Hence, live cells have bright centres, while dead cells have a uniform blue colour with no bright centres. The machine is then able to distinguish between dead and live cells.

Procedure for counting cells

After trypsinizing the cells and adding cell culture medium with FBS to inactivate the trypsin, take a representative aliquot of 30-50 µL of the cell suspension for cell counting. Add 10 µL of the cell suspension to 10 µL 0.4 % Trypan Blue Stain (Invitrogen #T10282). Mix gently by pipetting up and down. Apply 10 µL of the sample mixture to one side of the cell counting chamber slide and put the slide into a Countess™ Automated Cell Counter (Invitrogen™). Adjust the focus so that live cells have bright centres and dead cells are blue. Live cell, dead

cell, and total cell count is shown on the screen, as well as percentage viability. Count samples twice and use the average.

2.3 Glucose stimulation

2.3.1 Stimulation of HepG2 cells with glucose

HepG2 cells are maintained in 5 mM glucose DMEM. Seed the cells in 12-well-trays, at a concentration of 2×10^5/well in 1.5 mL DMEM with 5 mM glucose.

On the following day, inspect the cells to ensure that cells are equally confluent in all the wells. Change the medium from normal (5 mM) to high (25 Mm) or low (1 mM) glucose-containing medium: Remove the old medium, wash each well twice with 1 mL fresh medium, containing either high or low glucose depending on the treatment. In this project, we used this type of glucose treatment in a time-course experiment. Here cells were harvested before changing the medium (t0), and then 6, 12, 24 and 48 hours after changing to high or low glucose-containing medium, as outlined in **Figure 8.**

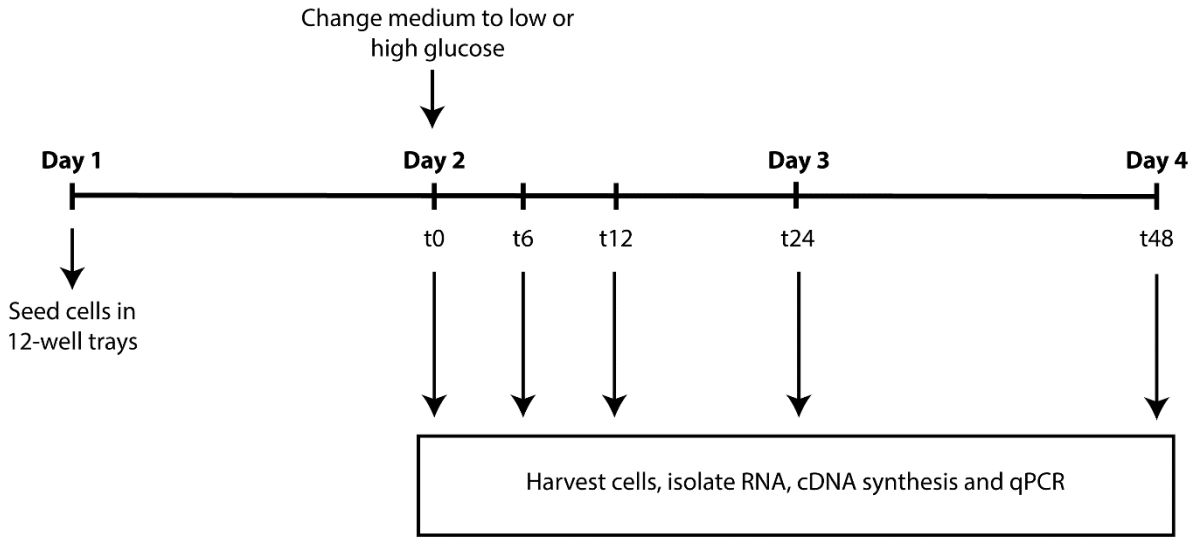

Figure 8: Flowchart of glucose stimulation experiment

HepG2 cells were seeded in 12-w trays in normal (5 mM) glucose. On day 2, the medium was changed to low (1 mM) or high (25 mM) glucose. Cells were harvested at baseline, and 6, 12, 24 and 48 hours after changing medium.

Harvesting: Inspect the cells. Wash all wells twice with 1 mL PBS. Add 400 µL RLT buffer with 0.1% β-ME (2-Mercaptoethanol). Scrape the cells with a cell scraper. Transfer the lysate to 15 mL tubes and store at -80 ºC. Proceed with RNA isolation and downstream analysis, as described in **Section 2.4**

2.4 Gene expression assays

2.4.1 Isolation of total RNA

RNA was isolated using the Qiagen RNeasy Mini Kit (#74104). The RNeasy procedure makes use of a silica membrane and a buffer system to isolate up to 100 µg of RNA from cells and tissue. RNA smaller than 200 nucleotides, such as 5.8S rRNA and 5S rRNA, are selectively excluded. The samples are first lysed and homogenized in the presence of a buffer containing guanidine thiocyanate and β-ME, which inactivates RNases. This ensures that the isolated RNA remains intact. Ethanol is added, ensuring appropriate binding of RNA to the silica membrane. Contaminants are washed away, and RNA is then eluted with Tris-buffered water. The purified RNA can then be used for downstream analysis such as cDNA synthesis and qPCR.

Procedure for isolating total RNA

Wash cells twice with 1 mL PBS. Add 10 µL β-ME pr. 1 mL Buffer RLT, supplied in the Qiagen RNeasy Mini Kit (#74104). Add 400 µL Buffer RLT per well in a 12-well cell culture dish. Scrape the cells with a rubber cell scraper and collect the lysate in a microcentrifuge tube. Remove any cell clumps by passing the lysate at least 5 times through a 21-gauge needle fitted to an RNase-free syringe. If the lysate is not to be used immediately, freeze at -80 º C. Otherwise, proceed according to the manufacturer's manual (2011) (118, 119). Measure RNA concentrations on NanoDrop® ND-1000 spectrophotometer (NanoDrop Technologies).

2.4.2 Assessing RNA quality

There is a linear relationship between the RNA quality and gene expression measurement (120, 121). It is therefore important to test RNA quality in order to obtain meaningful and reproducible data in downstream analyses. One method for assessing RNA quality is using the Agilent 2100 Bioanalyzer system, which uses automated electrophoresis to provide sizing,

quantitation, and purity assessments for RNA samples. The Bioanalyzer uses algorithms to determine the RNA quality, as expressed as an RNA integrity number (RIN). The RIN scale ranges from 1 to 10, where 1 is the lowest and 10 is the highest quality. For reproducible and reliable data in downstream analysis, a RIN higher than 5 is recommended, and higher than eight is considered as perfect total RNA (120).

Procedure for assessing RNA quality

Using the Agilent RNA 6000 Nano Kit (#5067-1511), prepare the gel-dye mix according to the manufacturer's instructions (2013) (122). Load the samples onto the chip supplied in the kit. Run the chip in the Agilent 2100 Bioanalyzer within 5 minutes.

2.4.3 Complementary DNA (cDNA) synthesis

Reverse transcriptase (RT) is an enzyme originally found in retroviruses which can synthesize DNA from RNA. RT can hence be used to synthesize complementary DNA (cDNA) from isolated mRNA. Random hexamers primers (5'-NNNNNN-3') can hybridize anywhere on the RNA, generating a double-stranded segment where RT can start the reverse transcription. By adding deoxynucleotides (dNTPs), RT can synthesize cDNA hybridized to mRNA.

The polymerase chain reaction (PCR) is quite sensitive to contamination. Hence it is important to follow good laboratory practices when doing PCR assays. When working with RNA, precautions should also be taken to avoid enzymatic RNA breakdown by ribonucleases (RNases). RNases are extremely stable and exist in virtually every cell, bacteria, and fungi. Always wear a clean lab coat and gloves, and change gloves often. Open and close sample tubes carefully to avoid spilling. Lab work should be performed on a clean lab bench using dedicated equipment and supplies.

Procedure for cDNA synthesis

cDNA was synthesized from mRNA using the Applied Biosystems High Capacity cDNA Reverse Transcription Kit (#4368813), following instructions supplied by the manufacturer (2010) (123). The kit includes deoxynucleotides (dNTPs), random hexamer primers, RT buffer and MultiScribe™ RT.

Dilute the RNA to 50 ng/µL in 10 µL RNase-free water. For each reaction, use 4.7 µL RNase-free water, 2 µL RT buffer (10×), 2 µL random primers (10×), 0.8 µL dNTPs (100 mM), 0.5 µL MultiScribe™ enzyme, and 10 µL of the diluted RNA template. The total reaction volume should be 20 µL and contain 500 ng of RNA. Run the reverse transcription reactions in PCR strips on a Veriti™ 96 Well Thermal Cycler (Applied Biosystems™), using the program outlined in **Figure 9**:

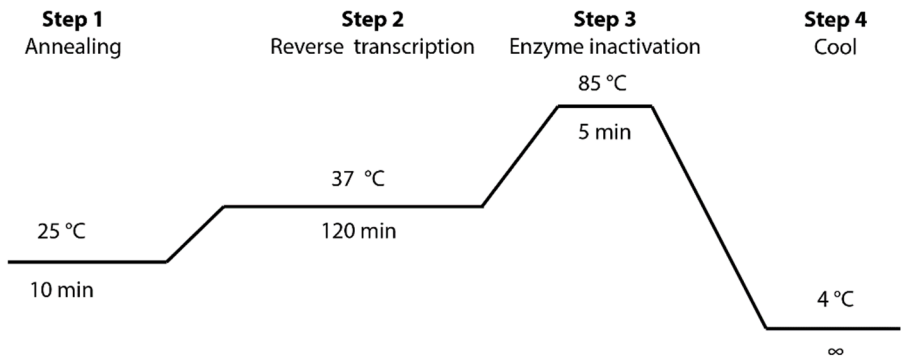

Figure 9: PCR temperature cycling for reverse transcription

As controls, prepare a sample without the MultiScribe™ enzyme to control for contamination of genomic DNA, and a sample using pure water without RNA to control for contamination of RNA in the reagents, as well as primer dimer formation. The cDNA can be stored short-term at 2-6°C, or long-term at -20 °C.

2.4.4 Quantitative Polymerase Chain Reaction (qPCR)

The polymerase chain reaction (PCR) is a method in which specific sequences within genomic DNA or the cDNA template are amplified using sequence-specific oligonucleotide primers, heat-stable DNA polymerase, and thermal cycling. In real-time quantitative PCR (qPCR), the PCR product is measured with each cycle of amplification. The amount of DNA is measured via reporters that yield an increasing fluorescent signal in direct proportion to the number of PCR product molecules generated. Data collected in the early and exponential phase of the reaction give quantitative information on the staring quantity of the amplification target. If a particular sequence is abundant, exponential amplification is observed in earlier cycles. If the sequence is scarce, exponential amplification is observed in later cycles.

Primers are short forward and reverse complementary nucleotides that anneal to the gene of interest. They direct the DNA polymerase to the starting point of replication. Primers used in this project were designed using Primer-BLAST from NCBI, except for the primers targeting *CHREBPA* and *CHREBPB*, which were found in literature (41) (**Appendix IV**). A primer pair should be sequence-specific so that only one particular DNA sequence is amplified, and in the case of cDNA amplification, preferably anneal to exon-exon junctions to avoid amplification of genomic DNA.

In order to measure the amplification of DNA during the qPCR, fluorescent probes or DNA-binding dyes and instruments that measure fluorescence during the thermal cycling can be used. SYBR Green® is a fluorescent dye that binds to double-stranded DNA. When SYBR Green® binds to DNA, it emits a stronger fluorescent signal than unbound dye. The cycle number at which the fluorescent signal crosses the threshold, i.e. detected above background, is expressed as the threshold cycle (C_T). The C_T value is used to calculate the initial DNA copy number and is inversely related to the amount of target (124).

SYBR Green® will bind to any amplified product, not just the target sequence. It is therefore important to assess specificity for every reaction. One common assessment is a melting curve analysis. The rationale for this assessment is that each amplicon has a specific melting temperature, T_m. Off-target products will therefore have detectable different T_m values. When double-stranded DNA (dsDNA) melts, DNA becomes single-stranded, the dye disassociates, and fluorescence decreases. The qPCR software transforms this into a peak, which should be narrow, symmetrical and devoid of other anomalies. Anomalies are an indicator of multiple products, such as primer dimers or other non-specific products.

Procedure for qPCR

Thaw qPCR reagents on ice and spin down before use. Prepare a master mix corresponding to 5.0 µL KAPA SYBR® FAST qPCR Master Mix (2×) Universal (KAPA Biosystems, #KK4601), 2.3 µL PCR water, and 0.1 µL of forward (10 µM) and reverse (10 µM) target gene primers per qPCR reaction. Pipette 7.5 µL from the master mix into the wells of a 96-well optical reaction plate. Dilute the cDNA samples 1:5 with PCR water and pipette 2.5 µL of the diluted cDNA into each well in the reaction plate, using a multichannel pipette. This yields a total reaction volume of 10 µL. Cover the top of the plate with an optical adhesive

sealing. Spin down the plate at 1000 rpm for 1 minute. Run the plate on a CFX96 Touch™ Real-Time PCR Detection System (Bio-Rad Laboratories), using a protocol suitable for KAPA SYBR® FAST qPCR Master Mix (2×). A subsequent melt curve analysis should be included in order to analyze the specificity of the qPCR reaction.

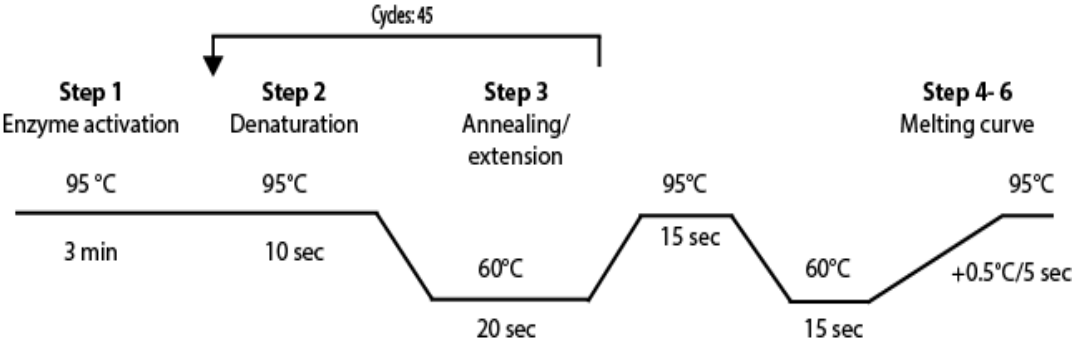

Figure 10: qPCR protocol

2.4.5 Processing of qPCR data

Relative mRNA expression was calculated using the comparative C_T method, also known as the $2^{-\Delta\Delta CT}$ method. Advantages of this method include ease of use and the ability to present data as 'fold change' in gene expression. The qPCR data were normalized to TATA-binding protein (TBP). ΔC_T is the target $C_T - C_T$ of the reference gene in each sample. $\Delta\Delta C_T$ is the ΔC_T value of the treatment – the ΔC_T value of the control. In this project, the control samples refer to cells cultivated in 5 mM glucose before treatment. The relative amount of target mRNA in a sample is given by $2^{-\Delta\Delta Ct}$. This will set the control samples to 1. Relative expression of PBMC data was normalized so that the average was equal to 1. $C_T > 35$ was considered negligible expression, and the sample was not considered further or set to C_T=35.

2.5 DNA cloning

DNA cloning refers to the process of replicating a small piece of DNA. Plasmids vectors are circular double-stranded DNA molecules, derived from plasmids that occur naturally in bacteria, yeast and some higher eukaryotic cells (125). Plasmids can be engineered to optimize their use as vectors in DNA cloning. The essential components of a plasmid vector include a replication origin (ORI), a region where exogenous DNA fragments can be inserted, and a drug-resistance gene. By treating the plasmid with restriction enzymes, which cleave dsDNA at specific sites, one can open the plasmid and prepare it for inserting a gene of

interest. This means that treating exogenous DNA, e.g. a human gene promoter, with the same restriction enzymes will result in a DNA fragment with a set of compatible ends. The DNA to be cloned is then added to the cut plasmid, and the fragments are covalently joined by DNA ligase, generating a recombinant plasmid. The recombinant plasmid can then be inserted into bacteria by transformation. Since the vector contains a drug-resistance gene, only the bacteria that have acquired the plasmid will survive when treated with the corresponding antibiotic. Plasmids are duplicated before every cell division and are passed on to the next generation of the host cell, and thus numerous copies of the plasmid can be generated.

The majority of the DNA plasmids used in the current project (**Appendix IV**) were either cloned and transformed at Department of Nutrition, University of Oslo from 2012 to 2017, or received as gifts. Plasmid stock solutions were stored at -20°C. In this project, the reporter plasmids pGL3b-mChREBPbeta-Exon-1B E-box-del and pGL3b-mChREBPbeta-Exon-1B DR4-del, and the expression plasmid pCMV4-FLAG-mChREBP-LID were cloned, transformed and purified by the procedures described below.

2.5.1 Site-directed mutagenesis

The sequence of a cloned DNA fragment can be changed by site-directed mutagenesis using PCR. By allowing synthetic, overlapping oligonucleotide primers with mutations to anneal to the template plasmid DNA, the mutated DNA is replicated in the PCR. The template plasmid DNA can later be removed by treating it with *DpnI*, an endonuclease which specifically digests methylated DNA (126). Since only plasmid DNA isolated from *E. coli* and not PCR DNA is modified by methylation, *DpnI* treatment can be used to separate the template from PCR products.

Procedure for PCR mutagenesis

Make dilutions so that all reagents have the appropriate concentrations. Mix 5.0 µL template, wild-type plasmid (5 ng/µL), with 1.25 µL forward primer (10 µM), 1.25 µL reverse primer (10 µM), 5.0 µL *PfuUltra* II reaction buffer (10×) (Agilent, #600670), 1.0 µL dNTP (5 mM), 1.0 *PfuUltra* II Fusion HotStart DNA Polymerase (2.3 IU/µL) (Agilent, #600670) and dH_2O to a total reaction volume of 50 µL. Run the PCR on a thermal cycler, using the program

outlined in **Figure 11.** In this project, we used a Veriti™ 96 Well Thermal Cycler (Applied Biosystems™).

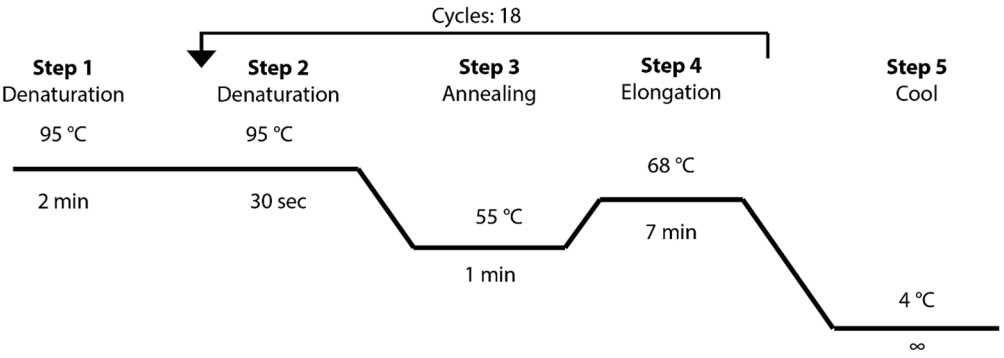

Figure 11: Temperature cycling for PCR mutagenesis

After the PCR is finished, add 1.0 µL of *DpnI* restriction enzyme to 25 µL of the PCR mix. Incubate at 37°C for 90 minutes to break down the template plasmid.

Procedure for cloning of pCMV4-FLAG-mChREBP-LID

Start by amplifying the desired DNA fragment using PCR, in this case, the low glucose inhibitory domain (LID) from ChREBPα: Dilute the PCR reaction solutions to appropriate concentrations. Mix 5.0 µL of the DNA template (5 ng/µL) with 2.5 µL forward primer (10 µM), 2.5 µL reverse primer (10 µM), 5.0 µL *PfuUltra* reaction buffer (10×) (Agilent, #600670), 2.5 µL dNTPs (10 mM), 1.0 µL *PfuUltra* II Fusion HotStart DNA Polymerase (2.5 U/µL) (Agilent, #600670). Add ddH2O to a total volume of 50 µL and run the reaction mix on a thermal cycler, using the program outlined in **Figure 12**.

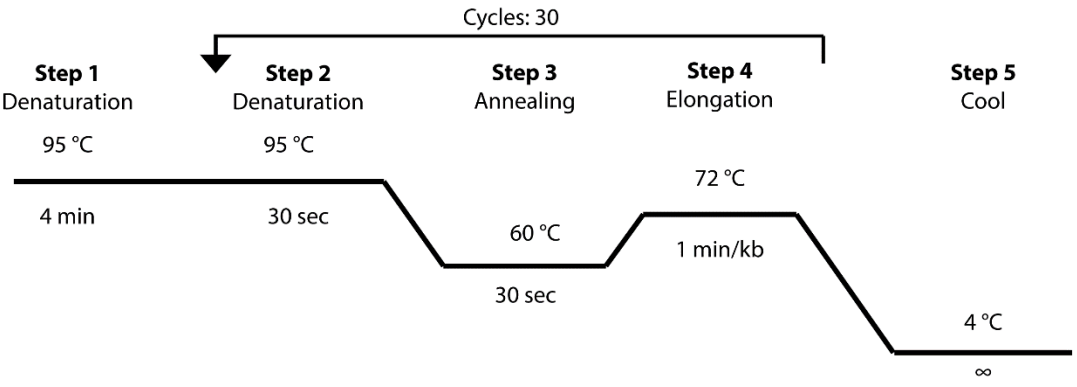

Figure 12: PCR amplification program

After the PCR, verify that the correct insert has been amplified by running an aliquot of the PCR mix on an agarose gel: Mix 5 µL of the reaction mix with 15 µL dH2O and 5 µL 5× loading dye. Run with a DNA ladder (Invitrogen, #10787018) on a 0.8 % agarose gel with TAE buffer at 100V for 30 min using Sub-Cell® GT Horizontal Electrophoresis System (Bio-Rad® laboratories, #1704401) and PowerPac™ Basic Power Supply (Bio-Rad® laboratories, #1645050).

Perform a PCR clean-up using the NucleoSpin® Gel and PCR Clean-up kit (Macherey-Nagel #740609) according to the manufacturer's instructions (2017) (127) with the following adjustments: incubate for 1 minute when binding DNA before spinning, and 1 minute when eluting DNA, before spinning. Elute DNA in 25 µL 1:10 TE buffer (**Appendix III**). Measure concentration on a NanoDrop® ND-1000 spectrophotometer (NanoDrop Technologies). Next, cut the PCR products and the vector with the appropriate restriction enzymes, in this project *BglII* and *HindIII*, which will generate so-called sticky ends that can later be ligated. Mix insert, vector, restriction enzymes and buffers as described in **Table 2** and incubate at 37ºC for 1.5-2 hours.

Table 2: Cutting reaction of insert and vector

Reagent	Volume (µL)	
	Insert	Vector
Insert	23.0	-
Vector	-	4.0
BglII	2.0	2.0
HindIII	2.0	2.0
NEBuffer 3.1 (10x)	4.0	5.0
1:10 TE buffer	9.0	37.0

Run the cut vector along with a DNA ladder on a 0.8 % agarose gel to separate the desired products from uncut vector and artefacts such as non-specific amplicons and primer-dimers. Excise the desired DNA fragment from the gel and extract the DNA from the gel using the NucleoSpin® Gel and PCR Clean-up kit (Macherey-Nagel #740609). Follow the protocol provided by the manufacturer (2017) (127). Elute DNA in 25 µL 1:10 TE buffer and measure on a NanoDrop® ND-1000 spectrophotometer (NanoDrop Technologies).

Next, set up a ligation reaction and control. Mix the cut PCR products and vector with T4-DNA ligase (New England Biolabs, #M0202S/L), T4-DNA ligase buffer and 1:10 TE buffer to a total volume of 20 µL, as outlined in
Table 3. Incubate at room temperature for 30 minutes. Make sure to add the insert in at least 3-fold molar excess for efficient ligation.

Table 3: Ligation reaction and control

Reagent	Volume (µL)[1]	
	Ligation	Control
Vector, 4849 bp (30 ng/µL)	12.6	12.6
Insert, 556 bp (30 ng/µL)	4.4	-
T4-DNA ligase buffer (10×)	2.0	2.0
T4-DNA ligase	1.0	1.0
1:10 TE buffer	-	4.4

Procedure for preparation of agarose gel

For a 0.8 % agarose gel, mix 0.8 g agarose (Lonza, #50181) in 100 mL 1×TAE in an Erlenmeyer flask. Boil in a microwave oven at full effect for 3 minutes until the gel solution appears clear. Cool the gel solution under running water. Add 10 µL SYBR™ Safe DNA Gel Stain (Invitrogen™ # S33102) to 100 mL gel and gently swirl the liquid to mix. Pour the solution into a gel tray and put the comb into the gel solution. Wait 20 minutes until the gel solidifies before running gel electrophoresis.

2.5.2 Transformation of *E. coli*

Transformation is the genetic alteration of the cell caused by uptake and expression of foreign DNA. In bacteria, this can occur via uptake of naked DNA, transduction by bacteriophages, or conjugation (125). In order for the bacteria to be able to take up naked DNA, such as a plasmid, the cells must be made competent. This can be done chemically or by electroporation. The purpose of the transformation affects the choice of method. DH5α cells are an *E.coli* strain that is engineered for optimal transformation efficiency. When the cells are heat-shocked, they are triggered to take up foreign DNA through pores in the cell wall.

[1] Volumes depend on the length of insert and vector. We used an online ligation calculator (http://2011.igem.org/Team:UT_Dallas/ligation)

Procedure for transformation of DH5α

Thaw competent DH5α on ice and mix 200 µL of the bacteria with 5 µL of ligated or un-ligated plasmid by pipetting up and down. Incubate the bacteria on ice for 30 minutes, then heat shock at 42 °C for exactly 90 seconds before putting the bacteria back on ice for 2 minutes. Seed 50 µL of each bacteria suspension separate LB plates with the antibiotic of choice, in this case, ampicillin as the plasmids code for an ampicillin resistance gene. Incubate the plates overnight at 37 °C.

Identification of positive clones

Pick six colonies and use them to inoculate six 3 mL cultures. Incubate a 37 ºC overnight with shaking (250 rpm). Re-streak the culture on fresh LB-Ampicillin plates. Incubate at 37 ºC overnight, and keep them at 4 ºC for later use. The following day, isolate plasmid DNA using the Miniprep NucleoSpin® kit (Macherey Nagel, #740588), according to the instructions provided by the manufacturer (2017) (128). Measure DNA concentrations on the NanoDrop® ND-1000 spectrophotometer (NanoDrop Technologies).

A test cutting can be performed to identify plasmids with the correct sized insert before sending them off for sequencing. In this project, a test cutting was performed on pCMV4-FLAG-mChREBP-LID by mixing 4.0 µL plasmid DNA (100ng/µL), 0.5 µL *BglII*, 0.5 µL *HindIII*, and 2 µL NEBuffer 3.1, adjusted to a total volume of 20 µL with 1:10 TE buffer. As uncut controls, 4 µL plasmid DNA and 16 µL 1:10 TE was mixed. After incubation at 37 º C for 1.5-2 hours, add 5 µL loading dye to each sample and run 25 µL of the plasmid mix on a 0.8 % agarose gel along with a DNA ladder in TAE buffer at 100V for 30 min.

Prepare the isolated DNA for Sanger sequencing at GATC Biotech (Germany). Dilute the plasmid DNA to a concentration of 80-100 ng/µL. Mix 5 µL DNA with 5 µL sequencing primers (5 µM) in a 1.5 mL microcentrifuge tube. Sequencing primers are listed in **Appendix V.** Choose one clone for maxi preparation based on sequence integrity.

Maxi preparation

When a positive clone has been identified, start a 200 mL bacterial culture by inoculating the medium with bacteria from the corresponding re-streaked colony. Incubate at 37 ºC with

shaking (250 rpm) overnight. Perform a maxi preparation by using the Nucleobond ® Xtra Maxi Plus kit (Macherey Nagel, #740416) according to manufacturer's manual (2017) (129). For long-term storage of plasmids, prepare glycerol stocks. Add 1000 µL of bacterial culture to 500 µL 50 % glycerol in a 2 mL screw-top tube and gently mix. Freeze and store at -80ºC.

2.6 Transfection

Transfection refers to the process of artificially introducing foreign nucleic acids into mammalian cells. The main purpose of transfection is to study the function of genes or gene products, by enhancing or inhibiting specific gene expression in cells, and to produce recombinant proteins (130). The introduced nucleic acids may exist stably or transiently in the cell. In stable transfection, the foreign DNA is integrated into the genome of the cell or maintained as an episomal plasmid. This leads to persistent expression of the gene, which can also be passed on through multiple generations. In transient transfection, the introduced nucleic acid exists in the cells only for a limited period of time and is not integrated into the genome. However, the high copy number of the transfected genetic material ensures high levels of expressed protein within the period it exists in the cell. Peak transient expression is generally seen 24-72 hours after transfection.

Transfection of DNA into mammalian cells can be achieved by several methods, including microinjection, electroporation, and lipofection. Lipofection is a popular method in cell biology and related research fields, as it is fast, simple and highly reproducible (131). Lipofection is based on the use of cationic lipids, such as Lipofectamine, which complexes the negatively charged nucleic acids and forms a transfection complex. The interaction with the cell membrane is mediated by this positive charge of the liposomes, and the DNA is taken up into the cell, assumingly by endocytosis.

In this project, HuH-7 and COS-1 cells were transfected with DNA plasmids with reporter genes and expression genes to be used in a dual-luciferase gene activity assay, described in **Section 2.7.1**. COS-1 cells were also transfected with expression plasmids and used to study protein-protein interactions, described in **Section 2.8**.

Procedure for transfection of COS-1 and HuH-7 cells

Seed cells in a 24-well culture plate at a concentration of 0.70×10^5/0.5mL/well. Incubate the cells for 24 hours. Inspect the cells under a light microscope to ensure that the cells have an acceptable confluence level. For optimum transfection efficiency and subsequent cell viability, the cells should be 90-95 % confluent.

Prepare DNA plasmids in 1:10 TE buffer according to the experimental setup. The plasmids used in this project are described in **Appendix IV**. Pre-warm DMEM without FBS in a 37 °C water bath. Prepare a master mix of DMEM and Lipofectamine® 2000 (Invitrogen™, #11668-019). Mix the components by pipetting up and down 3-4 times and incubate at room temperature for 5 minutes. Add DMEM to the DNA samples before adding the Lipofectamine master mix. The ratio of DNA to Lipofectamine should be between 1:2 and 1:3 w/v. Add the Lipofectamine master mix to the DNA samples and mix by pipetting up and down 3-4 times. Incubate at room temperature for 20 minutes. Then add the transfection complex solutions to each well dropwise to avoid damaging the cells. Incubate the cells at 37 °C.

Procedure for adding agonist

A nuclear receptor agonist, in this case, the LXR agonist GW3965, can be added to the cells four to six hours after transfection. Dilute GW3965 in DMSO to the desired concentrations. Add the agonist to DMEM with FBS to a final concentration of 0.1 % DMSO. Add 50 µL of the treatment solution to each well dropwise. Incubate at 37 °C for 18-24 hours before collecting the cells.

2.7 Reporter gene assays

2.7.1 Luciferase

Reporter genes are indicators of transcriptional activity. The reporter gene is typically joined to a promoter sequence in a circular DNA vector, which is transfected into cells. Expression of the reporter protein correlates with transcriptional activity of the reporter gene promoter. The function of cis-acting transcriptional elements can be investigated by cloning the promoter region upstream or downstream of the reporter gene. This allows the characterization of promoter and enhancer elements that regulate gene expression. The effect

of trans-acting factors can be assayed by co-transfection of the reporter gene with a cloned DNA plasmid, expressing the trans-acting protein of interest, or by activating trans-acting factors through treatment of the cell culture (132).

Commonly used reporter genes that induce visually identifiable characteristics usually involve fluorescent and luminescent proteins. Firefly luciferase is a 61 kDa enzyme cloned from the firefly *Photinus pyralis*, encoded by the *Luc* gene. It catalyzes a two-step reaction which involves the oxidation of D-luciferin, a reaction that produces light at about 550-570 nm. *Renilla* luciferase is a 36 kDa enzyme from sea pansy (*Renilla reniformis*), encoded by the *Rluc* gene. It catalyzes the oxidation of coelenterazine, which produces a blue light of 480 nm. The oxidation reactions are shown in **Figure 13**. The enzymes use different substrates and produce light at different wavelength. This allows for discrimination between their respective bioluminescence reactions, making them suitable for use in a dual-reporter assay. The most common dual-reporter assay uses both firefly and *Renilla* (132). First, the Firefly substrate is added, and luminescence is measured. Next, *Renilla* substrate is added, extinguishing firefly activity, and initiating the second luciferase reaction.

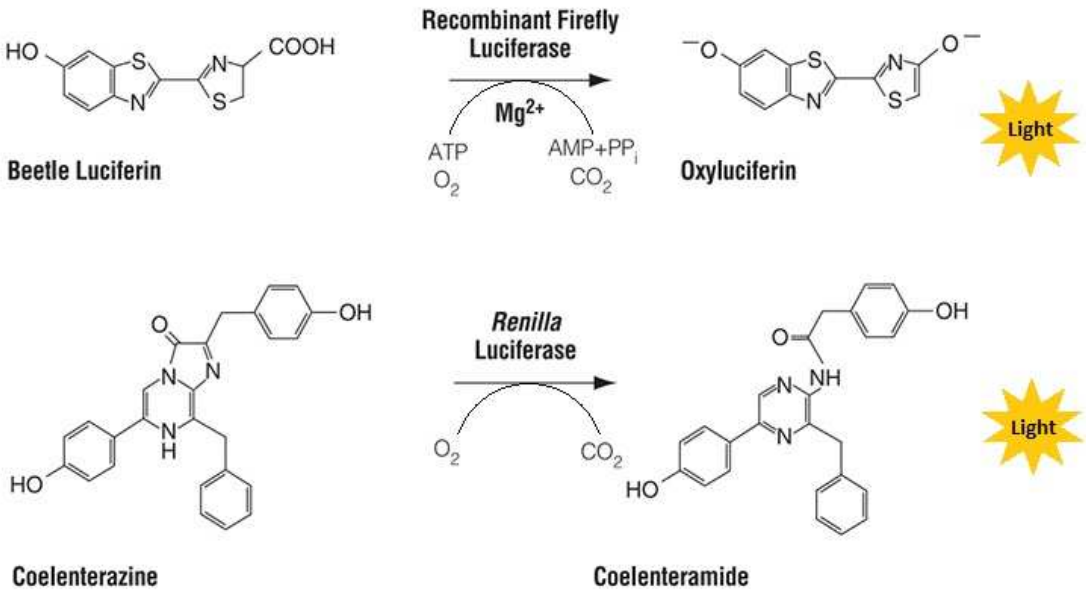

Figure 13: Simplified illustration of the bioluminescent reactions catalyzed by Firefly and *Renilla* luciferases

Substrates and known co-factors for the luciferases are presented. Modified from (133).

Procedure for luciferase assay

The Dual-Luciferase Reporter Gene Assays were performed using Dual-Luciferase® Reporter Assay System kit (Promega, #E1960). The Firefly luciferase substrate, LARII, and the *Renilla* luciferase substrate, Stop&Glo® reagent, supplied in the kit were prepared according to instructions supplied by the manufacturer (2009) (134). The prepared substrates should be kept out of light and can be stored at -20 °C for about a month.

Incubate the cells for 18-24 hours. Inspect the cells to ensure that the transfection or treatments have not affected cell viability or cell number. Remove the medium from the wells and wash cells twice with 0.5 mL PBS. Make sure to remove all liquid from the wells. Passive lysis buffer (5× PLB) is supplied in the kit and must be diluted 1:5 before use. Add 100 µL 1×PLB to each well. Incubate the cells for 15 minutes on an orbital shaker at 600 rpm. Transfer duplicates of 30 µL lysate to a 96-well white polystyrene microplate (Thermo Fischer Scientific, #136101) and measure samples using the Synergy 2™ Multi-Mode Reader (Bio-Tek® Instruments).

Synergy 2 is a single-channel microplate reader which injects reagents into the wells and measures light. Before reading the plate, prime and purge the dispensers with ddH_2O. Prime the dispensers with 1500 µL of the substrate reagents. Read the microplate using a protocol where 30 µL LARII reagent is injected into each well and Firefly luciferase activity is measured before 30 µL Stop&Glo® reagent is injected, and *Renilla* luciferase activity is measured. Apply a 2-second delay between adding the substrate and measure of the luciferase activity, and a 10 second light integration time. When the microplate readings are finished prime and purge the dispensers first with 70 % ethanol, and subsequently with ddH_2O.

2.7.2 Processing of gene activity data

Data from the dual-luciferase reporter gene assay are presented as relative light units (RLU). In order to calculate the RLU for each sample, Firefly luciferase activity (LUC) was divided by activity from the internal *Renilla* luciferase control (RLUC). Data from different biological replicates were normalized to each other using a normalization factor. Means, standard deviations (SD) and relative standard deviations (RSD) were calculated. RSD is the SD divided by the mean. The Solver add-in in Excel was used to calculate the normalization

factor for each biological replicate that yields the lowest sum of RSD. Sample means were normalized to their respective controls, and the control sample mean was set to 1.

2.8 Protein-protein interaction studies

2.8.1 Co-immunoprecipitation

Immunoprecipitation is the technique of precipitating a protein out of a solution by using an antibody that binds specifically to an antigen on that protein. In this way, it is possible to isolate and concentrate a specific protein from thousands of proteins in a cell. Co-immunoprecipitation (CoIP) is a classic technique for investigating protein-protein interactions, where intact protein complexes are precipitated from a solution. In the CoIP, cell lysates are generated, and antibodies that target a known protein of the complex are added. The antigen is then precipitated, and proteins that are not bound to the precipitate are washed away. Finally, the proteins that are bound to the antibody, either directly or indirectly via protein complexes, are eluted and analysed, for example by SDS-PAGE and western blotting (135) as described in **2.8.2.**

One method for precipitating proteins uses magnetic beads, such as Dynabeads®. These are conjugated to bacterial proteins, such as proteins A and G, which bind to different domains of immunoglobulins. The beads are incubated with the antibody of the target protein. By incubating the cell lysate with the beads, the target protein will form complexes with the antibody bound to the beads.

Procedure for CoIP

Preparing cell lysates: Seed cells in 6-well trays at a concentration of 3.5×10^5 per tray, 2 mL/well. For sufficient amount of protein for CoIP, seed six wells per treatment. The following day, inspect the cells to ensure that they are confluent or close to confluent. Prepare DNA solutions according to the experimental purpose and setup. Transfect the cells as described in **Section 2.6**. After 24 hours, remove the medium and wash cells in 500 µL cold PBS. Work on ice. Add 250 µL cold PBS-T (0.1% Tween20) to each well. Scrape the cells and transfer to chilled centrifuge tubes. Centrifuge the tubes for 3 minutes at 500 rcf. Aspirate the supernatant and re-suspend the pellet in 500 µL Lysis buffer, described in **Appendix III**.

Leave the tubes on ice for 10 minutes. Freeze on dry ice for 2 minutes or at -80°C for 10 minutes. Thaw on ice and centrifuge for 10 minutes at 1800 rcf at 4°C. Pipette the supernatant into a fresh tube.

Immunoprecipitation: Equilibrate the Protein A or G Dynabeads, depending on the antibody (host and subtype) used in the experiment, by mixing 20 µL Dynabeads with 1000 µL lysis buffer in a microcentrifuge tube. Put the tubes on a magnet and remove the lysis buffer. Vortex the lysates and transfer 200 µL of each treatment to separate tubes. Save 10 % for Input samples. Add 1-1.5 µg antibody per 100 µL of lysate. Incubate on a rotator for 2-3 hours at 4 °C.

Wash the beads with wash buffer, described in **Appendix III**, for 5 minutes with rotation. Place on a magnet and remove as much of the wash buffer as possible to ensure thorough washing. Repeat this step twice.

Add 45 µL 1×SDS loading dye to the beads. Mix by careful vortexing to re-suspend all of the beads. Spin down at 500 rcf for 30 seconds. For the Input samples, add 15 µL lysis buffer and 10 µL 5×loading dye to 20 µL of the sample for a final volume of 45 µL. Boil all samples at 95ºC for 5 minutes. Re-suspend beads and load 20 µL of the IP reactions and 20 µL of the Input samples on an SDS-PAGE. Store the remaining lysates at -20ºC.

2.8.2 SDS-PAGE and western blotting

Western blotting is a technique used to identify, quantify and determine the size of specific proteins (136). It involves separation of proteins by electrophoresis, transfer of the protein to a membrane and detection by antibodies specific to the protein of interest. Proteins can be separated by an isoelectric point, molecular weight, electric charge, or a combination. A common method is to use polyacrylamide gels and sodium dodecyl sulphate (SDS)-containing buffers (136). SDS is a strong, anionic detergent that denatures proteins, complexes with peptide chains and gives them a uniform negative charge. The proteins can then be separated based on molecular weight only. Voltage is applied to the gel, leading the negatively charged protein:SDS complexes to migrate towards the cathode with at a speed inversely correlated to the size. The proteins become separated into bands within each lane. The gel should include a molecular weight marker in order to determine the molecular weight

of the target protein, and preferentially a lane with a positive control. The separated proteins are then transferred from the gel onto a membrane. Electroblotting ensures speed and complete transfer (136). It uses electric current to pull proteins from the gel onto the membrane in a gel-membrane sandwich. To prevent nonspecific binding of the antibody, the membrane is blocked in a diluted solution of bovine serum albumin (BSA) or skim milk powder. The membrane is then incubated with the primary antibody, which binds specifically to the target protein. After washing, the membrane is incubated with the secondary antibody, which is linked to a fluorophore or an enzyme, usually horseradish peroxidase (HRP), which is able to cleave a chemiluminescent substrate. This reaction produces luminescence, which is directly proportional to the amount of protein. Blots can be washed in buffer and stripped, which entails removing the bound antisera to enable reuse of the blot. This will, however, result in a reduced signal from the re-blot (137).

Procedure for SDS-PAGE and western blotting

Dilute samples so that each sample has the same protein concentration. Prepare 5×loading dye and add to each sample 1:4 v/v. Mix samples and put on a heating block at 95 ºC for 5 minutes. Centrifuge samples at 400 rcfrcf for 2 minutes.

Mount the gel of choice in a gel chamber. We used 10 % 12+2w Criterion Tris-HCl precast gels in the Criterion Cell system. Slide the gel into position and lock everything into place. Fill the inner chamber with running buffer (**Appendix III**) and ensure there is no leakage. Then fill the outer chamber with buffer. Remove the comb gently. Apply 5 µL of Precision Plus Protein™ All Blue standard (Bio-Rad #161-0373) and 5 µL of Precision Plus Protein™ Dual Color standard (Bio-Rad #161-0374) to the small wells on each side of the gel. Load samples and run the gel at constant voltage (200 V) for approximately 60 minutes or until the blue dye front reaches the end of the gel.

Activate the PVDF membrane by soaking it for 5 seconds in 100 % methanol, then 2 minutes in ddH_2O and finally in transfer buffer (**Appendix III**) until use. Pre-soak sponges and filter paper in transfer buffer for a few minutes before use. Place an ice block in the back chamber of the blotter. Fill the tank of the Criterion Blotter with transfer buffer and place a magnetic stir bar inside the tank. Once the gels have stopped running, crack the plastic gel cassette open with the cassette-opening tool built into the Criterion cell lid.

Assemble the transfer cassette: Pour chilled transfer buffer into each compartment of the assembly tray, open the cassette and place the black plate in the tray. Place a pre-wetted sponge on the black plate of the cassette. Then, place a pre-wetted filter paper onto the sponge. Carefully lift the gel from the gel-cassette and submerge it briefly in transfer buffer before laying it on the filter paper. Layer the PVDF membrane onto the gel and place a filter paper and sponge on top. Use a blot roller to remove air bubbles trapped between the layers for the blot assembly. Close the sandwich, lock everything into position and place the entire sandwich into the Criterion Blotter apparatus. Add transfer buffer up to the fill level. Put the apparatus on a magnetic stirrer at low speed. Connect the Criterion blotter to a power supply and transfer the gel at 0.6 A for 1 hour. The voltage should be approximately 70-90.

Disassemble the sandwich when the transfer is complete. Discard the gel and the filter paper. Rinse membrane with 1×TBS-T, described in **Appendix III**. Incubate membrane in blocking buffer (**Appendix III**) at room temperature with agitation for 1 hour or at 4 °C overnight. The next day, remove the blocking solution. Dry the edges of the membrane quickly on a paper towel before incubation with primary antibody. Dilute primary antibody 1:1000 in TBS-T with 3 % BSA. Incubate with rotation for 1 hour at room temperature or at 4°C overnight. Rinse membrane once in TBS-T. Then wash membrane 3×10 minutes in TBS-T. Dilute secondary antibody (Jackson Laboratories, #115-035-174) 1:10 000 in TBS-T and incubate the membrane with rocking. Tilt the box with the membrane slowly for 45-60 minutes. Rinse membrane once in TBS-T. Then wash membrane 3 × 10 minutes in TBS-T. Dry the edges of the membrane quickly on a paper towel before developing. Develop using an enhanced chemiluminescent (ECL) horseradish peroxidase (HRP) substrate kit (Thermo-Scientific, Dura #34076, Pico #34080). Mix equal amount of Solution 1 and Solution 2 to generate working solution. Make enough solution to be able to cover the entire membrane (100 μL/cm^2). Place the membrane on a straight surface, preferably onto a plastic/glass plate. Add working solution to the membrane and move the plate gently so that the solution covers the entire membrane. Incubate membrane with working solution for 2 minutes. Do not shake membrane during this period. Drain off the excess working solution. Develop the membrane by recording the chemiluminescent signal using a Chemdoc station, e.g. the Bio-Rad Image Lab camera.

2.9 Statistical analysis

Statistical analyses were performed using IBM® SPSS® Statistics 25 and GraphPad Prism 7. Data are presented as means and standard error of the mean (SEM) unless otherwise specified. Statistical differences between groups were determined by two-way analysis of variance (ANOVA), followed by Tukey's multiple comparison tests. To test for the assumptions of the two-way ANOVA, residual analysis was performed. Outliers were assessed by inspection of a boxplot, normality was assessed using Shapiro-Wilk's normality test, and homogeneity of variances was assessed by Levene's test. For all statistical tests, $p < 0.05$ was considered significant.

Correlation between blood biomarkers and gene expression in peripheral blood mononuclear cells was assessed. To assess linearity, a scatter plot of the two variables was plotted. Bivariate normal distribution was assessed by Shapiro-Wilk's normality test. For assessing effect sizes, guidelines by Cohen were used, where $r \geq 0.5$ is a large size effect, $r \geq 0.3$ is a medium-size effect and $r \geq 0.1$ is a small size effect (138). Due to the exploratory nature of the cohort, we chose not to adjust for multiple tests.

3 Results

3.1 Site-directed mutagenesis

Unpublished data from our research group has indicated a co-regulatory role for LXRα and ChREBPα in the regulation of *Chrebpb* expression (Nørgaard, unpublished data). In order to investigate the function of putative regulatory elements in the *Chrebpb* promoter, we wanted to delete an E-box (half-site of putative ChoRE) and DR4 (putative LXRE) element the pGL3b-mChREBPbeta-Exon-1B reporter plasmid, and compare the activities from the mutated promoters with the wild-type promoter. The wild-type reporter was a gift from Prof. Mark Herman and has been described previously (41).

Site-directed PCR mutagenesis was performed with the intention to create two new reporters: pGL3b-mChREBPbeta-Exon-1B-E-box-del, in which the E-box is deleted, and pGL3b-mChREBPbeta-Exon-1B-DR4-del, in which a DR4 response element is deleted. For this, we used mutated, overlapping primers (**Appendix V**). After the PCR, the reaction mix was treated with *DpnI*, which breaks down methylated DNA and thus removes the template DNA while leaving the PCR product intact. *E.coli* DH5α were transformed with the cut PCR product and the uncut PCR product as a control. For each reporter, six colonies were selected for plasmid mini-preparation and sequencing at GATC Biotech, Cologne, Germany. For both plasmids, a clone with 100 % sequence identity in the coding region was chosen for maxi-preparation (**Appendix VI-VII**).

3.2 Cloning of ChREBP-LID expression construct

LXR has been shown to interact with ChREBPα, but not ChREBPβ (Nørgaard, unpublished data). Since ChREBPβ lacks the low-glucose inhibitory domain (LID) in the N terminal, we hypothesized that LXR interacts with the LID. In order to test this hypothesis, an expression plasmid was cloned in which only the LID (178 first amino acids) of the ChREBPα protein is expressed. In addition, LID was tagged with a FLAG-tag to allow us to detect or capture this relatively small protein domain. The FLAG-LID insert was amplified from the template plasmid pCMV4-FLAG-mCHREBPalpha in a PCR using specific primers (**Appendix V**). In order to verify that the correct insert was amplified in the PCR, the PCR product was run on

an agarose gel and visualized using SYBR Safe. The electrophoresis resulted in a DNA fragment at 500-650 bp, which corresponds to the FLAG-LID insert (556 bp) (**Figure 14**)

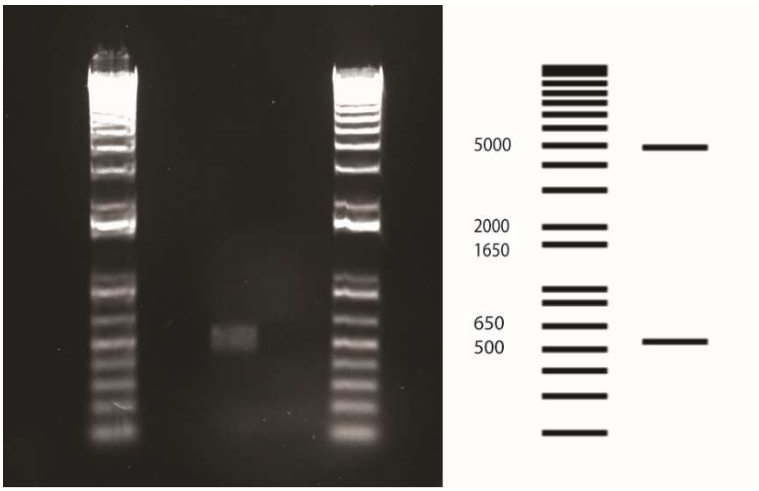

Figure 14: Verification of PCR product on agarose gel

The FLAG-LID insert was amplified from the template plasmid pCMV4-FLAG-mCHREBPalpha in a PCR using specific primers. To verify that the correct insert was amplified in the PCR, the PCR product was run on an agarose gel and visualized using SYBR Safe. The standard reference is modified from restriction analysis of pPMV4-FLAG-mCHREBPalpha cut with *BglII* and *HindIII*, using Serial Cloner v.2.6 (Serial Basics).

After trimming of the FLAG-LID and the pCMV4-FLAG-mCHREBPalpha vector with *BglII* and *HindIII* restriction enzymes, the insert was subcloned into the vector. A schematic outline of the cloning strategy is shown in **Figure 15**.

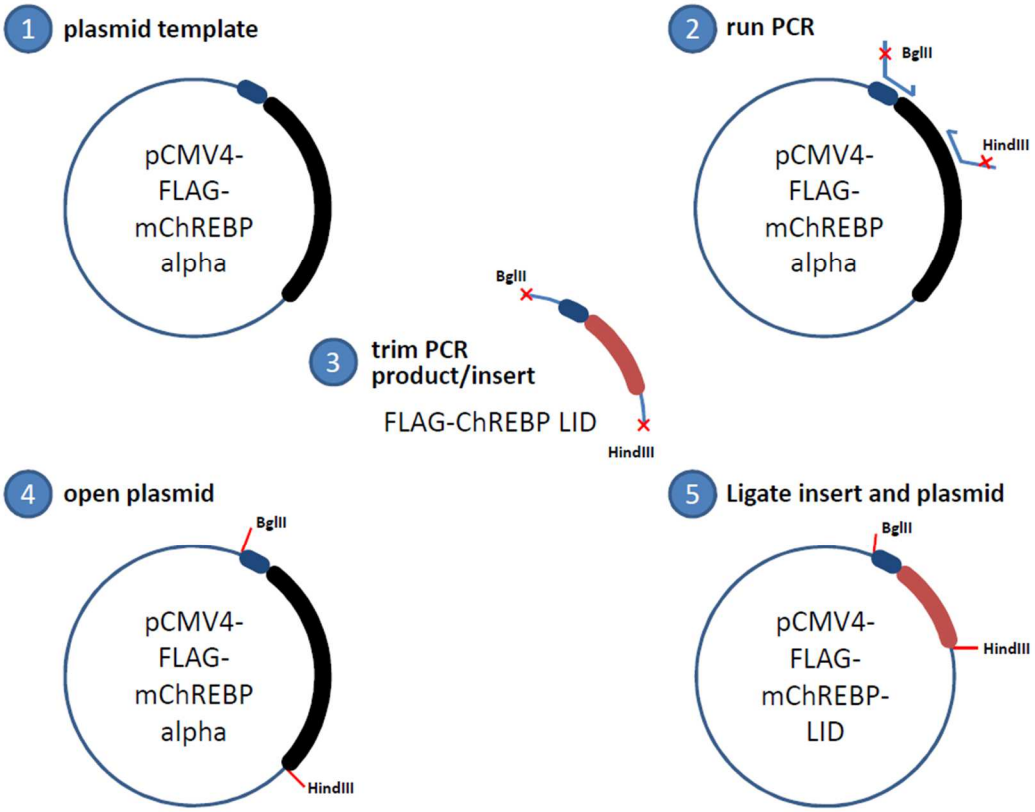

Figure 15: Cloning strategy for the ChREBP-LID construct

1: The pCMV4-FLAG-mChREBP-α vector was used as a template for cloning. **2:** The FLAG-ChREBP-LID insert was amplified from the plasmid template in a PCR using specific primers. **3:** The PCR product was trimmed using *BglII* and *HindIII* restriction enzymes. **4:** The plasmid template was opened using the same restriction enzymes. **5:** The trimmed insert and plasmid template were ligated using T4-DNA ligase. LID: Low-glucose inhibitory domain.

The ligation and control mix was transformed into *E.coli* DH5α. The colony growth on the ligation reaction plate was 3:1 compared with the control. Six colonies were picked for mini-preparation. These were test cut with *BglII* and *HindIII* and run on an agarose gel. All colonies produced a fragment at approximately 500 bp, which corresponds to FLAG-LID (556 bp) (**Figure 16**). Four clones were selected for sequencing. Clone no. 2 was chosen for maxi preparation. The cloned sequence chromatogram for the ChREBP-LID construct is given in **Appendix VIII**, aligned to the pCMV4-FLAG-mCHREBPalpha plasmid between bp positions 400-1660, covering the full open reading frame.

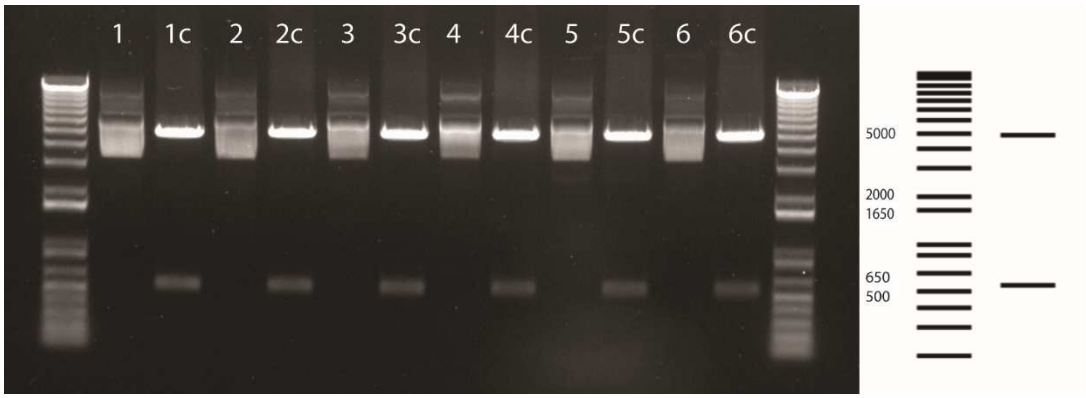

Figure 16: Verification of DNA plasmid clones on an agarose gel.

FLAG-LID was cut with *BglII* and *HindIII*, sub-cloned into a pCMV4-FLAG-ChREBPalpha-vector and transformed into *E.coli* DH5α. After mini preparation of the clones, the plasmids were test cut with *BglII* and *HindIII* and verified on 0.8 % agarose gel along with uncut plasmids for control. Numbers represent the ID for the plasmids isolated from separate colonies, c: cut plasmid. The standard reference is modified from restriction analysis of pPMV4-FLAG-mCHREBPalpha cut with *BglII* and *HindIII*, using Serial Cloner v.2.6 (Serial Basics).

3.3 Regulatory element-dependent activation of the *ChREBPβ* promoter

In order to investigate the role of different motifs in regulating the ChREBPβ promoter, HuH-7 cells were transfected with five different LUC reporters driven by the murine *Chrebpb* promoter. The wild-type reporter (pGL3b-mChREBPbeta-Exon-1B) and the two mutated reporters (pGL3b-mChREBPbeta-Exon-1B-ChoREdel) and (pGL3b-mChREBPbeta-Exon-1B-ChoRE-E-box-del) were gifts from Prof. Mark Herman and have been described previously (41). The two remaining reporters (pGL3b-mChREBPbeta-Exon-1B DR4-del and pGL3b-mChREBPbeta-Exon-1B-E-box-del) were cloned as a part of this project, as described in **Section 3.1**. A schematic representation of the different ChREBPβ reporter constructs is shown in

Figure 17. The cells were co-transfected with LXRα and/or ChREBPα expression plasmids, as well as their respective heterodimerization partners RXRα and Mlxγ. Six hours post transfection, the cells were treated with GW3965, a potent, selective agonist for LXRα and LXRβ, or DMSO as a control.

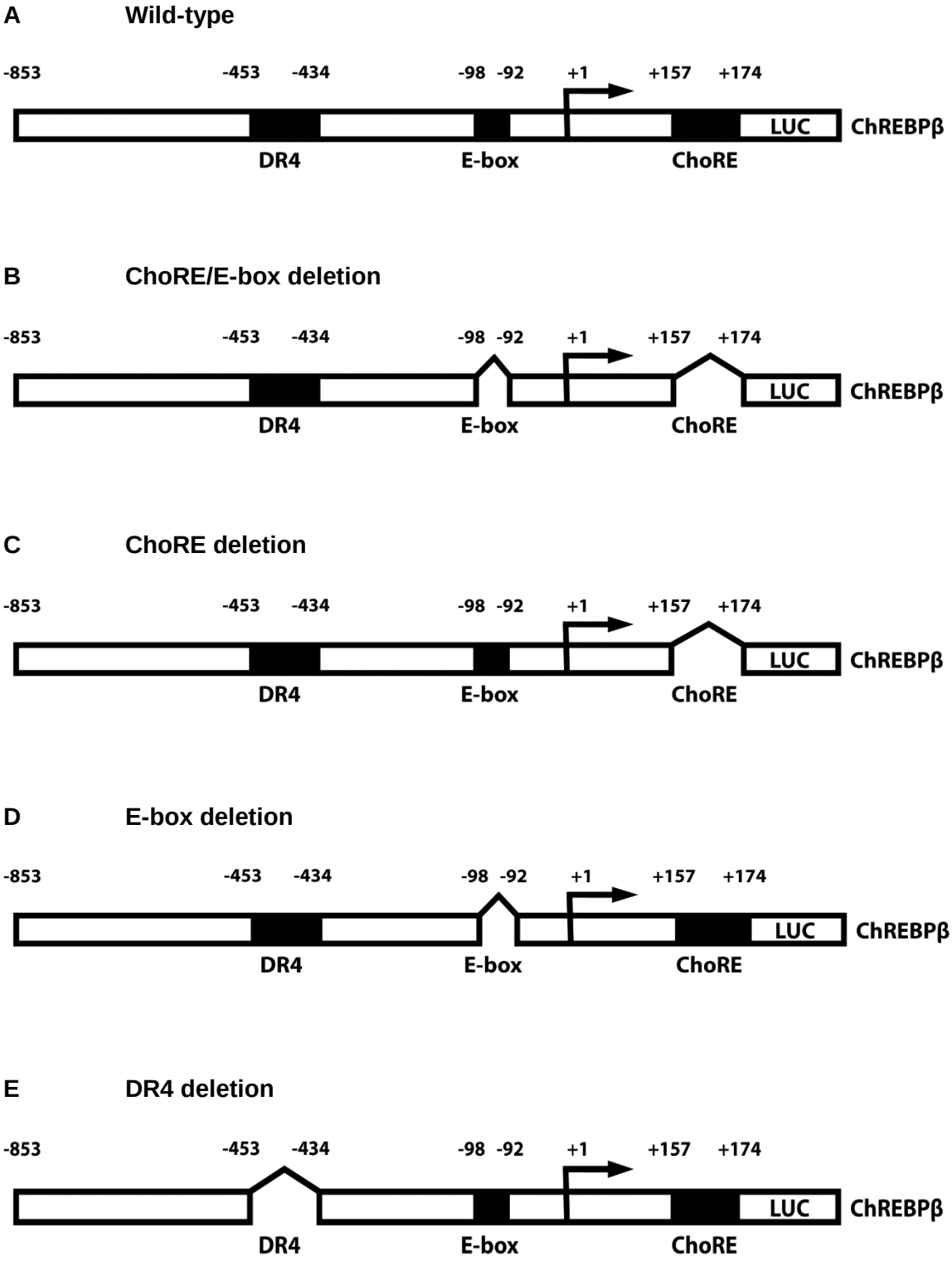

Figure 17: Schematic representation of the different *ChREBPβ* reporter construct

The wild-type murine *Chrebpb* reporter and four other reporters construct with different deletions were used in this project. The DR4 (putative LXRE), upstream E-box and ChoRE, are highlighted. ChoRE: carbohydrate response element; DR4: Direct repeat 4.

As can be seen in **Figure 18**, both LXRα and ChREBPα induce expression from the wild-type reporter. For LXRα this induction is ligand-dependent. Co-transfection with LXRα and ChREBPα did not have the expected additive or synergistic effect in regulating the *Chrebpb* promoter. Even more surprisingly, when adding the agonist, we saw slightly reduced activity in cells transfected with both LXRα and ChREBPα, compared to cells transfected with ChREBPα alone.

Deletion of both the ChoRE and E-box leads to a complete loss of the effect of ChREBPα on the *Chrebpb* promoter (**Figure 18B**), as previously shown by Herman *et al*. (41). The LXRα-effect is on the other hand retained. We then wanted to investigate the individual effects of the ChoRE and E-box. Interestingly, deletion of ChoRE did not affect *Chrebpb* promoter activity in any substantial way (**Figure 18C**), while the E-box deletion led to loss of activity, similar to that of the double deletion (**Figure 18D**).

Finally, we wanted to investigate the effects of deleting a DR4 type response element (RE) in the *Chrebpb* promoter. We expected that deletion of DR4 type RE would lead to loss of LXR's ability to regulate the promoter. Despite that, we could observe that the effect of LXR was retained, and the reporter even showed a slightly higher activity than the wild-type reporter (**Figure 18E**). When comparing the reporters directly, we only observed a significant reduction in the LXR-response with the ChoRE-deletion. (**Figure 19**)

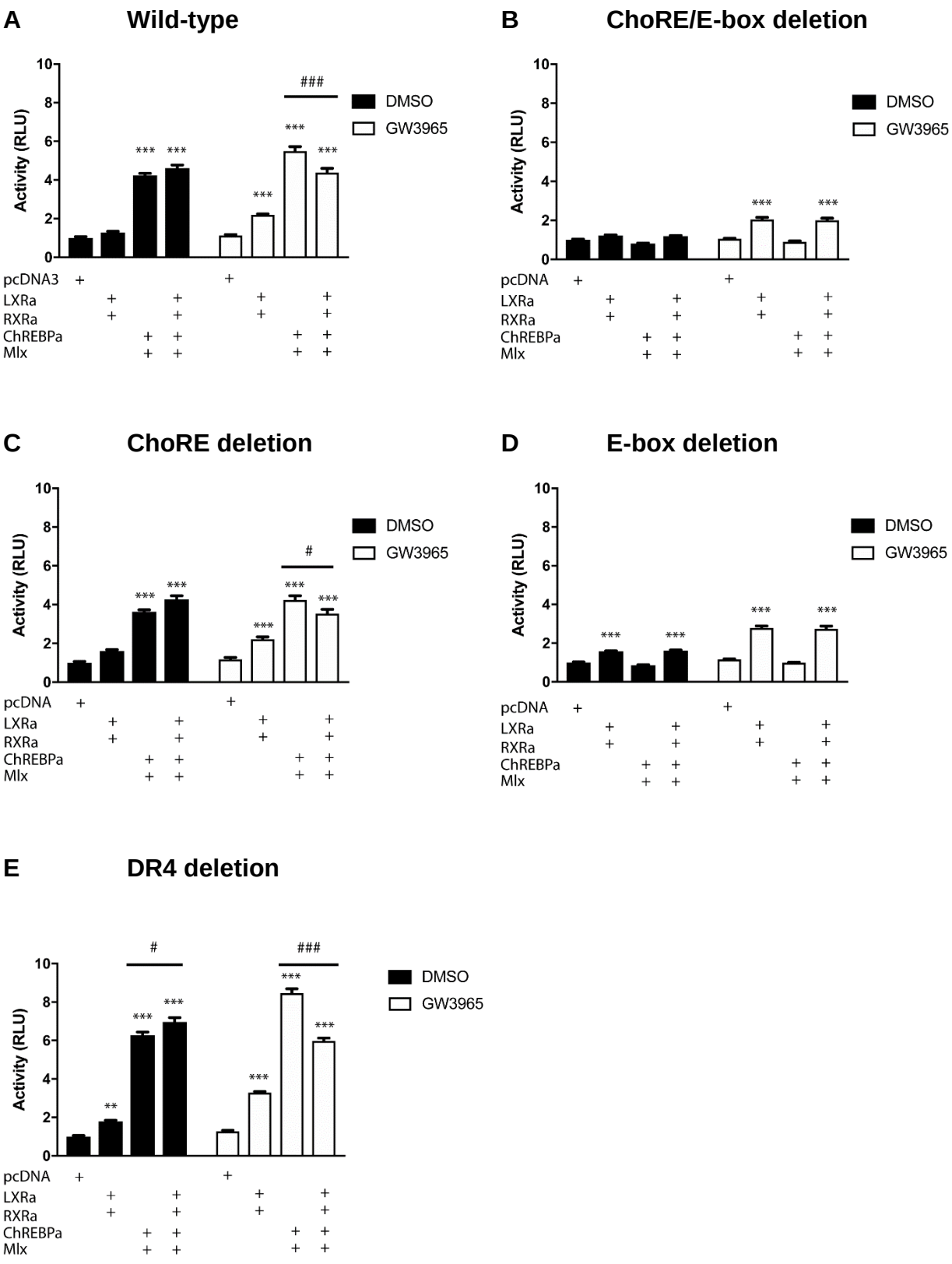

Figure 18: Activity data for different reporters

HuH-7 cells were transfected with plasmids expressing LXRα, RXRα, ChREBPα and Mlxγ, and different ChREBPβ-Exon1B-driven Luciferase reporters as indicated. The *Renilla* Luciferase plasmid

pRL-CMV was used as an internal control. Cells were stimulated with 10 µM GW3965 dissolved in 0.1 % DMSO for 18 hours. 0.1 % DMSO was used as a control. Cells were lysed, and Dual luciferase assay was performed 24 hours after transfection. The data represents at least three independent assays performed in duplicates normalized to DMSO control. All values are given as mean±SEM. Statistical differences were assessed by two-way ANOVA, followed by Tukey's multiple comparison test: **p≤0.01, ***p≤0.001 compared to control, and #p≤0.05, ###p≤0.001 compared to the indicated group. RLU: Relative light units.

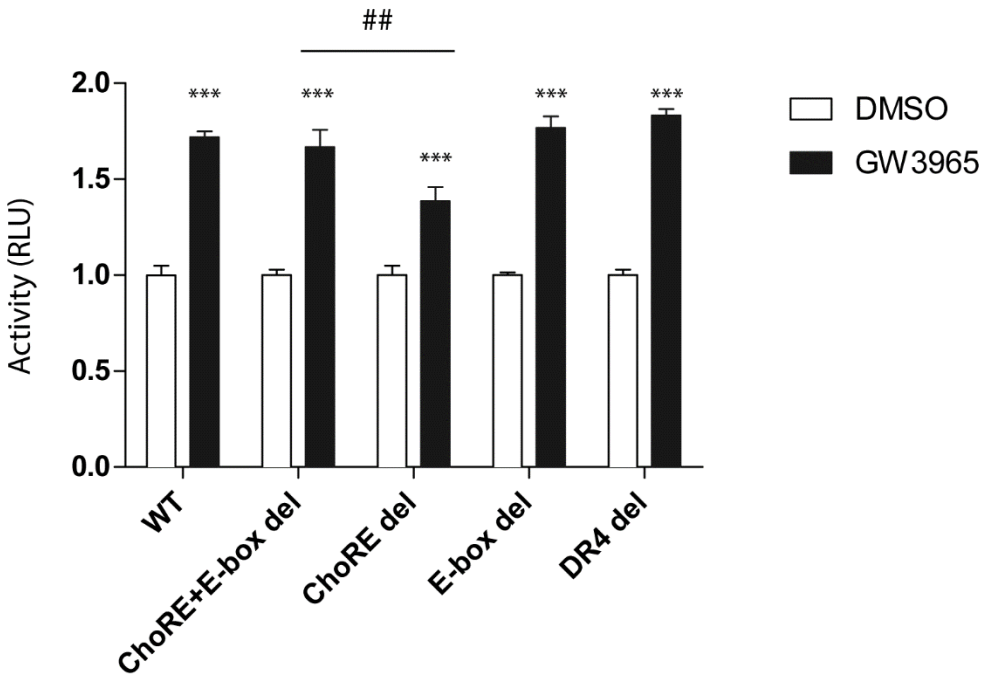

Figure 19: The effect of LXR agonist treatment on the different ChREBPβ reporters

HuH-7 cells were transfected with plasmids expressing LXRα, RXRα, and different ChREBPβ-Exon1B-driven Luciferase reporters. The *Renilla* Luciferase plasmid pRL-CMV was used as an internal control. Cells were stimulated with 10 µM GW3965 dissolved in 0.1 % DMSO for 18 hours. 0.1 % DMSO was used as a control. Cells were lysed, and Dual luciferase assay was performed 24 hours after transfection. The data represents at least three independent assays performed in duplicates normalized to DMSO control. All values are given as mean±SEM. Statistical differences were assessed by two-way ANOVA followed by Tukey's multiple comparison test: ***p≤0.001 compared to DMSO control, and ##p≤0.01, compared to agonist of different reporter. RLU: Relative light units.

3.4 Glucose stimulation of HepG2 cells

Having observed that both ChREBPα and LXRα is involved in regulating the activity of the *Chrebpb* promoter at 25 mM glucose, we wanted to investigate how the expression of ChREBPα, ChREBPβ, LXRα and selected target genes changes in response to elevated glucose level over time. We, therefore, performed a time course experiment in which HepG2 cells were stimulated with 25 mM glucose and compared that to cells grown at 1 mM glucose. We choose not to transfect the cells and instead rely on the endogenous factors. The cells were harvested at baseline and after 6, 12, 24 and 48 hours, and total RNA was isolated. Expression of *CHREBPA*, *CHREBPB*, *LXR*, *FASN*, *SREBF1*, and *PKLR1* was assessed by qPCR.

As expected, expression of *CHREBPB*, but not *CHREBPA*, was increased by high glucose treatment compared to low glucose (**Figure 20**). However, there was no substantial change in expression of *LXRA* and ChREBP/LXR target genes.

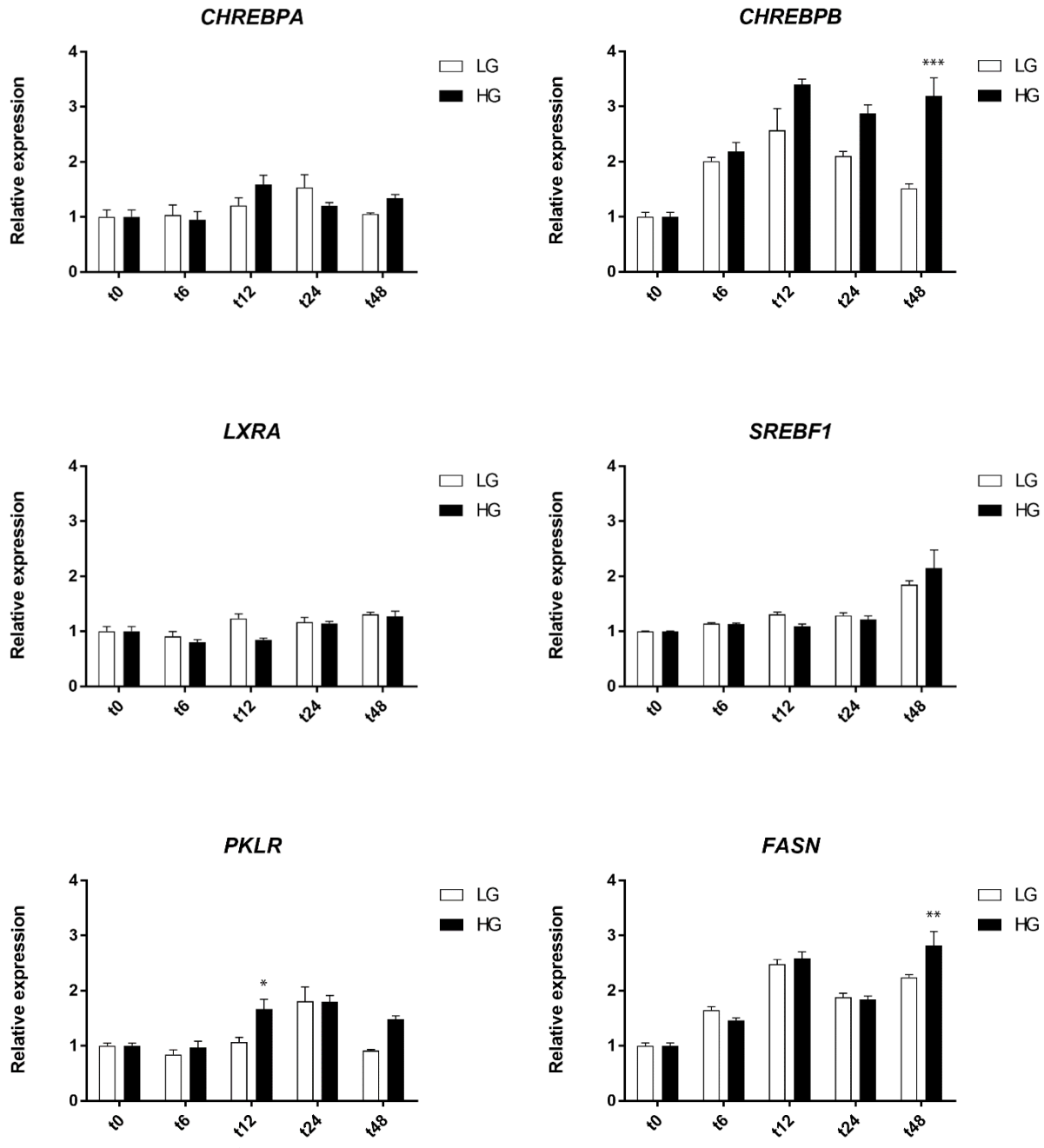

Figure 20: Relative expression of ChREBP, LXR and selected target genes in HepG2 cells

HepG2 cells were maintained and seeded in normal (5mM) glucose medium. 24 hour after seeding the medium was changed to low (1 mM) or high (25 mM) glucose medium. Cells were harvested at baseline (t0), and 6, 12, 24 and 48 hours after changing the media. The data represents two biological replicates analyzed in triplicates. Relative expression was normalized to t0. All values are presented as mean ±SEM. Statistical differences between treatments were assessed by two-way ANOVA, followed by Tukey's multiple comparisons test: *p≤0.05, **p≤0.01, ***p≤0.001. HG: high glucose (25 mM); LG: low glucose (1 mM).

3.5 Peripheral blood mononuclear cells

In adipose tissue, expression of *CHREBPB*, but not *CHREBPA*, mRNA has been shown to correlate with insulin sensitivity in obese non-diabetic subjects (41, 96, 97). Due to the difficulty of obtaining liver biopsies, few studies have measured *CHREBP* expression in liver tissue. We, therefore, wanted to investigate whether PBMCs could serve as a proxy for studying ChREBP and ChREBP target gene expression in the liver. Moreover, we wanted to assess whether expression of *CHREBP* and *CHREBP* target gene expression in PBMCs correlates with biochemical data such as insulin sensitivity or serum glucose.

3.5.1 Study population

The PBMCs used in the current project were collected in a previous pilot study conducted in 2008, which included 25 middle-aged adults previously diagnosed with diabetes or pre-diabetes. For one of the participants, biological material was not available, and this individual was not included in further analyses. There was a skewed distribution of men and women among the subjects, with 19 men and 5 women. Characteristics and biochemical data for the study population are shown in **Table 4.**

Table 4: Characteristics of the study population

Variable	
Male/female, n	19/5
Age, years	55 ± 8.9
Fasting glucose, mmol/L	8.2 ± 2.42
Insulin, pmol/L	86 (50.3–126.0)
C-peptide, nmol/L	1.10 (0.72–1.78)
HOMA-IR	4.9 ± 2.92
Total cholesterol, mmol/L	4.5 ± 0.86
LDL-C, mmol/L	2.8 ± 0.80
HDL-C, mmol/L	1.1 ± 0.26
Fasting triglycerides, mmol/L	1.8 ± 0.81
Free fatty acids, nmol/L	499 ± 191.6
ALAT, U/L	35 (24.0–51.8)
ASAT, U/L	26 (23.0–36.3)
Vitamin B12, pmol/L	240 (203.8–336.3)
Creatinine, µmol/L	73 ± 13.7
CRP, mg/L	1.9 (1.5–4.0)
Folate, nmol/L	12.6 (9.4, 16.1)
Homocysteine, µmol/L	11 ± 3.0

Values are presented as frequencies, mean ±SD or median and 25^{th} – 75^{th} percentiles. ALAT: Alanine aminotransferase; ASAT: aspartate aminotransferase; CRP: C-reactive protein; HDL: high-density lipoprotein cholesterol; HOMA-IR: Homeostatic Model Assessment for Insulin Resistance; LDL: low-density lipoprotein cholesterol.

RNA was isolated, and RNA quality was assessed using automated electrophoresis on an Agilent Bioanalyzer. An RNA integrity number (RIN) >5 is considered acceptable for qPCR. Average RIN was 7.91±0.71 (**Figure 21**). Electropherograms for two high-quality RNA samples are shown in **Figure 22**.

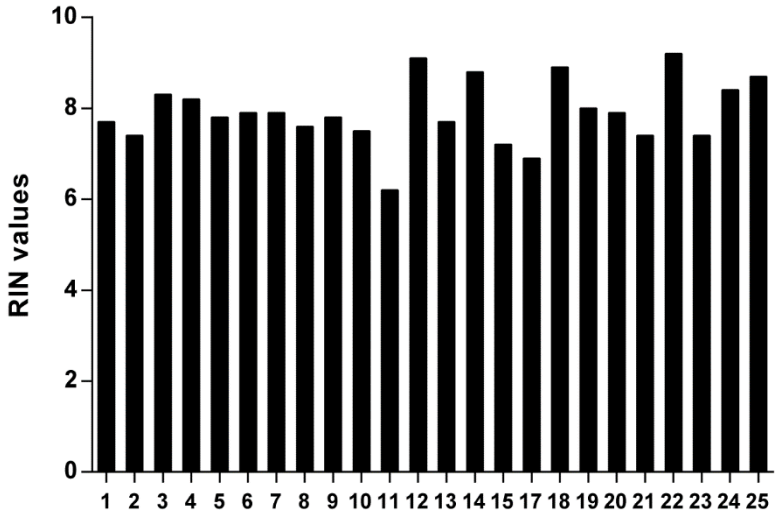

Figure 21: RIN values for PMBC RNA

RNA was isolated from PBMCs from 24 diabetic and pre-diabetic patients and RNA quality were assessed using the Agilent Bioanalyzer. Mean RIN was 7.91±0.71. PBMC: Peripheral mononuclear cells; RIN: RNA integrity number.

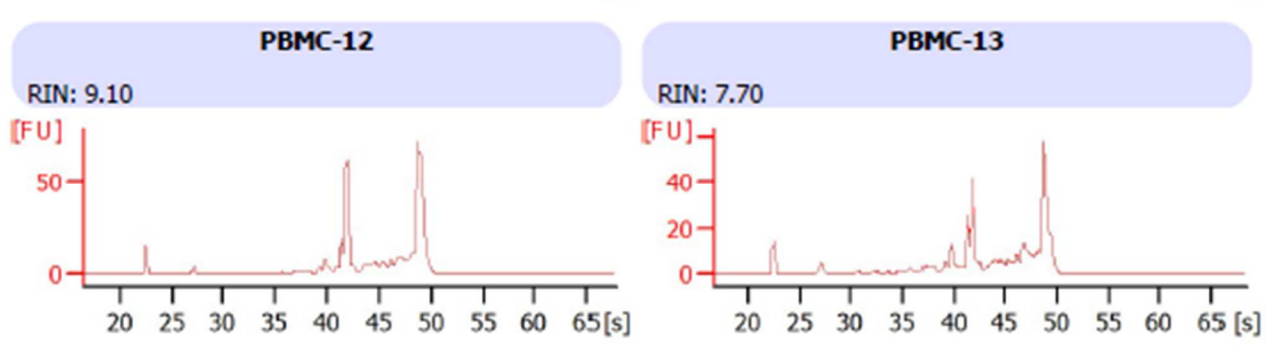

Figure 22: Electropherogram for assessing RNA integrity

RNA integrity was assessed on an Agilent 2100 Bioanalyzer. Integrity of the RNA is assessed by visualization of the 18S and 28S ribosomal RNA bands. Figure shows electropherogram for two high-quality RNA samples isolated from PBMCs, displaying a small 5S RNA peak and high 18S and 28S peaks. PBMC: Peripheral blood mononuclear cells; RIN: RNA integrity number.

3.5.2 Expression of *LXRA*, *SREBF1* and *FASN*

We continued by assaying the expression of *LXRA*, as well as *SREBF1* and *FASN*. *SREBF1* is a well-characterized LXR target gene, while *FASN* is regulated by both LXR and ChREBP. The expression of these genes was within normal range (*LXRA* C_T: 28.3±0.46, *SREBF1* C_T:

26.4±0.61, *FASN* C_T: 26.2±0.80). *LXRA*, *SREBF1*, and *FASN* are part of the same lipogenic gene regulatory network (see **Figure 1** in introduction), where LXR regulate *SREBF1* expression, and both factors regulate *FASN*. Therefore, we first wanted to see if their regulation correlated in the PBMCs. Preliminary analyses showed the relationship to be linear with both variables normally distributed, as assessed by Shapiro-Wilk's test ($p > 0.05$), and there were no outliers. As can be seen in **Figure 23**, there was a strong positive correlation between expression of *SREBF1* and *FASN, r = 0.72, p<0.001*. There was no correlation between *LXRA* and *SREBF1* or *LXRA* and *FASN*.

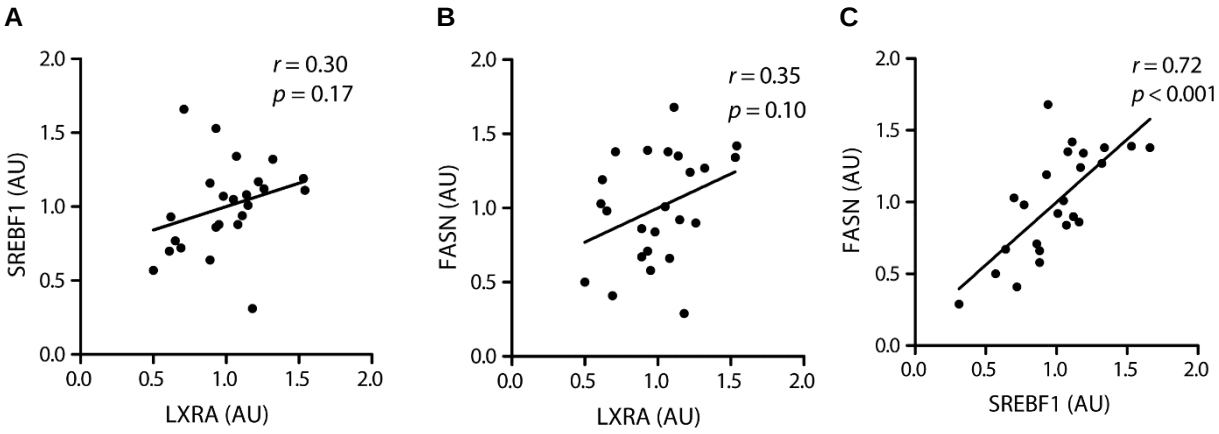

Figure 23: Correlations between *LXRA* and LXR target genes in PBMCs

RNA was isolated from PBMCs from 24 diabetic and pre-diabetic subjects. A qPCR was run for with primers targeting *LXRA*, *SREBF1,* and *FASN*. Dots represent three technical replicates normalized to the mean relative expression of *TBP*. Pearson's *r* and unadjusted *p* value is presented. AU: arbitrary units; PBMC: peripheral blood mononuclear cells.

3.5.3 Effect of serum glucose and cholesterol on lipogenic gene expression in PBMCs

Although the study population included diabetic and pre-diabetic patients, there was considerable variation in fasting glucose levels within the study sample, ranging from normal and near-normal to levels indicating severe insulin resistance. We were therefore interested in how levels high glucose and insulin resistance affect gene expression of *LXR*, *FASN*, and *SREBF1* in these cells.

Preliminary analyses suggested a linear relationship between the variables. All variables were normally distributed, as assessed by Shapiro-Wilk's test ($p > 0.05$). For HOMA-IR, there was

one outlier. Correlation was run with and without the outlier, and was found not to affect the results.

As shown in **Figure 24**, there was a medium-size negative correlation between fasting serum glucose and expression of *SREBF1* and *FASN*, while there was no significant correlation with *LXRA*. There was a medium-size negative correlation between total serum cholesterol and *FASN* (r = -0.44, p = 0.03). There was no significant correlation between TC and *LXRA* or *SREBF1*, as shown in **Figure 25**. HOMA-IR did not correlate with expression of any of the genes (not shown).

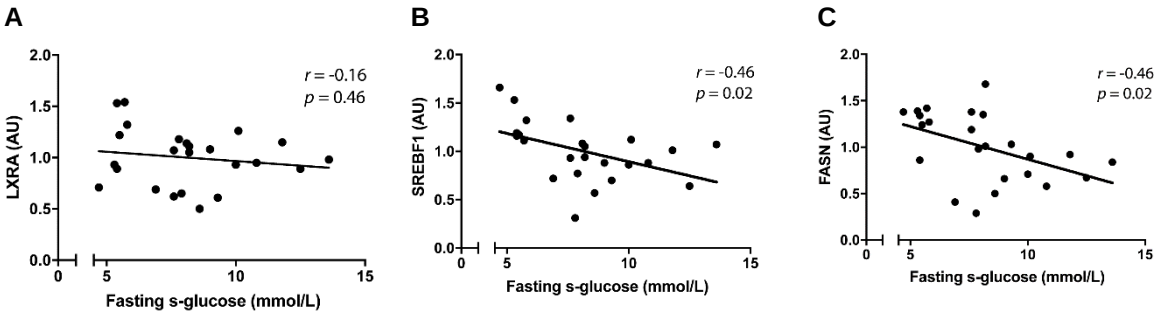

Figure 24: Correlations between fasting serum glucose and gene expression in PBMCs

RNA was isolated from PBMCs from 24 patients with diabetes and pre-diabetes. qPCR was run for with primers targeting *LXRA*, *SREBF1,* and *FASN*. Dots represent three technical replicates normalized to *TBP*. Pearson's *r* and unadjusted *p* value is presented. AU: arbitrary units; PBMC: peripheral blood mononuclear cells.

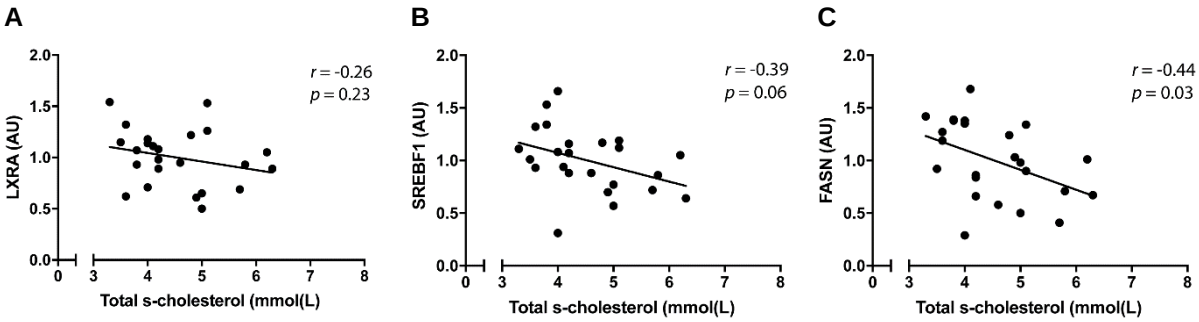

Figure 25: Correlations between total cholesterol and gene expression in PBMCs

RNA was isolated from PBMCs from 24 patients with diabetes and pre-diabetes. qPCR was run with primers targeting *LXRA*, *SREBF1,* and *FASN*. Dots represent three technical replicates normalized to *TBP*. Pearson's *r* and unadjusted *p* value is presented. AU: arbitrary units; PBMC: peripheral blood mononuclear cells.

3.5.4 Expression of ChREBPα and ChREBPβ

To our regret, the expression of *CHREBPA* and *CHREBPB* in the PBMCs assayed was negligible (C_T>33) in all samples, as shown in **Figure 26**, and no further analyses were performed on these data.

A

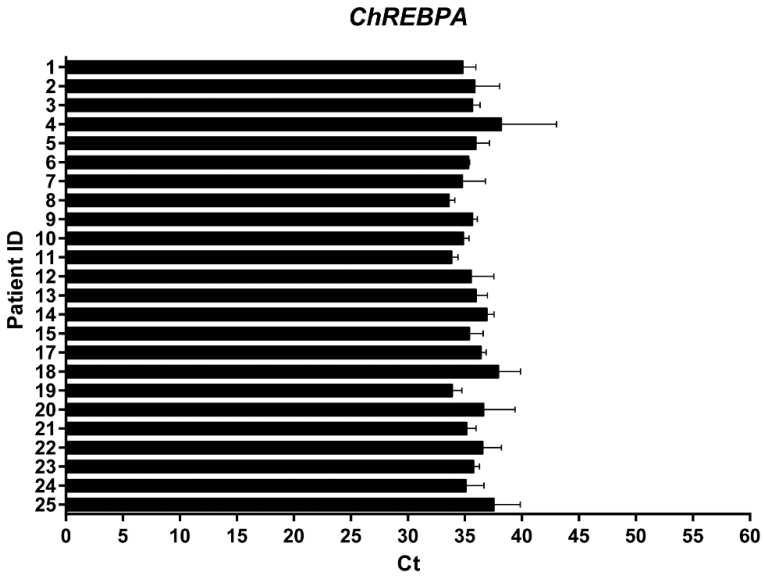

B

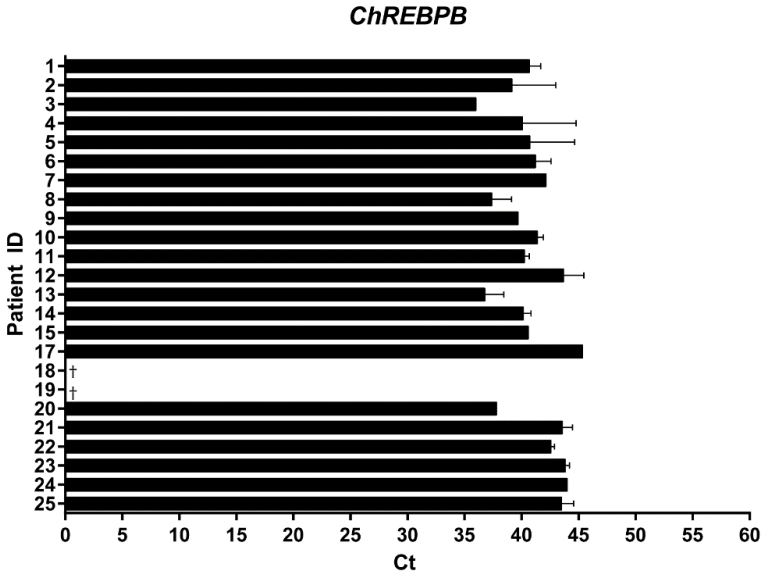

Figure 26: mRNA expression of ChREBP isoforms in PBMCs from diabetic and pre-diabetic patients.

Expression of ChREBPα and ChREBPβ in PBMCs from 24 diabetic and pre-diabetic subjects was assessed using qPCR. **A**: *CHREBPA*, Mean C_T: 35.7±1.3. **B**: *CHREBPB*, Mean C_T: 40.9±1.5. †: gene

was not detectable in the sample. No statistical analyses were performed on these data. C_T: threshold cycle; PBMC: Peripheral blood mononuclear cells.

3.6 Co-immunoprecipitation

LXRα has been shown to interact with ChREBPα, but not with ChREBPβ (Nørgaard, unpublished data). ChREBPβ is the shorter isoform of ChREBP that lacks most of the LID in the N-terminal. A schematic representation of ChREBPα and ChREBPβ proteins are shown in **Figure 4**. Because of this difference in affinity, we hypothesized that LXRα interacts with ChREBPα via LID. To test this hypothesis, we transfected COS-1 cells with FLAG-ChREBPα, FLAG-ChREBP-LID, and LXRα, alone and in combination, and immunoprecipitated the cell lysates with both LXR and FLAG antibodies.

When using a FLAG antibody (middle panel), both FLAG-tagged ChREBPα and LID are immunoprecipitated. As can be seen, LXRα is detected in both precipitates. When reversing the experiment, we could show that both LID and ChREBPα is co-immunoprecipitated together with LXR (right panel). Together, this confirms that LXR interacts with ChREBPα and show for the first time that this interaction is relayed through the LID. The experiment was conducted twice, and a representative blot is shown in **Figure 27**.

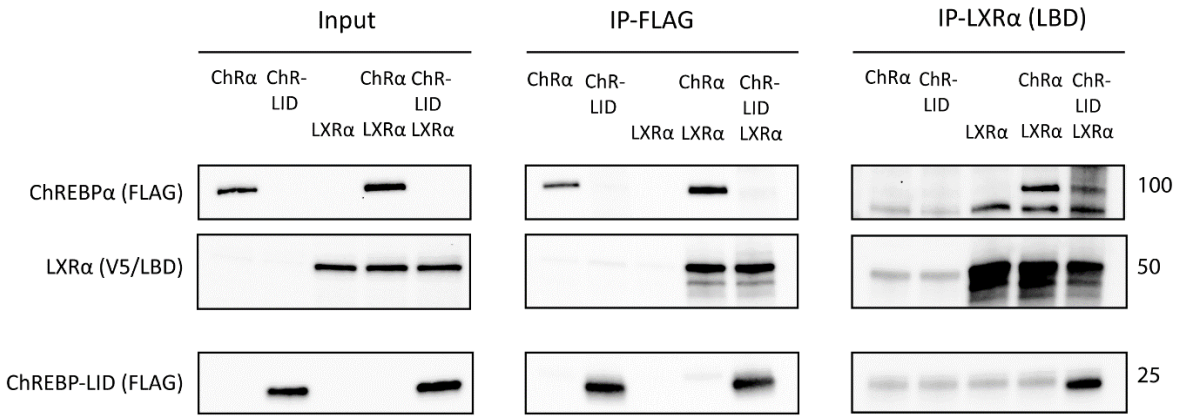

Figure 27: Co-immunoprecipitation experiments with ChREBPα, LID, and LXRα.

COS-1 cells maintained in 25 mM glucose were transfected with a FLAG-ChREBPα or FLAG-ChREBP-LID expression vector, with or without a V5-LXRα expression vector. Overexpressed ChREBP and LXRα were immunoprecipitated with FLAG and LXRα antibodies. Input and immunoprecipitated proteins were immunoblotted with FLAG and LXRα antibodies. ChR: ChREBP; LBD: ligand-binding domain; LID: low glucose inhibitory domain; FL: full-length.

4 Discussion

4.1 Methodological considerations

Research in molecular biology is often based on model systems. These systems include *in vivo* model organisms such as the bacterium *E.coli*, the fly *Drosophila melanogaster*, and the mouse *Mus musculus*, as well as *in vitro* cell systems. All models have advantages and disadvantages and represent invaluable, but imperfect methods for investigating molecular mechanisms.

4.1.1 *In vitro* cell systems in biomedical research

In vitro cell systems have the advantage that exposure to specific compounds can be more closely regulated with regards to concentrations and duration, than in *in vivo* models. Primary human hepatocytes are considered to be the best *in vitro* model for studying the liver. There are, however, some disadvantages which limit their usages, such as their limited lifespan, scarce availability and genotypic variability between donors (139). Obtaining tissues from animal or human experiments is also associated with a number of ethical issues. Immortalized hepatic cell lines may therefore be a good alternative. Hepatic cell lines can be cultured in almost unlimited supply, with minimal variation between cells, thus avoiding inter-individual variation. Since cells lines are relatively homogenous, the need for statistical analysis of variance is limited (140). However, cell cultures in general do differ from cells growing in their natural niche *in vivo* in some important ways. The culture medium does to a great extent lack systemic components involved in the homeostatic regulation *in vivo*, *i.e.* components of the nervous and endocrine system. Cellular metabolism may hence be more constant and not truly representative of metabolism *in vivo*. The cells are also cultured under low oxygen tension, which implies that energy metabolism is achieved largely by glycolysis. The TCA cycle is still functional but plays a lesser role (140). For these reasons, caution must be taken in generalizing conclusion from *in vitro* data to biological processes *in vivo*.

To ensure cell proliferation, the cell medium is commonly supplied with serum. Serum contains growth factors, which promote cell proliferation, and adhesion factors and antitrypsin activity, which promote cell attachment. Serum is also a source of minerals, lipids

and hormones. The most commonly used sera are calf and foetal bovine serum (141). Proteins are a major component of serum, but the function of many of these proteins *in vitro* remains unclear. In addition, serum contains amino acids, glucose, keto acids, as well as other nutrients and intermediary metabolites. As sera are biological products, it is to be expected that their composition varies from batch to batch. This variation may result from differing methods of preparation and sterilization, storage conditions, as well as variations in the animals stocks from which the serum was derived. Because of this batch-to-batch variation, standardization of the experiments between different times and different labs can be challenging. Despite this, most relevant and robust biological effects will still be detectable and reproducible, also in cell cultures

Another concern is that the as the cells grow over time, they will exhibit genotypic and phenotypic variation. This may happen when cells are exposed to different environments, and because fast-growing and less representative cells may be selected for when the cells are passaged. By avoiding indefinite passaging and not distributing cell cultures uncritically between labs, this issue is minimized (142). In the current project, we decided not to exceed 30 passages in total.

4.1.2 Reporter gene assays

Reporter gene technology is widely used to study the cellular events associated with signal transduction and gene expression. Reporter genes were first used to study *cis*-acting genetic elements such as enhancers and promoters in the upstream region of genes, but more recently they are also used in, e.g. the characterization of receptors and their ligands, signalling pathways, and toxicological effect. Several reporter genes are available, including chloramphenicol acetyltransferase, β-galactosidase, alkaline phosphatase and different luciferases. The choice of reporter depends on the cell line used, the nature of the experiment, and the adaptability of the assay to the appropriate detection method.

In the current project, we used five different varieties of the mouse *Chrebpb* promoter cloned upstream of a gene encoding the firefly luciferase. Advantages of the firefly luciferase include high specific activity, no endogenous activity, and a broad dynamic range (143). Light produced by luciferase is measured quantitatively, and correlate with promoter activity. Variability in transfection efficacy and cell viability may obfuscate the results from a

luciferase reporter gene assay. This can be avoided by including a co-reporter such as *Renilla* luciferase as an internal control in a dual luciferase assay. The results can then be normalized to the expression of *Renilla* luciferase, and consequently minimizing the problem.

4.1.3 Ligand treatment

The LXR ligand-binding pocket is able to accommodate ligands with widely varying structures, including both natural, steroidal ligands, and non-steroidal synthetic ligands such as GW3965 and Tularik. Different ligands may alter the 3D structure of the receptor in different ways, which may result in different effects. While a natural ligand may mimic a physiological response more correctly, they are often less potent. Thus, it can be more challenging to detect their effect.

In the current project, HuH-7 cells were treated with GW3965, which is a potent synthetic non-steroidal LXR agonist. GW3965 was added in a concentration of 10 µM, a concentration which is not realistic in a physiological setting. However, it can be argued that since LXRα, ChREBPα and their heterodimers are overexpressed, this concentration is necessary to maintain the stoichiometry to be able to detect any agonist effect. Since we wanted to determine what happens when LXRα is activated, we chose to use a synthetic agonist in an artificial system. However, it could be useful to investigate whether treatment with a natural agonist would lead to the same effects on *Chrebpb* activation, as it would strengthen our hypothesis that LXR is involved also in a physiological context.

Finally, as LXR heterodimerize with RXR, it can be argued that an RXR ligand should be included in this type of experiments. In one study, the addition of RXR agonist led to a 1.8-fold increase in expression of the LXR target gene ChREBPα, while addition of LXR agonist increased expression 2-fold, and the addition of both lead to a 3-fold increase in expression (28). This suggests that activation of RXR also may also be important for LXR activation. Still, RXR agonists are often omitted in nuclear receptor research to reduce the number of variables to take into account.

4.1.4 RNA quality control

Before proceeding with downstream analyses, it is important to assess RNA quantity and quality, as this can influence the accuracy of the gene expression data (120). The starting RNA should be free of proteins, genomic DNA, enzymatic inhibitors of the RT and other contaminants. In the current project, genomic DNA was removed by treating the samples with DNase before proceeding with cDNA synthesis. Quality and quantity of starting RNA were assessed by measuring absorbance at 230 nm, 260 nm and 280 nm using the Nanodrop® ND-100 spectrophotometer. These wavelengths represent background absorbance and possible contaminants (230 nm), nucleic acids (260 nm), and proteins (280 nm) present in the sample. An absorbance of 260/280 nm ratio of more than 1.8 is generally considered an indicator of good RNA quality (120).

RNA is sensitive to degradation by sample handling and storage due to its chemical instability and susceptibility to RNases in the environment. In this project, RNA was isolated from PBMCs collected in a previous study. Blood cells have been shown to have high RNA integrity compared to some other tissues (120). However, these cells had been in storage for about ten years, and we therefore wanted to assess RNA integrity using the Agilent 2100 Bioanalyzer. An RNA integrity number (RIN) higher than 5 is considered acceptable for downstream analysis (120). The RNA displayed varying concentrations and integrity. Mean RIN was 7.91±0.71, with none of the samples showing values below 6. RNA integrity was not assessed in samples from cell lines. Our laboratory has previously assessed the integrity of RNA isolated from Huh7 and COS-1 cell cultures, consistently showing RIN values > 9.7 (unpublished observations). RNA integrity analyses for these samples were therefore not considered to be necessary.

4.1.5 qPCR

A qPCR provides a snapshot of the amount of a particular gene transcript at a given time. The amount of mRNA can be determined by absolute or relative quantification. In order to determine the absolute amount of a gene transcript, a standard curve of samples of known quality is prepared. To determine the relative amount of gene transcript, the expression in the sample is compared to that of a control sample. In this project, we used the relative quantification method because we wanted to investigate the differences between glucose

concentrations and ligand treatment, and therefore it was not required to determine the absolute expression of any gene.

In a qPCR, errors will be introduced due to minor differences in starting amount of RNA, quality of RNA or differences in efficiency of cDNA synthesis and PCR amplification. To minimize these errors and correct for variation between samples, an internal reference RNA is simultaneously amplified with the target, against which other RNA values can be normalized. These genes, called housekeeping genes, should theoretically be expressed at a constant level in different tissues, at all stages of development and their expression should remain relatively constant even in differing experimental conditions. However, no ideal housekeeping gene exists, and it is therefore important to select the one that is the most relevant to the cells of interest and the experimental setup. It is also recommended to select a reference gene that's not expressed at very high or very high levels, i.e. between C_T 30-15 (144). In the current project, TATA-box binding protein (TBP; C_T~23) was used as an internal control, as it has appropriate C_T values and is relatively stable in differing nutritional conditions (145).

In general, there are two technologies available for amplicon detection: double-stranded DNA-intercalating dyes and fluorescent probes. In this project, we used SYBR® Green DNA-intercalating dye. Unbound SYBR Green exhibits very little fluorescence. During primer extension and polymerization, the dye binds to dsDNA, resulting in an increase in detected fluorescence. The intensity of the signal depends on the quantity of dsDNA present in the reaction. This technique is relatively cheap and can be used with any pair of primers for any target. However, the method is susceptible to unspecific fluorescent signals causes by primer-dimers and amplification of non-specific products (146). Therefore, the qPCR should be followed by melt-curve analysis. The amplicon will display a characteristic peak at the melting temperature (T_M) that distinguishes it from amplification artefacts such as primer-dimers, which melt at lower temperatures at broader peaks. This was done for all primer pairs used in this thesis.

Since a PCR reaction is sensitive to small amounts of contaminating molecules, it is essential to follow good laboratory practices to avoid random contamination or contamination of reagents. Also, no RNA/no RT samples should be included in the qPCR to control for primer-

dimers and contaminating DNA/genomic DNA. In the current project, work with RNA and qPCR was performed on designated workstations and with equipment reserved specifically for these purposes. Samples with abnormal melt curves were excluded from further analysis, as they were considered not to be reliable.

To study our hypotheses, we chose to investigate the expression of *LXRA*, *CHREBPA*, *CHREBPB* and a selection of previously characterized target genes. *PKLR1* seems to be uniquely regulated by ChREBP and unaffected by LXRs or SREBP-1c (28, 147). *SREBF1* is a well-characterized LXR target gene (29), while *FASN* which is a target gene of both (148).

4.1.6 Protein-protein interactions

There are several methods for studying protein-protein interactions. One of the most commonly used methods is co-immunoprecipitation (CoIP) of proteins. In a CoIP, protein complexes are typically captured from, e.g. a cell lysate using a specific antibody. The antibody is immobilized using protein A or G attached to sepharose or magnetic beads. After washing the beads, the antibody and the associated proteins are eluted. The bound proteins can then be identified by mass spectrometry or by immunoblotting.

The CoIP can be carried out using lysates from cell lines or tissues expressing endogenous proteins, or from cells that have been transfected with plasmids encoding a tagged protein. By studying endogenous protein interactions, any artificial effects of tags or overexpression conditions are avoided. This may therefore be more reliable but also requires highly specific antibodies to the proteins of interest. By transfecting cells with plasmids encoding a tagged protein, it is possible to use an antibody against the tag, such as anti-FLAG. In this way, it is possible to study proteins for which an antibody does not exist. Moreover, by using tags the possibility that the antibody reacts with other proteins is limited.

In the current project, COS-1 cells were transfected with plasmids encoding V5-tagged LXRα, and FLAG-tagged ChREBPα and ChREBP-LID. COS-1 cells were chosen because they show higher transfection efficiency than hepatoma cell lines such as HepG2 and HuH-7. We chose to transfect the cells because LXRα shows low expression and ChREBPα is not detectable in COS-1. Furthermore, we chose to use tagged proteins, because no reliable antibody has yet been generated towards the N-terminal of ChREBP. For the study of

interactions with LID, using a tag strategy is the only possibility. A CoIP usually generates significant background, and it is important to include parallel negative controls (149). Ideally, ChREBPβ should have been included as a negative control. However, this is complicated by the fact that ChREBPβ is unstable because of a short half-life, and is therefore difficult to detect, even in an overexpressed state (150).

A positive CoIP of proteins does not necessarily mean that they interact directly, as they can be part of larger complexes. In the current project, we identified a possible interaction of LID with LXRα. However, the presence of mediating proteins cannot be ruled out and warrants further investigations. Confirmation of a suspected direct interaction can be done by a pull-down assay with, e.g. bacterially expressed proteins. In this way, it is possible to produce a large quantity of proteins, larger than what is possible in endogenous conditions. These protein preparations can be purified, and by this avoid that other interacting proteins affect the result. A positive pull-down thus suggests that the proteins interact directly. By proceeding with a peptide array screening, it is possible to map the precise binding sites of the protein. In peptide arrays, 20-30-mer peptides derived from one of the proteins of interest are spotted onto a solid support and then incubated with the partner protein. The protein-bound peptides can den be detected by immunoblotting.

Finally, based on a positive CoIP, we cannot be absolutely sure that the interaction takes place in the cell and is not just as a consequence of cell lysis. One prerequisite for defining protein-protein interactions *in vivo* is that they co-localize in the cell, or at least show overlapping distribution within the cell. The intracellular localization of two or more proteins should therefore be assessed by confocal microscopy.

4.1.7 Statistical analysis

In scientific research, the statistical significance level, also known as the α level, is frequently set to 0.05, which means that there is a 5 % chance that the observed difference is due to sampling or experimental error. When running multiple statistical procedures, such as Students t-test or Pearson's correlation, the probability of detecting a significant finding just by chance, i.e. type I error, increases. This is called the problem of multiplicity (151). The Bonferroni correction is frequently applied to adjust probability (p) values when making

multiple statistical tests so that the α level over all the tests is kept at 0.05. The correction is simple:

Adjusted $\alpha = \alpha/k$, where k is the number of tests.

However, this correction is extremely conservative and comes at the expense of increasing the probability of a type II error, i.e. not detecting an effect even though it exists. Thus, as the number of statistical tests increases, the likelihood of not detecting a real effect increases, leading to loss of statistical power. For this reason, the routine correction for multiple tests is, although common, also much debated. It is important to consider the risk of type I and type II errors before deciding to adjust *p* values. One consideration is whether the study is hypothesis-driven or hypothesis-generating. In an exploratory context, it can be argued that it is better not to miss a possible effect that would be worthy of further study, that is, to avoid a type II error, and therefore not use Bonferroni correction. Conversely, if the objective is to be confident that the effect is real, a more conservative method would be more appropriate. In an exploratory context, it can also be argued that a certain number of false positives is tolerable since these will be discarded when the study is replicated. The Bonferroni correction also becomes increasingly conservative when the outcomes are correlated with each other, such as in a *post hoc* test following a significant F test (ANOVA). In such circumstances, Bonferroni or related corrections may not be appropriate (151).

The current project includes a cohort of pre-diabetic and diabetic patients, where we wanted to investigate whether *ChREBP*, *LXRA* and target gene expressions related to blood biomarkers in peripheral blood mononuclear cells. Since this cohort is primarily exploratory, we chose not to adjust *p* values, and instead accept a higher probability of type I errors. To limit the number of tests, we chose to include only the variables relevant to our hypotheses. Also, the direction and the magnitude of the effect was considered, as significant findings in the same direction strengthen our confidence in the results.

4.2 Discussion of the results

4.2.1 Activation of the ChREBPβ promoter by ChREBPα and LXRα

ChREBP has been established as a central transcriptional regulator of glucose metabolism. In 2012, Herman and colleagues identified a shorter ChREBP isoform, termed ChREBPβ, which they found was highly active in WAT and transcribed from an alternative promoter upstream of exon 1a. Furthermore, they showed that glucose metabolism induces the transcriptional activity of ChREBPα and the binding of ChREBPα to a ChoRE in exon1b, consequently promoting transcription of *Chrebpb* (41). This shorter isoform has been shown to be different with respect to transcriptional activity, induction, and degradation pattern (41, 50), and since most studies so far have been conducted on the full-length ChREBPα, our interest has been in unravelling how ChREBPα regulates the *Chrebpb* promoter.

Recent data has shown that the expression of *Chrebpb* and *L-pk* was almost abolished in LXR double knock-out mice compared to wild type (152). Moreover, LXRα has been shown to regulate the expression of *Chrebpb* and *L-pk* in the livers of mice fed a high-glucose diet (153). This has led to the hypothesis that LXRα regulates the *Chrebpb* promoter; either directly, or indirectly by regulating the expression of ChREBPα.

We hypothesized that ChREBPα and LXRα would work synergistically to activate the *Chrebpb* promoter. In the current project, we show that both LXRα and ChREBPα induce *Chrebpb* expression from the wild-type reporter. For LXRα this induction is ligand-dependent. However, LXRα and ChREBPα did not show an additive or synergistic effect on the promoter. Interestingly, when adding the agonist, we saw slightly reduced activity in cells transfected with both LXRα and ChREBPα, compared to cells transfected with ChREBPα alone. This is in line with previous observations (Nørgaard, unpublished data). A possible explanation could be that ligand-bound LXRα somehow inhibits glucose from inducing the conformational change required for ChREBPα activity.

Next, we were interested in investigating the role of different parts of the *Chrebpb* promoter. Herman *et al*. identified a highly conserved region containing a ChoRE 17 kb upstream of the mouse *Chrebp* transcriptional start site, as well as a separate E-box 255 base pairs (bp) upstream of the putative ChoRE (41). They showed that deletion of either the ChoRE or the

upstream E-box attenuated both glucose-induced and basal induction of *Chrebpb* promoter activity, while this effect was completely abolished with the deletion of both (41). Our lab received the wild-type, ChoRE and E-box deleted promoters as gifts from the Herman lab. Upon verifying the sequence of these promoters, we discovered that the E-box-deleted promoter was also lacking additional segments, which put the results from Herman into question. Therefore, a new reporter was cloned as a part of this project, and its integrity was verified by sequencing.

We found that deletion of the E-box led to a loss of activity of the *Chrebpb* promoter, similar to that we observed for the double deletion, while deletion of ChoRE did not have any appreciable effect on *Chrebpb* promoter. This suggests that the upstream E-box is a part of a functional site that conveys ChREBP activity. This E-box is proximal to an E-box like sequence, spaced by 5 base pairs (**CGGCTG**nnnnn**CACGTG)**. Thus, this site can be termed ChoRE-like. Interestingly, this finding is in line with chromatin immunoprecipitation (ChIP) sequencing data analyzed by our group, which shows that ChREBP aligns with the ChoRE-like sequence and not the ChoRE, as shown in **Figure 28** (unpublished data).

A

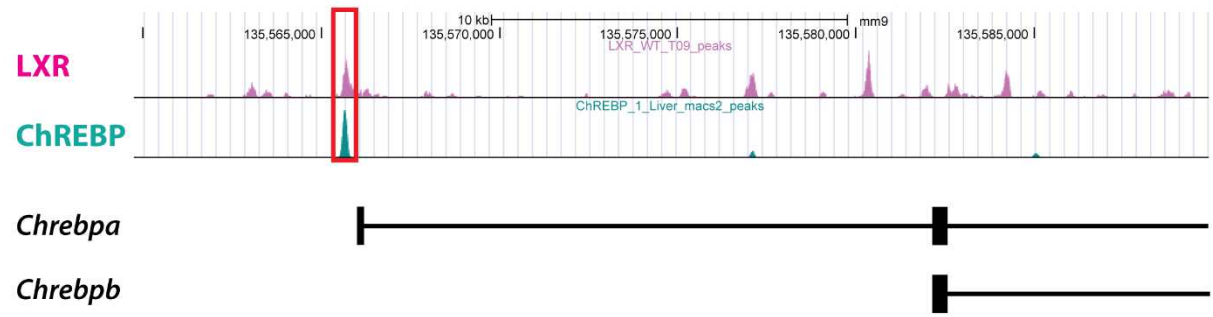

B

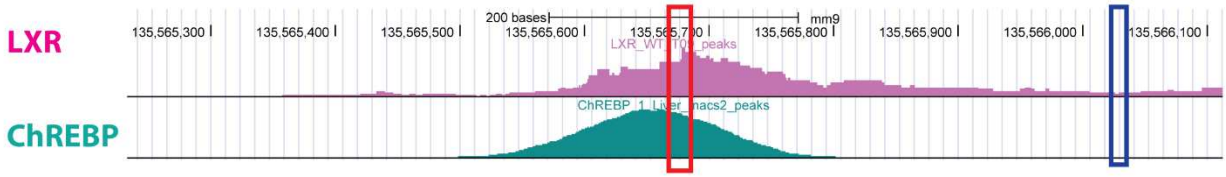

Figure 28: ChIP-sequencing data of LXR and ChREBP in mice liver.

A: ChIP-sequencing data of the mouse *Chrebp* (*Mlxipl*) gene showing alignment of ChREBP (teal) and LXR (pink) on the ChoRE-like sequence (red box) in the *Chrebpb* promoter 255 base pairs upstream of the canonical ChoRE. **B:** 100x zoom of the high peak in figure 29A. The ChoRE-like sequence (red box) and the canonical ChoRE (blue box) are indicated. ChoRE: Carbohydrate response element.

While ChREBPα has at least two functional LXREs in its promoter (28), no functional LXRE has been established in the *Chrebpb* promoter. However, data from our group has shown that LXRα induced *Chrebpb* and *L-pk* expression and that this induction was dependent on a functional DBD (Nørgaard, unpublished data). This could indicate that LXRα binds to the *Chrebpb* promoter through its DBD through a hitherto unknown LXRE. We were therefore interested in investigating the possibility that LXRα directly regulates the *Chrebpb* promoter activity through a putative LXRE. The *Chrebp* gene was searched for DR4 type response element using the JASPAR TF binding motif database (http://jaspar.genereg.net). One putative site was identified 434 base pairs upstream of the *Chrebpb* promoter. As a part of the current project, a *Chrebpb*-driven luciferase reporter was cloned in which this DR4 element was deleted. If this element were a functional LXRE, we would expect that deletion would reduce LXRα's ability to regulate the promoter. However, we observed that the effect of LXRα was retained, suggesting that this is not a functional LXRE. Nevertheless, only a small fraction of LXR/RXR binding sites contains a well-defined DR4/LXRE (154). It is therefore

still possible that LXRα directly activates the *Chrebpb* promoter via another binding site not identified in our bioinformatics search. Another possibility is that LXRα acts primarily through an indirect mechanism, e.g. by inducing expression of another transcription factor which in turn promotes *CHREBPB* expression. This transcription factor could indeed be ChREBPα, however, when we deleted the E-box of the ChREBPα binding site, LXRα was still able to induce *CHREBPB* expression in response to ligand treatment, suggesting that this effect is not mediated by ChREBPα.

4.2.2 Glucose treatment in hepatoma cells

The ChREBP isoforms have shown different dynamics regarding expression in response to glucose. Upon discovering the ChREBPβ isoform, Herman and collaborators proposed a feed-forward model in which glucose induces ChREBPα transcriptional activity, resulting in increased *CHREBPB* expression, while *CHREBPA* expression is not affected by glucose concentrations (41). In support of this model, studies in mice have shown that *Chrebpa*, but not *Chrebpb*, is expressed in the liver in mice during fasting and that only *Chrebpb* is responsive to high-carbohydrate refeeding (44, 155). Moreover, high glucose treatment in human primary hepatocytes increased expression of *CHREBPB* and the target genes *ACC*, *FASN* and *TXNIP* (44).

In the current project, expression of *CHREBPB*, but not *CHREBPA*, was increased by high glucose treatment compared to low glucose. However, there was no substantial change in expression of ChREBP target genes. A possible explanation for this may be that hepatocytes are able to make use of a wide variety of substrates for their metabolism, including amino acids. In physiological conditions, hepatocytes only use glucose as their substrate to a minimal degree. Since the serum added to the culture medium may contain a considerate amount of amino acids and other gluconeogenic substrates, it would have been beneficial to replicate the experiment in cells that have been subjected to serum starvation. In addition, HepG2 cells express low levels of glucokinase, which may account for the poor glucose response (156). For this reason, another cell line or primary hepatocytes could provide more insight about glucose-regulated genes.

We did not observe any substantial differences in *LXRA.* This was expected as we did not add LXR agonist in this setup. The role of LXR as a glucose sensor is debated. Mitro *et al.*

reported that glucose can bind and activate LXR (157), which was questioned because the ligand-binding pocket of LXR accommodates hydrophobic, and not hydrophilic, compounds (158). In support of this, Denechaud *et al*. found that induction of *Chrebp*, *L-pk* and *Acc* by glucose or high-carbohydrate diet was similar in LXR double knock-out mice compared with wild-type, suggesting an LXR-independent mechanism (60). However, Nørgaard demonstrated a significant difference between LXR double knock-out mice and LXRβ knock-out mice on *Chrebpb* and *L-pk* expression, suggesting that these genes are dependent on LXRα (unpublished data). Because of these conflicting results, more investigations should be done, in particular on the role of the different LXR isoforms in glucose metabolism.

4.2.3 Gene expression in peripheral blood mononuclear cells

Expression of both ChREBP isoforms is associated with improved insulin sensitivity in human adipose tissue (41, 96, 97), while decreased expression in adipose tissue and increased expression in liver predicts insulin resistance (41, 97). However, few studies have investigated the expression of ChREBP and its target genes in the liver. The largest study to date included 165 patients, in which *CHREBPB* mRNA in the liver correlated with insulin resistance. Kursawe *et al*. found similar results with a significant increase in HOMA-IR with increasing levels of both ChREBP isoforms in the liver in eight adolescents with pre-diabetes or early T2DM (96). Due to limited tissue availability, these studies did not include protein analysis. Conversely, another study found that *CHREBP* mRNA expression in the liver was inversely correlated with insulin resistance in patients with NASH (86).

To our knowledge, no one has so far investigated the expression of ChREBP in peripheral blood mononuclear cells. Collection of liver tissue from healthy volunteers is ethically problematic because of the risks involved with the procedure. There is therefore interest in discovering tissues or cells that can serve *as in vivo* liver models. PBMCs share more than 80 % of the transcriptome with the liver and have been shown to reflect hepatic regulation of cholesterol metabolism on the level of gene expression (159) They are also responsive to physiological stimuli such as fasting and feeding (106, 160). In this project, we were therefore interested in determining whether PBMCs could serve as a surrogate tissue to study the role of ChREBP in liver metabolism.

Disappointingly, we discovered that both ChREBP isoforms were negligibly expressed in these cells. Moreover, a correlation analysis revealed an inverse relationship between serum glucose and the expression of the LXR and ChREBP target genes *SREBF1* and *FASN*. This is in contrast to *in vitro* and *in vivo* studies in hepatocytes, which have shown that glucose induces hepatic ChREBP and target gene expression (44, 155). Moreover, we found an inverse relationship between total serum cholesterol and expression of *FASN*. This may be due to chance, especially since most of the subjects had cholesterol levels within the normal range. Lastly, there was no correlation between HOMA-IR and expression of any of the genes of interest.

The major disadvantage of using these cells is that they have been in storage for approximately ten years, which may have led to RNA degradation and consequently obscured downstream analyses. However, RNA integrity was assessed and found to be within acceptable levels. Also, expression of *LXRA*, *SREBF1* and *FASN* were all in the normal range, which rules out general mRNA degradation. Another limitation is that the blood was sampled in the fasting state. This may explain the undetectable levels of *CHREBPB*, which is the isoform that responds to glucose by increased expression. However, we would have expected to detect the glucose non-responsive, more stably expressed *CHREBPA*, also in fasting conditions. However, the possibility that the fasting might have changed the expression of both ChREBP isoforms cannot be excluded.

The term PBMC covers different cells with varying properties, including monocytes, dendritic cells, CD4 and CD8 T cells, B cells and NK cells. Therefore, the possibility that gene expression varies according to the proportion of cell types that makes up the PBMC preparation cannot be ruled out. For example, the expression of *ABCA1* and *ABCG1* has been shown to be lower in PBMCs than primary monocytes (161). Recent studies have also indicated that activated T cells downregulate the LXR pathway while upregulating the SREBP-1 pathway (162), which introduces inflammation as a confounding factor. Similarly, glucose is the primary fuel source of lymphocytes and is vital for their proliferation, but resting lymphocytes have low energy needs (163). The expression of genes related to glucose and lipid metabolism may therefore be affected by inflammation.

Ultimately, PBMCs are immune cells whose main function is to respond to pathogens through differentiation, proliferation and antigen production. Even though they share a large proportion of active genes with the liver, the regulation of their genes may be considerably different to that of hepatocytes. Our analyses revealed that lipogenic genes are regulated in the opposite direction of what we would expect in the liver. Our inability to detect both ChREBP isoforms in PBMCs suggests that this might not be an important pathway in these cells. For these reasons, results on metabolic mechanisms from PBMCs should be interpreted with great caution, as they do not necessarily mimic metabolism in other tissues.

4.2.4 Interaction between LXRα and ChREBPα

An interesting observation in the current project is that LXRα ligand treatment reduces ChREBPα-mediated *Chrebpb* expression. One way this repression may come about is through an interaction between these transcription factors. Activation of LXRα may lead to binding of LXRα to the LID, thus inhibiting the glucose-mediated transcriptional activity of ChREBPα.

Previous data have shown that both LXRα and LXRβ interact with ChREBPα, but not with ChREBPβ (Nørgaard, unpublished data). The fact that ChREBPβ lacks the N-terminal low glucose inhibitory domain (LID) suggests that LXRα interacts with ChREBPα through this domain. In the current project, an expression plasmid coding only for the LID was cloned and transfected into COS-1 cells. A co-immunoprecipitation assay was performed, showing that, in support of our hypothesis, LXRα is pulled down by LID and vice versa.

The interaction between LXRα and ChREBPα may be affected by post-translational modifications, which can change protein conformation and thus its affinity for other proteins. A particularly interesting post-translational modification in this aspect is O-GlcNAcylation, which is a dynamic and reversible modification, influenced by glucose flux through the hexosamine biosynthetic pathway. It can therefore be characterized as a glucose-sensing pathway. Moreover, increased O-GlcNAcylation has been associated with glucose toxicity and insulin resistance, as well as hepatic steatosis, (62, 164), linking aberrant glucose signalling to pathologies commonly associated with obesity. O-GlcNAcylation is catalysed by O-linked β-*N*-acetylglucosamine transferase (OGT), which transfers the nucleotide sugar UDP-GlcNAc to a serine or threonine residue on a target protein, while the modification is removed by O-GlcNAcase (OGA). Both LXR and ChREBP are subjected to O-

GlcNAcylation in response to glucose, leading to an upregulation of their activity and target genes activation (62, 76, 152). Interestingly, loss of LXR led to reduced O-GlcNAcylation of ChREBPα (152). It could therefore be possible that LXR mediates O-GlcNAcylation of ChREBP by co-recruiting OGT, as LXR has been shown to interact strongly with OGT.

Recently, ChREBP has also been found to physically interact with the nuclear receptors hepatocyte nuclear factor 4 alpha (HNF-4α) (165) and farnesoid X receptor (FXR) (166). HNF-4α is abundant in foetal and adult liver and intestine and regulates expression of a large number of genes involved in glucose, fatty acid, cholesterol, and drug metabolism in the liver. HNF-4α was found to interact with ChREBPα, promote ChREBP transcription in response to glucose and to synergistically promote ChREBPβ expression (165). FXR acts as an intracellular sensor for bile acids and controls bile acid, lipid and glucose homeostasis, much in the opposite direction to that of LXR. While LXR promotes storage of lipids, FXR decreases TAG levels and modulates glucose metabolism (167). In high glucose concentrations, FXR and ChREBP co-occupy the *L-PK* promoter. FXR activation by the ligand GW4064 decreases ChREBP binding, reduces binding of co-activators CBP and p300 to the FXR:ChREBP complex, and instead induces recruitment of the SMRT co-repressor to the *L-pk* promoter (166).

FXR binds to ChREBP both via its AF-1 and LBD (166). Studies by Nørgaard suggested that LXRα interacts with ChREBPα through its hinge/LBD (unpublished data), which is interesting because FXR and LXR show significant homology within their LBD. This opens for the possibility that LXRα interacts with ChREBPα in a similar way, but with opposite results on metabolic regulation. While we have suggested that LXRα interacts only with ChREBPα, it is not clear which ChREBP isoforms interact with FXR.

Our findings suggest that LXRα mediates its effects on the *CHREBPB* promoter through the regulation of ChREBPα activity and that this regulation involves the LID. The fact that LXRα seems to require a functional DBD indicates that LXRα is bound to DNA. This regulation also seems to depend on ligand activation. Moreover, the ChIP-seq data show co-occupancy of ChREBPα and LXRα on the ChREBPα ChoRE-like binding site. Moreover, we have not been able to identify an LXRE in the ChREBPβ promoter. All this considered, we therefore propose a model in which LXRα mediates is gene regulatory effects by binding to a hitherto

unidentified binding site on the DNA, interacting with ChREBPα through DNA looping, as shown in **Figure 29**.

A

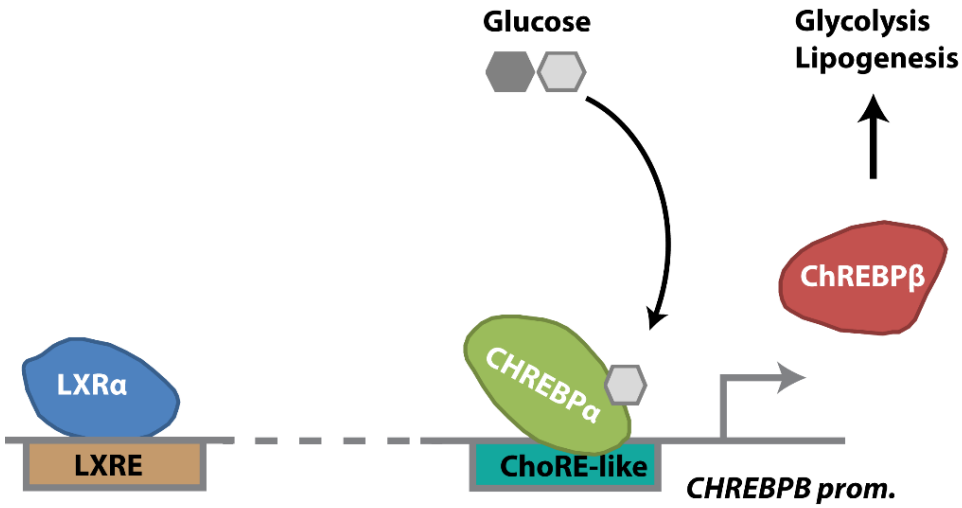

B

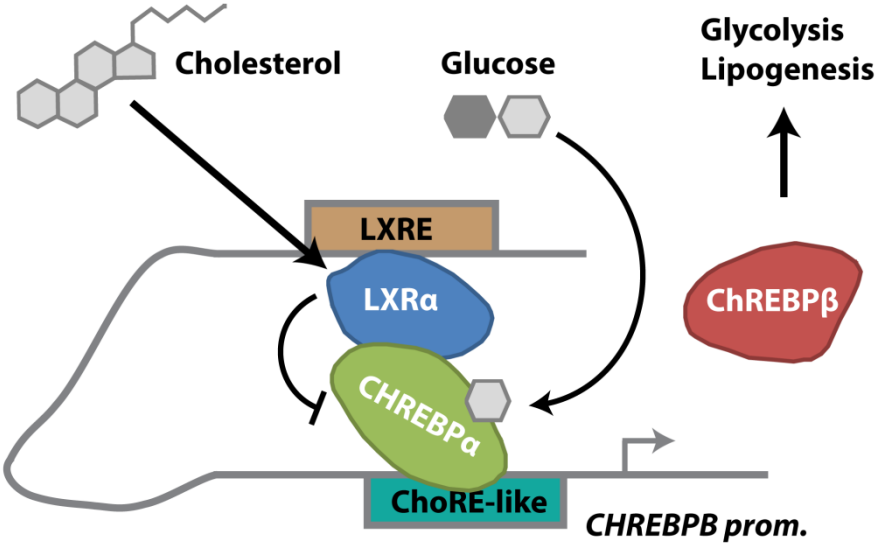

Figure 29: Proposed model of the interaction between LXRα and ChREBPα

A: Upon glucose activation, ChREBPα binds to a ChoRE-like regulatory element to enhance transcription from the ChREBPB promoter. **B:** A proposed model in which LXRα binds to an LXRE distally of the CHREBPB promoter. Upon ligand activation, LXRα interacts directly or indirectly with the LID of ChREBPα, leading to repression of the transcriptional activity of ChREBPα.

Furthermore, this switch activates the transcription of *CHREBPB* under high glucose conditions, while it partly represses this activation when the concentration of cholesterol and cholesterol metabolites is high. This model permits co-occupancy but does not necessitate an LXR binding site in the *CHREBPB* promoter. However, it does not explain how LXRα is able to activate CHREBPB expression independently of a functional ChoRE/ChoRE-like. One possibility is that the *CHREBPB* promoter contains an unknown LXR binding site, another is that induce expression of or mediate the recruitment of unknown proteins. Thus, this is an issue which needs to be investigated further.

4.2.5 Physiological implications of LXRα and ChREBP crosstalk

In physiological conditions, ChREBP and LXRα work in concert to regulate hepatic glycolysis and lipogenesis in response to feeding. These two transcription factors play complementary roles, where ChREBP expression and activity is induced by glucose metabolites, while LXRα is activated by cholesterol metabolites. Moreover, LXRα increases expression of ChREBPα, which in turn regulates the expression of the shorter and more potent ChREBPβ isoform. Adding to this, our data show that the activity of the ChREBPβ promoter is reduced by LXR ligands, suggesting that LXRα activation by oxysterols may have suppressive effects on ChREBPα transcriptional activity.

Such a negative regulation could make sense both from a mechanistic point of view and in a physiological context, e.g. when considering a diet high in both cholesterol and simple sugars. A high intake of sugar may result in a surplus of glucose, which increases the transcriptional activity of ChREBPα, leading to increased ChREBPβ activity and hepatic lipogenesis. Cholesterol and bile acid metabolism give rise to oxysterols, which may lead to LXRα activation and a concomitant reduction in the lipogenic activity of ChREBPβ. In the liver, this could be beneficial, as a too high lipogenic rate contributes to hepatic steatosis. Since NAFLD is associated with increased ChREBP mRNA expression (86), it is also possible that such a repressive mechanism could be subject to metabolic dysregulation. Interestingly, it has been recently suggested that ChREBP also plays a role in hepatic cholesterol biosynthesis (168). Taken together, this indicates that LXR and ChREBP integrate the sugar and cholesterol sensing pathways in quite sophisticated ways, worthy of further investigations.

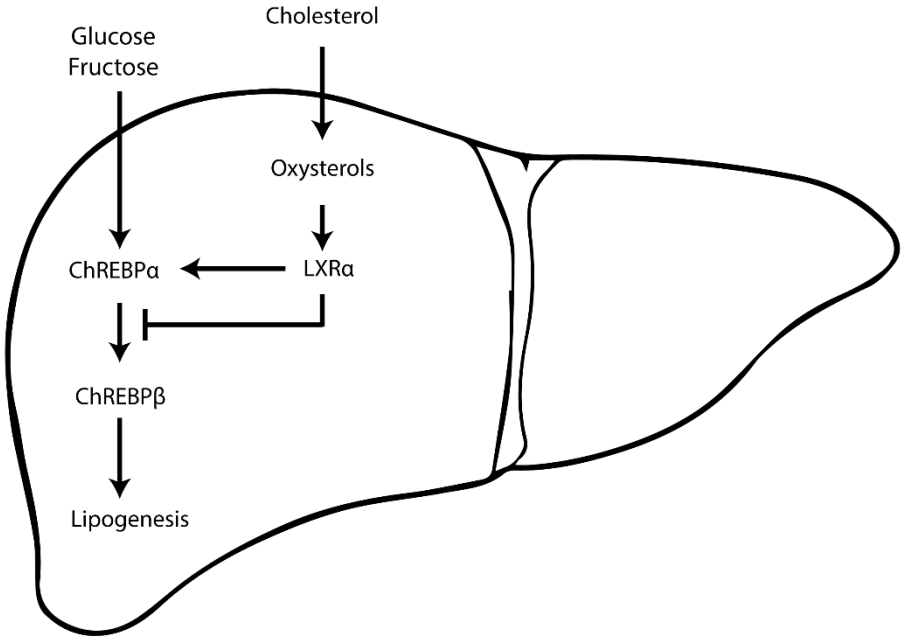

Figure 30: Physiological role of a putative sugar and cholesterol-responsive transcriptional switch

While fructose and glucose activate ChREBPα to induce expression of ChREBPβ, cholesterol metabolites activate LXRα, which increase the expression of ChREBPα but also inhibits its transcriptional activity of ChREBPα. This inhibition results in decreased lipogenesis.

5 Conclusions

Through *in vitro* cell studies, we identified that an E-box localized upstream of the canonical ChoRE is a key regulatory sequence in the ChREBPβ promoter. This E-box and an E-box-like site are separated by 5 base pairs and constitute a possible ChREBP binding site, which we termed ChoRE-like. We characterized PBMCs as an inadequate model for studying ChREBP *in vivo*, which may have implications for its validity as a liver model also in other metabolic studies. We have also provided more data in favour of the hypothesis that ChREBPα interacts with LXRα via its low glucose inhibitory domain. Finally, we propose a model in which LXRα binds to a yet unidentified site on the ChREBP gene, and represses ChREBPα transcriptional activity through an interaction with the LID.

5.1 Further perspectives

ChREBP, LXRs and other transcription factors are involved in the direct and indirect transcriptional response to nutrient, which facilitates fine-tuning of the cellular responses. Most promoters of important metabolic genes contain multiple binding sites for different transcription factors (169). This may seem redundant, but ensures a complex, integrative and tight regulation of important enzymes of metabolic pathways. Furthermore, transcription factors may interact with each other, resulting in feed-forward or feed-back mechanisms. Future investigations of the carbohydrate and cholesterol-responsive transcriptional switch in the liver should focus on the interplay between ChREBP, nuclear receptors, as well as the effect of post-translational modifications.

References

1. Zhang X-Y, Shu L, Si C-J, Yu X-L, Liao D, Gao W, et al. Dietary Patterns, Alcohol Consumption and Risk of Coronary Heart Disease in Adults: A Meta-Analysis. Nutrients. 2015;7(8):5300.
2. Ma J, Fox CS, Jacques PF, Speliotes EK, Hoffmann U, Smith CE, et al. Sugar-sweetened beverage, diet soda, and fatty liver disease in the Framingham Heart Study cohorts. Journal of hepatology. 2015;63(2):462-9.
3. Green AK, Jacques PF, Rogers G, Fox CS, Meigs JB, McKeown NM. Sugar-sweetened beverages and prevalence of the metabolically abnormal phenotype in the Framingham Heart Study. Obesity (Silver Spring, Md). 2014;22(5):E157-63.
4. Malik VS, Popkin BM, Bray GA, Despres JP, Willett WC, Hu FB. Sugar-sweetened beverages and risk of metabolic syndrome and type 2 diabetes: a meta-analysis. Diabetes Care. 2010;33(11):2477-83.
5. DeFronzo RA, Ferrannini E, Groop L, Henry RR, Herman WH, Holst JJ, et al. Type 2 diabetes mellitus. Nature reviews Disease primers. 2015;1:15019.
6. World Health Organization. Global report on diabetes. Geneva, Switzerland; 2016.
7. Helsedirektoratet. Nasjonal faglig retningslinje for diabetes Oslo, Norway; 2017.
8. Chalasani N, Younossi Z, Lavine JE, Diehl AM, Brunt EM, Cusi K, et al. The diagnosis and management of non-alcoholic fatty liver disease: practice Guideline by the American Association for the Study of Liver Diseases, American College of Gastroenterology, and the American Gastroenterological Association. Hepatology (Baltimore, Md). 2012;55(6):2005-23.
9. Kleiner DE, Brunt EM, Van Natta M, Behling C, Contos MJ, Cummings OW, et al. Design and validation of a histological scoring system for nonalcoholic fatty liver disease. Hepatology (Baltimore, Md). 2005;41(6):1313-21.
10. Angulo P. Long-term mortality in nonalcoholic fatty liver disease: is liver histology of any prognostic significance? Hepatology (Baltimore, Md). 2010;51(2):373-5.
11. Ahmed MH, Barakat S, Almobarak AO. Nonalcoholic fatty liver disease and cardiovascular disease: has the time come for cardiologists to be hepatologists? Journal of obesity. 2012;2012:483135.
12. Vernon G, Baranova A, Younossi ZM. Systematic review: the epidemiology and natural history of non-alcoholic fatty liver disease and non-alcoholic steatohepatitis in adults. Alimentary pharmacology & therapeutics. 2011;34(3):274-85.
13. Machado M, Marques-Vidal P, Cortez-Pinto H. Hepatic histology in obese patients undergoing bariatric surgery. Journal of hepatology. 2006;45(4):600-6.
14. Donnelly KL, Smith CI, Schwarzenberg SJ, Jessurun J, Boldt MD, Parks EJ. Sources of fatty acids stored in liver and secreted via lipoproteins in patients with nonalcoholic fatty liver disease. The Journal of clinical investigation. 2005;115(5):1343-51.
15. Nakamuta M, Kohjima M, Higuchi N, Kato M, Kotoh K, Yoshimoto T, et al. The significance of differences in fatty acid metabolism between obese and non-obese patients with non-alcoholic fatty liver disease. International journal of molecular medicine. 2008;22(5):663-7.
16. Latchman DS. Transcription factors: an overview. International Journal of Experimental Pathology. 1993;74(5):417-22.
17. Ferrier DR. Lippincott's Illustrated reviews. 6th ed. ed. Ferrier DR, Harvey RA, editors. Philadelphia :: Wolters Kluwer Health/Lippincott Williams & Wilkins; 2014.
18. Thorens B, Mueckler M. Glucose transporters in the 21st Century. American Journal of Physiology - Endocrinology and Metabolism. 2010;298(2):E141-E5.
19. Frayn KN. Metabolic Regulation. A Human Perspective. 3 ed. Oxford, UK: Wiley-Blackwell; 2013. 371 p.
20. Lodhi IJ, Wei X, Semenkovich CF. Lipoexpediency: de novo lipogenesis as a metabolic signal transmitter. Trends in endocrinology and metabolism: TEM. 2011;22(1):1-8.
21. Hodson L, Fielding BA. Stearoyl-CoA desaturase: rogue or innocent bystander? Progress in lipid research. 2013;52(1):15-42.
22. Strable MS, Ntambi JM. Genetic control of de novo lipogenesis: role in diet-induced obesity. Critical reviews in biochemistry and molecular biology. 2010;45(3):199-214.
23. Ferre P, Foufelle F. Hepatic steatosis: a role for de novo lipogenesis and the transcription factor SREBP-1c. Diabetes, obesity & metabolism. 2010;12 Suppl 2:83-92.

24. Magana MM, Lin SS, Dooley KA, Osborne TF. Sterol regulation of acetyl coenzyme A carboxylase promoter requires two interdependent binding sites for sterol regulatory element binding proteins. Journal of lipid research. 1997;38(8):1630-8.
25. Foufelle F, Gouhot B, Pegorier JP, Perdereau D, Girard J, Ferre P. Glucose stimulation of lipogenic enzyme gene expression in cultured white adipose tissue. A role for glucose 6-phosphate. The Journal of biological chemistry. 1992;267(29):20543-6.
26. Girard J, Ferre P, Foufelle F. Mechanisms by which carbohydrates regulate expression of genes for glycolytic and lipogenic enzymes. Annual review of nutrition. 1997;17:325-52.
27. Towle HC. Glucose as a regulator of eukaryotic gene transcription. Trends in endocrinology and metabolism: TEM. 2005;16(10):489-94.
28. Cha JY, Repa JJ. The liver X receptor (LXR) and hepatic lipogenesis. The carbohydrate-response element-binding protein is a target gene of LXR. The Journal of biological chemistry. 2007;282(1):743-51.
29. Repa JJ, Liang G, Ou J, Bashmakov Y, Lobaccaro JM, Shimomura I, et al. Regulation of mouse sterol regulatory element-binding protein-1c gene (SREBP-1c) by oxysterol receptors, LXRalpha and LXRbeta. Genes & development. 2000;14(22):2819-30.
30. Joseph SB, Laffitte BA, Patel PH, Watson MA, Matsukuma KE, Walczak R, et al. Direct and indirect mechanisms for regulation of fatty acid synthase gene expression by liver X receptors. The Journal of biological chemistry. 2002;277(13):11019-25.
31. Sun Y, Hao M, Luo Y, Liang CP, Silver DL, Cheng C, et al. Stearoyl-CoA desaturase inhibits ATP-binding cassette transporter A1-mediated cholesterol efflux and modulates membrane domain structure. The Journal of biological chemistry. 2003;278(8):5813-20.
32. Grønning-Wang LM, Bindesbøll, Christian, Nebb, Hilde I. The Role of Liver X Receptor in Hepatic de novo Lipogenesis and Cross-Talk with Insulin and Glucose Signaling. Lipid Metabolism. Rijeka: InTech; 2013.
33. Wang N, Lan D, Chen W, Matsuura F, Tall AR. ATP-binding cassette transporters G1 and G4 mediate cellular cholesterol efflux to high-density lipoproteins. Proceedings of the National Academy of Sciences of the United States of America. 2004;101(26):9774-9.
34. Lodish H BA, Zipursky SL, et al. Molecular Cell Biology. 4th ed. New York: W. H. Freeman; 2000.
35. Inamoto I, Chen G, Shin JA. The DNA target determines the dimerization partner selected by bHLHZ-like hybrid proteins AhRJun and ArntFos. Molecular bioSystems. 2017;13(3):476-88.
36. Aronsson C, Dånmark S, Zhou F, Öberg P, Enander K, Su H, et al. Self-sorting heterodimeric coiled coil peptides with defined and tuneable self-assembly properties. Scientific reports. 2015;5:14063.
37. Gronemeyer H, Gustafsson J-Å, Laudet V. Principles for modulation of the nuclear receptor superfamily. Nature Reviews Drug Discovery. 2004;3:950.
38. Aagaard MM, Siersbaek R, Mandrup S. Molecular basis for gene-specific transactivation by nuclear receptors. Biochimica et biophysica acta. 2011;1812(8):824-35.
39. Filhoulaud G, Guilmeau S, Dentin R, Girard J, Postic C. Novel insights into ChREBP regulation and function. Trends in endocrinology and metabolism: TEM. 2013;24(5):257-68.
40. Stoeckman AK, Ma L, Towle HC. Mlx is the functional heteromeric partner of the carbohydrate response element-binding protein in glucose regulation of lipogenic enzyme genes. The Journal of biological chemistry. 2004;279(15):15662-9.
41. Herman MA, Peroni OD, Villoria J, Schon MR, Abumrad NA, Bluher M, et al. A novel ChREBP isoform in adipose tissue regulates systemic glucose metabolism. Nature. 2012;484(7394):333-8.
42. Iizuka K, Bruick RK, Liang G, Horton JD, Uyeda K. Deficiency of carbohydrate response element-binding protein (ChREBP) reduces lipogenesis as well as glycolysis. Proceedings of the National Academy of Sciences of the United States of America. 2004;101(19):7281-6.
43. Osorio JS, Lohakare J, Bionaz M. Biosynthesis of milk fat, protein, and lactose: roles of transcriptional and posttranscriptional regulation. Physiological genomics. 2016;48(4):231-56.
44. Stamatikos AD, da Silva RP, Lewis JT, Douglas DN, Kneteman NM, Jacobs RL, et al. Tissue Specific Effects of Dietary Carbohydrates and Obesity on ChREBPalpha and ChREBPbeta Expression. Lipids. 2016;51(1):95-104.
45. Jing G, Chen J, Xu G, Shalev A. Islet ChREBP-β is increased in diabetes and controls ChREBP-α and glucose-induced gene expression via a negative feedback loop.
46. Nakagawa T, Ge Q, Pawlosky R, Wynn RM, Veech RL, Uyeda K. Metabolite regulation of nucleo-cytosolic trafficking of carbohydrate response element-binding protein (ChREBP): role of ketone bodies. The Journal of biological chemistry. 2013;288(39):28358-67.

47. Dentin R, Benhamed F, Pegorier JP, Foufelle F, Viollet B, Vaulont S, et al. Polyunsaturated fatty acids suppress glycolytic and lipogenic genes through the inhibition of ChREBP nuclear protein translocation. The Journal of clinical investigation. 2005;115(10):2843-54.
48. Shih HM, Liu Z, Towle HC. Two CACGTG motifs with proper spacing dictate the carbohydrate regulation of hepatic gene transcription. The Journal of biological chemistry. 1995;270(37):21991-7.
49. Ma L, Tsatsos NG, Towle HC. Direct role of ChREBP.Mlx in regulating hepatic glucose-responsive genes. The Journal of biological chemistry. 2005;280(12):12019-27.
50. Abdul-Wahed A, Guilmeau S, Postic C. Sweet Sixteenth for ChREBP: Established Roles and Future Goals. Cell metabolism. 2017;26(2):324-41.
51. Fukasawa M, Ge Q, Wynn RM, Ishii S, Uyeda K. Coordinate regulation/localization of the carbohydrate responsive binding protein (ChREBP) by two nuclear export signal sites: discovery of a new leucine-rich nuclear export signal site. Biochemical and biophysical research communications. 2010;391(2):1166-9.
52. Davies MN, O'Callaghan BL, Towle HC. Glucose activates ChREBP by increasing its rate of nuclear entry and relieving repression of its transcriptional activity. The Journal of biological chemistry. 2008;283(35):24029-38.
53. Davies MN, O'Callaghan BL, Towle HC. Activation and repression of glucose-stimulated ChREBP requires the concerted action of multiple domains within the MondoA conserved region. American Journal of Physiology - Endocrinology and Metabolism. 2010;299(4):E665-E74.
54. Li MV, Chang B, Imamura M, Poungvarin N, Chan L. Glucose-dependent transcriptional regulation by an evolutionarily conserved glucose-sensing module. Diabetes. 2006;55(5):1179-89.
55. Billin AN, Ayer DE. The Mlx network: evidence for a parallel Max-like transcriptional network that regulates energy metabolism. Current topics in microbiology and immunology. 2006;302:255-78.
56. Villar-Palasi C, Guinovart JJ. The role of glucose 6-phosphate in the control of glycogen synthase. FASEB journal : official publication of the Federation of American Societies for Experimental Biology. 1997;11(7):544-58.
57. Kabashima T, Kawaguchi T, Wadzinski BE, Uyeda K. Xylulose 5-phosphate mediates glucose-induced lipogenesis by xylulose 5-phosphate-activated protein phosphatase in rat liver. Proceedings of the National Academy of Sciences of the United States of America. 2003;100(9):5107-12.
58. Dentin R, Tomas-Cobos L, Foufelle F, Leopold J, Girard J, Postic C, et al. Glucose 6-phosphate, rather than xylulose 5-phosphate, is required for the activation of ChREBP in response to glucose in the liver. Journal of hepatology. 2012;56(1):199-209.
59. Arden C, Tudhope SJ, Petrie JL, Al-Oanzi ZH, Cullen KS, Lange AJ, et al. Fructose 2,6-bisphosphate is essential for glucose-regulated gene transcription of glucose-6-phosphatase and other ChREBP target genes in hepatocytes. The Biochemical journal. 2012;443(1):111-23.
60. Denechaud PD, Bossard P, Lobaccaro JM, Millatt L, Staels B, Girard J, et al. ChREBP, but not LXRs, is required for the induction of glucose-regulated genes in mouse liver. The Journal of clinical investigation. 2008;118(3):956-64.
61. Bricambert J, Miranda J, Benhamed F, Girard J, Postic C, Dentin R. Salt-inducible kinase 2 links transcriptional coactivator p300 phosphorylation to the prevention of ChREBP-dependent hepatic steatosis in mice. The Journal of clinical investigation. 2010;120(12):4316-31.
62. Guinez C, Filhoulaud G, Rayah-Benhamed F, Marmier S, Dubuquoy C, Dentin R, et al. O-GlcNAcylation increases ChREBP protein content and transcriptional activity in the liver. Diabetes. 2011;60(5):1399-413.
63. Song C, Hiipakka RA, Kokontis JM, Liao S. Ubiquitous receptor: structures, immunocytochemical localization, and modulation of gene activation by receptors for retinoic acids and thyroid hormones. Annals of the New York Academy of Sciences. 1995;761:38-49.
64. Auboeuf D, Rieusset J, Fajas L, Vallier P, Frering V, Riou JP, et al. Tissue distribution and quantification of the expression of mRNAs of peroxisome proliferator-activated receptors and liver X receptor-alpha in humans: no alteration in adipose tissue of obese and NIDDM patients. Diabetes. 1997;46(8):1319-27.
65. Willy PJ, Umesono K, Ong ES, Evans RM, Heyman RA, Mangelsdorf DJ. LXR, a nuclear receptor that defines a distinct retinoid response pathway. Genes & development. 1995;9(9):1033-45.
66. Apfel R, Benbrook D, Lernhardt E, Ortiz MA, Salbert G, Pfahl M. A novel orphan receptor specific for a subset of thyroid hormone-responsive elements and its interaction with the retinoid/thyroid hormone receptor subfamily. Molecular and cellular biology. 1994;14(10):7025-35.
67. Yan D, Olkkonen VM. Chapter Seven - Characteristics of Oxysterol Binding Proteins. In: Jeon KW, editor. International Review of Cytology. 265: Academic Press; 2008. p. 253-85.

68. Jakobsson T, Treuter E, Gustafsson JA, Steffensen KR. Liver X receptor biology and pharmacology: new pathways, challenges and opportunities. Trends in pharmacological sciences. 2012;33(7):394-404.
69. Farnegardh M, Bonn T, Sun S, Ljunggren J, Ahola H, Wilhelmsson A, et al. The three-dimensional structure of the liver X receptor beta reveals a flexible ligand-binding pocket that can accommodate fundamentally different ligands. The Journal of biological chemistry. 2003;278(40):38821-8.
70. Cao G, Liang Y, Broderick CL, Oldham BA, Beyer TP, Schmidt RJ, et al. Antidiabetic action of a liver x receptor agonist mediated by inhibition of hepatic gluconeogenesis. The Journal of biological chemistry. 2003;278(2):1131-6.
71. Dalen KT, Ulven SM, Bamberg K, Gustafsson JA, Nebb HI. Expression of the insulin-responsive glucose transporter GLUT4 in adipocytes is dependent on liver X receptor alpha. The Journal of biological chemistry. 2003;278(48):48283-91.
72. Huuskonen J, Fielding PE, Fielding CJ. Role of p160 coactivator complex in the activation of liver X receptor. Arteriosclerosis, thrombosis, and vascular biology. 2004;24(4):703-8.
73. Chen M, Bradley MN, Beaven SW, Tontonoz P. Phosphorylation of the liver X receptors. FEBS letters. 2006;580(20):4835-41.
74. Li X, Zhang S, Blander G, Tse JG, Krieger M, Guarente L. SIRT1 deacetylates and positively regulates the nuclear receptor LXR. Molecular cell. 2007;28(1):91-106.
75. Ghisletti S, Huang W, Ogawa S, Pascual G, Lin ME, Willson TM, et al. Parallel SUMOylation-dependent pathways mediate gene- and signal-specific transrepression by LXRs and PPARgamma. Molecular cell. 2007;25(1):57-70.
76. Anthonisen EH, Berven L, Holm S, Nygård M, Nebb HI, Grænning-Wang LM. Nuclear receptor liver X receptor is O-GlcNAc-modified in response to glucose. The Journal of biological chemistry. 2010;285(3):1607-15.
77. Fan Q, Moen A, Anonsen JH, Bindesbøll C, Sæther T, Carlson CR, et al. O-GlcNAc site-mapping of liver X receptor-α and O-GlcNAc transferase. Biochemical and biophysical research communications. 2018;499(2):354-60.
78. Venteclef N, Jakobsson T, Ehrlund A, Damdimopoulos A, Mikkonen L, Ellis E, et al. GPS2-dependent corepressor/SUMO pathways govern anti-inflammatory actions of LRH-1 and LXRbeta in the hepatic acute phase response. Genes & development. 2010;24(4):381-95.
79. Kennedy MA, Venkateswaran A, Tarr PT, Xenarios I, Kudoh J, Shimizu N, et al. Characterization of the human ABCG1 gene: liver X receptor activates an internal promoter that produces a novel transcript encoding an alternative form of the protein. The Journal of biological chemistry. 2001;276(42):39438-47.
80. Venkateswaran A, Laffitte BA, Joseph SB, Mak PA, Wilpitz DC, Edwards PA, et al. Control of cellular cholesterol efflux by the nuclear oxysterol receptor LXR alpha. Proceedings of the National Academy of Sciences of the United States of America. 2000;97(22):12097-102.
81. Repa JJ, Mangelsdorf DJ. The liver X receptor gene team: potential new players in atherosclerosis. Nature medicine. 2002;8(11):1243-8.
82. Zelcer N, Hong C, Boyadjian R, Tontonoz P. LXR regulates cholesterol uptake through Idol-dependent ubiquitination of the LDL receptor. Science (New York, NY). 2009;325(5936):100-4.
83. Agellon LB, Drover VA, Cheema SK, Gbaguidi GF, Walsh A. Dietary cholesterol fails to stimulate the human cholesterol 7alpha-hydroxylase gene (CYP7A1) in transgenic mice. The Journal of biological chemistry. 2002;277(23):20131-4.
84. Joseph SB, McKilligin E, Pei L, Watson MA, Collins AR, Laffitte BA, et al. Synthetic LXR ligand inhibits the development of atherosclerosis in mice. Proceedings of the National Academy of Sciences of the United States of America. 2002;99(11):7604-9.
85. Levin N, Bischoff ED, Daige CL, Thomas D, Vu CT, Heyman RA, et al. Macrophage liver X receptor is required for antiatherogenic activity of LXR agonists. Arteriosclerosis, thrombosis, and vascular biology. 2005;25(1):135-42.
86. Benhamed F, Denechaud PD, Lemoine M, Robichon C, Moldes M, Bertrand-Michel J, et al. The lipogenic transcription factor ChREBP dissociates hepatic steatosis from insulin resistance in mice and humans. The Journal of clinical investigation. 2012;122(6):2176-94.
87. Letexier D, Peroni O, Pinteur C, Beylot M. In vivo expression of carbohydrate responsive element binding protein in lean and obese rats. Diabetes & Metabolism.31(6):558-66.
88. Iizuka K, Miller B, Uyeda K. Deficiency of carbohydrate-activated transcription factor ChREBP prevents obesity and improves plasma glucose control in leptin-deficient (ob/ob) mice. American journal of physiology Endocrinology and metabolism. 2006;291(2):E358-64.

89. Dentin R, Benhamed F, Hainault I, Fauveau V, Foufelle F, Dyck JR, et al. Liver-specific inhibition of ChREBP improves hepatic steatosis and insulin resistance in ob/ob mice. Diabetes. 2006;55(8):2159-70.
90. Kim JK, Lee KS, Chang HY, Lee WK, Lee JI. Progression of diet induced nonalcoholic steatohepatitis is accompanied by increased expression of Kruppel-like-factor 10 in mice. Journal of translational medicine. 2014;12:186.
91. Ahn SB, Jang K, Jun DW, Lee BH, Shin KJ. Expression of liver X receptor correlates with intrahepatic inflammation and fibrosis in patients with nonalcoholic fatty liver disease. Digestive diseases and sciences. 2014;59(12):2975-82.
92. Ito A, Hong C, Rong X, Zhu X, Tarling EJ, Hedde PN, et al. LXRs link metabolism to inflammation through Abca1-dependent regulation of membrane composition and TLR signaling. eLife. 2015;4:e08009.
93. Jois T, Sleeman MW. The regulation and role of carbohydrate response element binding protein in metabolic homeostasis and disease. Journal of neuroendocrinology. 2017.
94. Cao H, Gerhold K, Mayers JR, Wiest MM, Watkins SM, Hotamisligil GS. Identification of a lipokine, a lipid hormone linking adipose tissue to systemic metabolism. Cell. 2008;134(6):933-44.
95. Kuriyama H, Liang G, Engelking LJ, Horton JD, Goldstein JL, Brown MS. Compensatory increase in fatty acid synthesis in adipose tissue of mice with conditional deficiency of SCAP in liver. Cell metabolism. 2005;1(1):41-51.
96. Kursawe R, Caprio S, Giannini C, Narayan D, Lin A, D'Adamo E, et al. Decreased transcription of ChREBP-alpha/beta isoforms in abdominal subcutaneous adipose tissue of obese adolescents with prediabetes or early type 2 diabetes: associations with insulin resistance and hyperglycemia. Diabetes. 2013;62(3):837-44.
97. Eissing L, Scherer T, Todter K, Knippschild U, Greve JW, Buurman WA, et al. De novo lipogenesis in human fat and liver is linked to ChREBP-beta and metabolic health. Nature communications. 2013;4:1528.
98. Chavez JA, Summers SA. A ceramide-centric view of insulin resistance. Cell metabolism. 2012;15(5):585-94.
99. Yu C, Chen Y, Cline GW, Zhang D, Zong H, Wang Y, et al. Mechanism by which fatty acids inhibit insulin activation of insulin receptor substrate-1 (IRS-1)-associated phosphatidylinositol 3-kinase activity in muscle. The Journal of biological chemistry. 2002;277(52):50230-6.
100. Laffitte BA, Chao LC, Li J, Walczak R, Hummasti S, Joseph SB, et al. Activation of liver X receptor improves glucose tolerance through coordinate regulation of glucose metabolism in liver and adipose tissue. Proceedings of the National Academy of Sciences of the United States of America. 2003;100(9):5419-24.
101. Stulnig TM, Steffensen KR, Gao H, Reimers M, Dahlman-Wright K, Schuster GU, et al. Novel roles of liver X receptors exposed by gene expression profiling in liver and adipose tissue. Molecular pharmacology. 2002;62(6):1299-305.
102. Pettersson AM, Stenson BM, Lorente-Cebrian S, Andersson DP, Mejhert N, Kratzel J, et al. LXR is a negative regulator of glucose uptake in human adipocytes. Diabetologia. 2013;56(9):2044-54.
103. Abbas AK, Lichtman AH. Basic Immunology: Functions and Disorders of the Immune System: W. B. Saunders; 2001.
104. de Mello VDF, Kolehmanien M, Schwab U, Pulkkinen L, Uusitupa M. Gene expression of peripheral blood mononuclear cells as a tool in dietary intervention studies: What do we know so far? Molecular Nutrition & Food Research. 2012;56(7):1160-72.
105. Liew CC, Ma J, Tang HC, Zheng R, Dempsey AA. The peripheral blood transcriptome dynamically reflects system wide biology: a potential diagnostic tool. The Journal of laboratory and clinical medicine. 2006;147(3):126-32.
106. Mohr S, Liew C-C. The peripheral-blood transcriptome: new insights into disease and risk assessment. Trends in Molecular Medicine. 2007;13(10):422-32.
107. Bouwens M, Grootte Bromhaar M, Jansen J, Müller M, Afman LA. Postprandial dietary lipid–specific effects on human peripheral blood mononuclear cell gene expression profiles. The American journal of clinical nutrition. 2010;91(1):208-17.
108. Boucher P, de Lorgeril M, Salen P, Crozier P, Delaye J, Vallon JJ, et al. Effect of dietary cholesterol on low density lipoprotein-receptor, 3-hydroxy-3-methylglutaryl-CoA reductase, and low density lipoprotein receptor-related protein mRNA expression in healthy humans. Lipids. 1998;33(12):1177-86.

109. Mutungi G, Torres-Gonzalez M, McGrane MM, Volek JS, Fernandez ML. Carbohydrate restriction and dietary cholesterol modulate the expression of HMG-CoA reductase and the LDL receptor in mononuclear cells from adult men. Lipids in health and disease. 2007;6:34.
110. Myhrstad MCW, Ulven SM, Günther CC, Ottestad I, Holden M, Ryeng E, et al. Fish oil supplementation induces expression of genes related to cell cycle, endoplasmic reticulum stress and apoptosis in peripheral blood mononuclear cells: a transcriptomic approach. Journal of internal medicine. 2014;276(5):498-511.
111. Matthews DR, Hosker JP, Rudenski AS, Naylor BA, Treacher DF, Turner RC. Homeostasis model assessment: insulin resistance and beta-cell function from fasting plasma glucose and insulin concentrations in man. Diabetologia. 1985;28(7):412-9.
112. Gayoso-Diz P, Otero-González A, Rodriguez-Alvarez MX, Gude F, García F, De Francisco A, et al. Insulin resistance (HOMA-IR) cut-off values and the metabolic syndrome in a general adult population: effect of gender and age: EPIRCE cross-sectional study. BMC Endocrine Disorders. 2013;13(1):47.
113. Lann D, LeRoith D. Insulin Resistance as the Underlying Cause for the Metabolic Syndrome. Medical Clinics of North America. 2007;91(6):1063-77.
114. Verma A. Animal Tissue Culture: Principles and Applications. Animal Biotechnology. San Diego: Academic Press; 2014. p. 211-31.
115. Nakabayashi H, Taketa K, Miyano K, Yamane T, Sato J. Growth of human hepatoma cells lines with differentiated functions in chemically defined medium. Cancer research. 1982;42(9):3858-63.
116. López-Terrada D, Cheung SW, Finegold MJ, Knowles BB. Hep G2 is a hepatoblastoma-derived cell line. Human Pathology. 2009;40(10):1512-5.
117. Donato MT, Tolosa L, Gómez-Lechón MJ. Culture and Functional Characterization of Human Hepatoma HepG2 Cells. In: Vinken M, Rogiers V, editors. Protocols in In Vitro Hepatocyte Research. New York, NY: Springer New York; 2015. p. 77-93.
118. RNeasy® Mini Kit, Part 1 Hilden, Germany: Qiagen; 2011 [04.12.2017]. Available from: https://www.qiagen.com/no/resources/resourcedetail?id=0e32fbb1-c307-4603-ac81-a5e98490ed23&lang=en.
119. RNeasy® Mini Kit, Part 2 Hilden, Germany: Qiagen; 2011 [04.12.2017]. Available from: https://www.qiagen.com/no/resources/resourcedetail?id=f9b2e5ef-9456-431a-85ed-2a2b9fbd503d&lang=en.
120. Fleige S, Pfaffl MW. RNA integrity and the effect on the real-time qRT-PCR performance. Molecular aspects of medicine. 2006;27(2-3):126-39.
121. Fleige S, Walf V, Huch S, Prgomet C, Sehm J, Pfaffl MW. Comparison of relative mRNA quantification models and the impact of RNA integrity in quantitative real-time RT-PCR. Biotechnology letters. 2006;28(19):1601-13.
122. Agilent RNA 6000 Nano Kit Guide Waldbronn, Germany: Agilent technologies; 2013 [Available from: https://www.agilent.com/cs/library/usermanuals/Public/G2938-90034_RNA6000Nano_KG.pdf.
123. High Capacity cDNA Reverse Transcription Kits Foster City, CA, USA: Applied Biosystems; 2010 [Available from: https://assets.thermofisher.com/TFS-Assets/LSG/manuals/cms_042557.pdf.
124. Real-time PCR Handbook. 3rd Edition ed: Thermo Fisher Scientific 2014. 68 p.
125. Alberts B, Johnson A, Lewis J, Wilson JH, Hunt T. Molecular biology of the cell. Abingdon; New York: Garland Science, Taylor & Francis Group; 2015.
126. Lacks S, Greenberg B. A deoxyribonuclease of Diplococcus pneumoniae specific for methylated DNA. The Journal of biological chemistry. 1975;250(11):4060-66.
127. NucleoSpin® Gel and PCR Clean-up User manual: Macherey-Nagel; 2017 [Available from: http://www.mn-net.com/Portals/8/attachments/Redakteure_Bio/Protocols/DNA%20clean-up/UM_PCRcleanup_Gelex_NSGelPCR.pdf.
128. NucleoSpin® Plasmid User manual: Macherey-Nagel; 2017 [Available from: http://www.mn-net.com/Portals/8/attachments/Redakteure_Bio/Protocols/Plasmid%20DNA%20Purification/UM_pDNA_NS.pdf.
129. NucleoBond® Xtra Plasmid DNA purification User manual: Macherey-Nagel; 2017 [Available from: http://www.mn-net.com/Portals/8/attachments/Redakteure_Bio/Protocols/Plasmid%20DNA%20Purification/UM_pDNA_NuBoXtra.pdf.
130. Kim TK, Eberwine JH. Mammalian cell transfection: the present and the future. Analytical and Bioanalytical Chemistry. 2010;397(8):3173-8.
131. Kaestner L, Scholz A, Lipp P. Conceptual and technical aspects of transfection and gene delivery. Bioorganic & Medicinal Chemistry Letters. 2015;25(6):1171-6.

132. Bioluminescence Reporters Promega Corporation; 2018 [Available from: https://no.promega.com/resources/product-guides-and-selectors/protocols-and-applications-guide/bioluminescent-reporters/.
133. Dual-Luciferase® Reporter Assay System: Promega Corporation; 2015 [Available from: https://no.promega.com/-/media/files/resources/protocols/technical-manuals/0/dual-luciferase-reporter-assay-system-protocol.pdf.
134. Dual-Luciferase® Reporter Assay and Dual-Luciferase® Reporter 1000 Assay Systems QuickProtocol: Promega Corporation; 2009 [23.01.2018].
135. Phizicky EM, Fields S. Protein-protein interactions: methods for detection and analysis. Microbiological reviews. 1995;59(1):94-123.
136. Jensen EC. The basics of western blotting. Anatomical record (Hoboken, NJ : 2007). 2012;295(3):369-71.
137. Alegria-Schaffer A, Lodge A, Vattem K. Performing and optimizing Western blots with an emphasis on chemiluminescent detection. Methods in enzymology. 2009;463:573-99.
138. Cohen J. Statistical Power Analysis for the Behavioral Sciences: Taylor & Francis; 2013.
139. Freshney RI. Specialized Cells. Culture of Animal Cells: John Wiley & Sons, Inc.; 2010. p. 383-432.
140. Freshney RI. Introduction. Culture of Animal Cells: John Wiley & Sons, Inc.; 2010. p. 1-10.
141. Freshney RI. Defined Media and Supplements. Culture of Animal Cells: John Wiley & Sons, Inc.; 2010. p. 99-114.
142. Masters JR. Human cancer cell lines: fact and fantasy. Nature reviews Molecular cell biology. 2000;1(3):233-6.
143. Naylor LH. Reporter gene technology: the future looks bright. Biochemical pharmacology. 1999;58(5):749-57.
144. Kozera B, Rapacz M. Reference genes in real-time PCR. Journal of applied genetics. 2013;54(4):391-406.
145. Gong H, Sun L, Chen B, Han Y, Pang J, Wu W, et al. Evaluation of candidate reference genes for RT-qPCR studies in three metabolism related tissues of mice after caloric restriction. Scientific reports. 2016;6:38513.
146. Arya M, Shergill IS, Williamson M, Gommersall L, Arya N, Patel HR. Basic principles of real-time quantitative PCR. Expert review of molecular diagnostics. 2005;5(2):209-19.
147. Yamashita H, Takenoshita M, Sakurai M, Bruick RK, Henzel WJ, Shillinglaw W, et al. A glucose-responsive transcription factor that regulates carbohydrate metabolism in the liver. Proceedings of the National Academy of Sciences of the United States of America. 2001;98(16):9116-21.
148. Poupeau A, Postic C. Cross-regulation of hepatic glucose metabolism via ChREBP and nuclear receptors. Biochimica et biophysica acta. 2011;1812(8):995-1006.
149. Berggard T, Linse S, James P. Methods for the detection and analysis of protein-protein interactions. Proteomics. 2007;7(16):2833-42.
150. Witte N, Muenzner M, Rietscher J, Knauer M, Heidenreich S, Nuotio-Antar AM, et al. The Glucose Sensor ChREBP Links De Novo Lipogenesis to PPARgamma Activity and Adipocyte Differentiation. Endocrinology. 2015;156(11):4008-19.
151. Streiner DL. Best (but oft-forgotten) practices: the multiple problems of multiplicity-whether and how to correct for many statistical tests. The American journal of clinical nutrition. 2015;102(4):721-8.
152. Bindesbøll C, Fan Q, Nørgaard RC, MacPherson L, Ruan HB, Wu J, et al. Liver X receptor regulates hepatic nuclear O-GlcNAc signaling and carbohydrate responsive element-binding protein activity. Journal of lipid research. 2015;56(4):771-85.
153. Fan Q, Nørgaard RC, Bindesbøll C, Lucas C, Dalen KT, Babaie E, et al. LXRalpha Regulates Hepatic ChREBPalpha Activity and Lipogenesis upon Glucose, but Not Fructose Feeding in Mice. Nutrients. 2017;9(7).
154. Boergesen M, Pedersen TA, Gross B, van Heeringen SJ, Hagenbeek D, Bindesboll C, et al. Genome-wide profiling of liver X receptor, retinoid X receptor, and peroxisome proliferator-activated receptor alpha in mouse liver reveals extensive sharing of binding sites. Molecular and cellular biology. 2012;32(4):852-67.
155. Jois T, Howard V, Youngs K, Cowley MA, Sleeman MW. Dietary Macronutrient Composition Directs ChREBP Isoform Expression and Glucose Metabolism in Mice. PloS one. 2016;11(12):e0168797.
156. Wang Y, Guo T, Zhao S, Li Z, Mao Y, Li H, et al. Expression of the Human Glucokinase Gene: Important Roles of the 5′ Flanking and Intron 1 Sequences. PloS one. 2012;7(9):e45824.

157. Mitro N, Mak PA, Vargas L, Godio C, Hampton E, Molteni V, et al. The nuclear receptor LXR is a glucose sensor. Nature. 2007;445(7124):219-23.
158. Lazar MA, Willson TM. Sweet dreams for LXR. Cell metabolism. 2007;5(3):159-61.
159. Powell EE, Kroon PA. Low density lipoprotein receptor and 3-hydroxy-3-methylglutaryl coenzyme A reductase gene expression in human mononuclear leukocytes is regulated coordinately and parallels gene expression in human liver. The Journal of clinical investigation. 1994;93(5):2168-74.
160. Bouwens M, Afman LA, Muller M. Fasting induces changes in peripheral blood mononuclear cell gene expression profiles related to increases in fatty acid beta-oxidation: functional role of peroxisome proliferator activated receptor alpha in human peripheral blood mononuclear cells. The American journal of clinical nutrition. 2007;86(5):1515-23.
161. Spartano NL, Lamon-Fava S, Matthan NR, Ronxhi J, Greenberg AS, Obin MS, et al. Regulation of ATP-binding Cassette Transporters and Cholesterol Efflux by Glucose in Primary Human Monocytes and Murine Bone Marrow-derived Macrophages. Experimental and clinical endocrinology & diabetes : official journal, German Society of Endocrinology [and] German Diabetes Association. 2014;122(8):463-8.
162. Hubler MJ, Kennedy AJ. Role of lipids in the metabolism and activation of immune cells. The Journal of nutritional biochemistry. 2016;34:1-7.
163. MacIver NJ, Jacobs SR, Wieman HL, Wofford JA, Coloff JL, Rathmell JC. Glucose metabolism in lymphocytes is a regulated process with significant effects on immune cell function and survival. Journal of Leukocyte Biology. 2008;84(4):949-57.
164. Karunakaran U, Jeoung NH. O-GlcNAc Modification: Friend or Foe in Diabetic Cardiovascular Disease. Korean diabetes journal. 2010;34(4):211-9.
165. Meng J, Feng M, Dong W, Zhu Y, Li Y, Zhang P, et al. Identification of HNF-4alpha as a key transcription factor to promote ChREBP expression in response to glucose. Scientific reports. 2016;6:23944.
166. Caron S, Huaman Samanez C, Dehondt H, Ploton M, Briand O, Lien F, et al. Farnesoid X receptor inhibits the transcriptional activity of carbohydrate response element binding protein in human hepatocytes. Molecular and cellular biology. 2013;33(11):2202-11.
167. Kalaany NY, Mangelsdorf DJ. LXRS and FXR: the yin and yang of cholesterol and fat metabolism. Annual review of physiology. 2006;68:159-91.
168. Zhang D, Tong X, VanDommelen K, Gupta N, Stamper K, Brady GF, et al. Lipogenic transcription factor ChREBP mediates fructose-induced metabolic adaptations to prevent hepatotoxicity. The Journal of clinical investigation. 2017;127(7):2855-67.
169. Wang Y, Viscarra J, Kim SJ, Sul HS. Transcriptional regulation of hepatic lipogenesis. Nature reviews Molecular cell biology. 2015;16(11):678-89.
170. Weedon-Fekjaer MS, Dalen KT, Solaas K, Staff AC, Duttaroy AK, Nebb HI. Activation of LXR increases acyl-CoA synthetase activity through direct regulation of ACSL3 in human placental trophoblast cells. Journal of lipid research. 2010;51(7):1886-96.

Appendix I: Materials, equipment and software

Reagents and kits	Manufacturer	Cat. no
2-mercaptoethanol	Sigma-Aldrich	7522
ALLN	Calbiochem	208719-5
Ampicillin sodium salt	Sigma-Aldrich	A0166
β-glycerophosphate	Sigma-Aldrich	G9422
BglII	New England Biolabs, Inc.	R0144S
Bovine serum albumin	Sigma-Aldrich	A8806
cOmplete™ protease inhibitor cocktail	Roche Applied Science	
Dimethyl sulfoxide (DMSO)	Sigma-Aldrich	D2650
Dithiothreitol (DTT)	Bio-Rad	161-0611
DNA Ladder, 1 Kb Plus	Invitrogen™	10787018
DpnI	New England Biolabs, Inc.	R0176S
Dual-Luciferase® Reporter Assay System kit	Promega	E1960
Dulbecco's modified Eagle's medium with L-Gln	Lonza	12-604F
Dulbecco's modified Eagle's medium, no glucose	Thermo Fisher Scientific	11966025
Dynabeads™ Protein A	Thermo Fisher Scientific	10001D
Fetal bovine serum	Sigma-Aldrich	F7524
Glucose solution, 100 g/L	Sigma-Aldrich	G8644
Glycerol	Sigma-Aldrich	G7793
GW3965 hydrochloride	Sigma-Aldrich	G629
Hepes buffer solution, 1 M	Sigma-Aldrich	59205C
High-Capacity cDNA Reverse Transcription Kit	Applied Biosystems™	4368814
HindIII	Promega	R6041
IGEPAL® CA-630	Sigma-Aldrich	I8896
KAPA SYBR FAST Universal	Kapa Biosystems	KK4601
L-Glutamine solution, 200 mM	Sigma-Aldrich	G7513
Lipofectamine® 2000 Reagent	Invitrogen™	11668019
MetaPhor™ Agarose	Lonza	50181
Methanol	Merck	1060091000
NEBuffer 3.1 (10×)	New England Biolabs, Inc.	B7203S
Nucleobond ® Xtra Maxi Plus kit	Macherey-Nagel	740416
NucleoSpin® Gel and PCR Clean-up kit	Macherey-Nagel	740609
NucleoSpin® Plasmid kit	Macherey-Nagel	740588
Penicillin-Streptomycin	Sigma-Aldrich	P4458
PMSF	Thermo Fisher Scientific	36978
Precision Plus Protein™ All Blue Standards	Bio-Rad	161-0373
Precision Plus Protein™ Dual Color Standards	Bio-Rad	161-0374
Purified BSA (100×)	New England Biolabs	B9001S
Restore™ PLUS Western Blot Stripping Buffer	Thermo Fisher Scientific	46430
RNA 6000 Nano Kit	Agilent Technologies	5067-1511
RNeasy® Mini Kit	Qiagen	74104
Skim milk powder	Sigma-Aldrich	70166
Sodium azide	Sigma-Aldrich	S8032
Sodium fluoride (NAF)	Fluka	71519
Sodium orthovanadate (Na2VO4)	Sigma-Aldrich	56508
Sodium pyruvate	Sigma-Aldrich	P5280

SuperSignal™ West Dura Extended Duration Substrate	Thermo Fisher Scientific	34076
SuperSignal™ West Pico PLUS Chemiluminescent Substrate	Thermo Fisher Scientific	34080
SYBR™ safe DNA Gel Stain	Invitrogen™	S33102
T4 DNA ligase	New England Biolabs	M0202S
T4 DNA ligase buffer	New England Biolabs	B0202S
Thiamet G	Sigma-Aldrich	SML0244
Tryphan Blue Stain 0.4 %	Invitrogen™	T10282
Trypsin-EDTA Solution	Sigma-Aldrich	T3924
Tween®20	Sigma-Aldrich	P1379

Equipment	**Manufacturer**	**Cat. no**
Biosphere Filter tips - 10 µL - 100 µL - 300 µL - 1000 µL	Sarstedt	 70.1131.210 70.760.212 70.765.210 70.762.211
Cell culture flasks - 25 cm^2 - 75 cm^2	Corning Inc., Falcon™	 353108 353136
Cell culture plates - 6 wells - 12 wells - 24 wells	Corning Inc., Falcon™	 353046 353043 353047
Cell scraper, 16 cm	Sarstedt	83.1832
Countess™ Cell Counting Chamber Slides	Invitrogen™	C10228
Criterion™ Tris-HCl Precast Gel - 10 %, 12+2 well - 4-20 %, 18 well	Bio-Rad	 3450009 3450033
Immobilion-P transfer membrane	Sigma-Aldrich	IPVH00010
Microcentrifuge tube - 1.5 mL - 2.0 mL	Axygen™ Scientific	 311-08-051
Nunc™ F96 MicroWell™ White Polystyrene Plate	Thermo Fischer Scientific	136101
Polypropylene conical centrifuge tubes - 15 mL - 50 mL	Corning Inc., Falcon™	 352095 352070
qPCR 96-well plate non-skirted, low profile, frosted	Eurogentec	RT-PL96-OP
qPCR optical adheasive seals	Eurogentec	RT-OPSL-100
Serological pipettes - 5 mL - 10 mL - 25 mL	Sarstedt	 86.1253.001 86.1254.001 86.1685.001
Sterican® cannulas 21G (0.8×40 mm)	B. Braun Medical	612-0142
Syringe, 2 mL	Terumo	SS-03S
Thick filter paper, Precut, 7.5×10 cm	Bio-Rad	1703932

Instruments	Manufacturer
2100 Bioanalyzer	Agilent Technologies
Avanti J-26XP centrifuge	Beckman Coulter
CFX96 Touch™ Real-Time PCR Detection Systems	Bio-Rad Laboratories
ChemiDoc™ XRS+ System	Bio-Rad
Countess™ Automated Cell Counter	Invitrogen™
Criterion™ Cell system	Bio-Rad Laboratories
Forma™ Steri-Cycle™ CO2 Incubator	Thermo Fischer Scientific
Heraeus Multifuge 3+ Centrifuge	Thermo Fischer Scientific
Heraeus Pico21 Centrifuge	Thermo Fischer Scientific
LD-76 rotator	Labinco BV
NanoDrop®ND-1000 spectrophotometer	NanoDrop Technologies
New Brunswick™ I26 incubator	Eppendorf®
Olympus CKX41 inverted microscope	Olympus®
PowerPac™ Basic Power Supply	Bio-Rad Laboratories
Spectrafuge™ Mini	Labnet International Inc.
Stuart SRT9D roller mixer	Cole-Parmer
Stuart SSL4 see-saw rocker	Cole-Parmer
Sub-Cell® GT Horizontal Electrophoresis System	Bio-Rad Laboratories
Synergy 2 Multi-Mode Reader	Bio-Tek® Instruments
Thermomixer® comfort	Eppendorf®
Veriti™ 96 Well Thermal Cycler	Applied Biosystems™
Vortex-Genie 2	Scientific Industries, Inc.

Software	Manufacturer
Adobe Illustrator CS6	Adobe Systems Inc.
Adobe Photoshop CS6	Adobe Systems Inc.
Bio-Rad CFX Manager 3.1	Bio-Rad Laboratories
CLC Sequence Viewer	Qiagen
EndNote X8.1 (Build 11010)	EndNote
Prism 7	GraphPad Software Inc.
IBM® SPSS® Statistics v.25	IBM Corporation
Image Lab ™ Software 6.0	Bio-Rad Laboratories
Microsoft Office Plus 2010	Microsoft Corporation
NanoDrop 1000 Operating Software (ND-1000) v.3.8.1	NanoDrop Technologies
Serial Cloner 2.6.1	Serial Basics

Appendix II: Antibodies

Primary antibodies	Manufacturer	Cat. No
ChREBP	Novus Biologicals	NB400-135
FLAG-tag	Sigma-Aldrich	F7425
LXRα LBD	R&D systems	PP-PP20412-00
V5-tag, mouse	Thermo Fisher Scientific	37-7500
Secondary antibodies		
HRP-conjugated Goat anti-mouse IgG	Jackson ImmunoResearch Laboratories	115-035-174

Appendix III: Buffers and reagents recipes

TE buffer 0.79 g Trizma® Hcl (MW=157.60 g/mol) 0.186 g EDTA $2H_2O$ (MW=372,24 g/mol) 450 ml dH_2O Adjust pH to 8.0 with NaOH dH2O to 500 ml	**SDS-PAGE running buffer (10×)** 250 mM Tris 30 g 1.92 M Glycine 144 g 1 % SDS 10 g dH_2O to 1 L
Lysis buffer (CoIP) 200 mM NaCl 20 mM Hepes pH 7.4 1% NP40 2× Protease inhibitor (PIC) and 1x ALLN. Phosphatase/GlcNAcase inhibitors etc. if needed	**10× Towbin buffer (Transfer buffer)** 30 g 250 mM Tris 144 g 1920 mM glycine dH_2O to 1 L
Wash buffer (CoIP) 200 mM NaCl 20 mM Hepes pH 7.4 0.1% NP40 1× Protease inhibitor (PIC)	**1× transfer buffer** 200 ml 10× Towbin buffer 1600 ml dH_2O 200 ml methanol
1× Laemmli sample buffer (Bio-Rad) 62. 5 mM Tris-HCl 10 % glycerol 2 % SDS 0.01 % Bromphenol Blue dH_2O 100 mM DTT	**Blocking solution** 3 % BSA or 3% milk powder, 3 g TBS-T to 100 ml
10× TBS 200 mM Tris base (Mw=121.14) 24 g 1370 mM NaCl 80.15 g dH_2O to 1 L Adjust pH to 7.5 with approximately 38 ml 1M HCl, then add up to 1l with dH_2O	**TBS-T** 10× TBS 100 ml 0.1 % Tween-20 1 ml dH_2O to 1 L
50× TAE buffer 242g Tris base 750ml ddH2O, mix until completely dissolved 100ml 0.5M EDTA 57.1ml anhydrous acetic acid Adjust pH 8.2 - 8.4, then add up to 1 L with ddH2O	

Appendix IV: DNA plasmids

Empty vectors	Description	Ref.
pCDNA3.1(+)	Mammalian expression vector with CMV promoter. Bought from Life Technologies, cat.no V79020.	
pCMV4 empty	Mammalian expression vector with CMV promoter.	(41)
Reporters		
pGL3b-mChREBPbeta-Exon-1B	Wild-type mChrebpbeta-driven luciferase reporter.	(41)
pGL3b-mChREBPbeta-Exon-1B DR4-del	Mutated from pGL3b-mChREBPbeta-Exon-1B, where the DR4 is deleted. Cloned in this project.	
pGL3b-mChREBPbeta-Exon-1B-E-box-del	Mutated from pGL3b-mChREBPbeta-Exon-1B, where the E-box is deleted. Cloned in this project.	
pGL3b-mChREBPbeta-Exon-1B-ChoREdel	Mutated from pGL3b-mChREBPbeta-Exon-1B, where the ChoRE is deleted.	(41)
pGL3b-mChREBPbeta-Exon-1B-ChoRE-E-box-del	Mutated from pGL3b-mChREBPbeta-Exon-1B, where the ChoRE and the E-box is deleted.	(41)
pRL-CMV	Mammalian *Renilla* luciferase co-reporter control plasmid with constitutive CMV promoter	
Expression plasmids		
pcDNA3-FLAG-hLXRα	FLAG-tagged hLXRalpha expression vector.	(76)
pcDNA3-FLAG-hRXRα	FLAG-tagged hRXRalpha expression vector.	(170)
pCMV4-FLAG-mChREBP-LID	Cloned in this project.	
pCMV4-FLAG-mCHREBPalpha	Cloned from GenBank: AF245475.1 with one base swap (lower letter)	(41)
pCMV4-HA-mMLXγ	HA-tagged mMLXgamma expression vector.	

Appendix V: Primer sequences

qPCR primers

Human target gene (GenBank acc. no.)	Primer sequence (5' → 3')		Amplicon (bp)	Ref.
CHREBPA *(MLXIPL v1)*	F	TTGTTCAGGCGGATCTTGTC	100	(41)
	R	AGTGCTTGAGCCTGGCCTAC		
CHREBPB *(MLXIPL v2)*	F	AGCGGATTCCAGGTGAGG	119	(41)
	R	TTGTTCAGGCGGATCTTGTC		
FASN (NM_004104.4)	F	GCAAATTCGACCTTTCTCAGAAC	71	
	R	AGTAGGACCCCGTGGAATGTC		
LXRA (NM_005693.3)	F	TGCATGCCTACGTCTCCATC	111	
	R	ACACTTGCTCTGAGTGGACG		
PKLR1 (NM_000298.5)	F	CCCAATATTGTCCGGGTCGT	89	
	R	TCTGGGCCGATTTTCTGGAC		
SREBF1 c (NM_001005291.2)	F	GGAGCCATGGATTGCACTTT	124	
	R	GTCAAATAGGCCAGGGAAGTCA		
TBP (NM_003194.4)	F	TTGTACCGCAGCTGCAAAAT	96	
	R	TATATTCGGCGTTTCGGGCA		

Sequencing primers

Plasmid target	Primer sequence (5' → 3')		Ref.
pGL3 basic vector	F	CTAGCAAAATAGGCTGTCCC	
	R	CTTTATGTTTTTGGCGTCTTCCA	
pCMV5	F	CGTTGACGCAAATGGGCGG	
	R	CCTCCACCCATAATATTATAG	
FLAG-LID	F	AATTCAGATCTATGGACTACAAGG	
	R	ATTCAAGCTTACATCACCACCTCGATGCGC	
mCHR-DR4del	F	GTCTGCTCTACCCTGAGTCCTCCCTAAGCTTCTC TTCTCTTC	
	R	GAAGAGAAGAGAAGCTTAGGGAGGACTCAGGGT AGAGCAGAC	
mCHR-Eboxdel	F	GTGCCTCCTTCTCTCCTTAGGATGGCAGCCGCTC CTCAGGC	
	R	GCCTGAGGAGCGGCTGCCATCCTAAGGAGAGAA GGAGGCAC	

Appendix VI: Sequence chromatogram, pGL3b-mChREBPbeta-Exon-1B-DR4-del

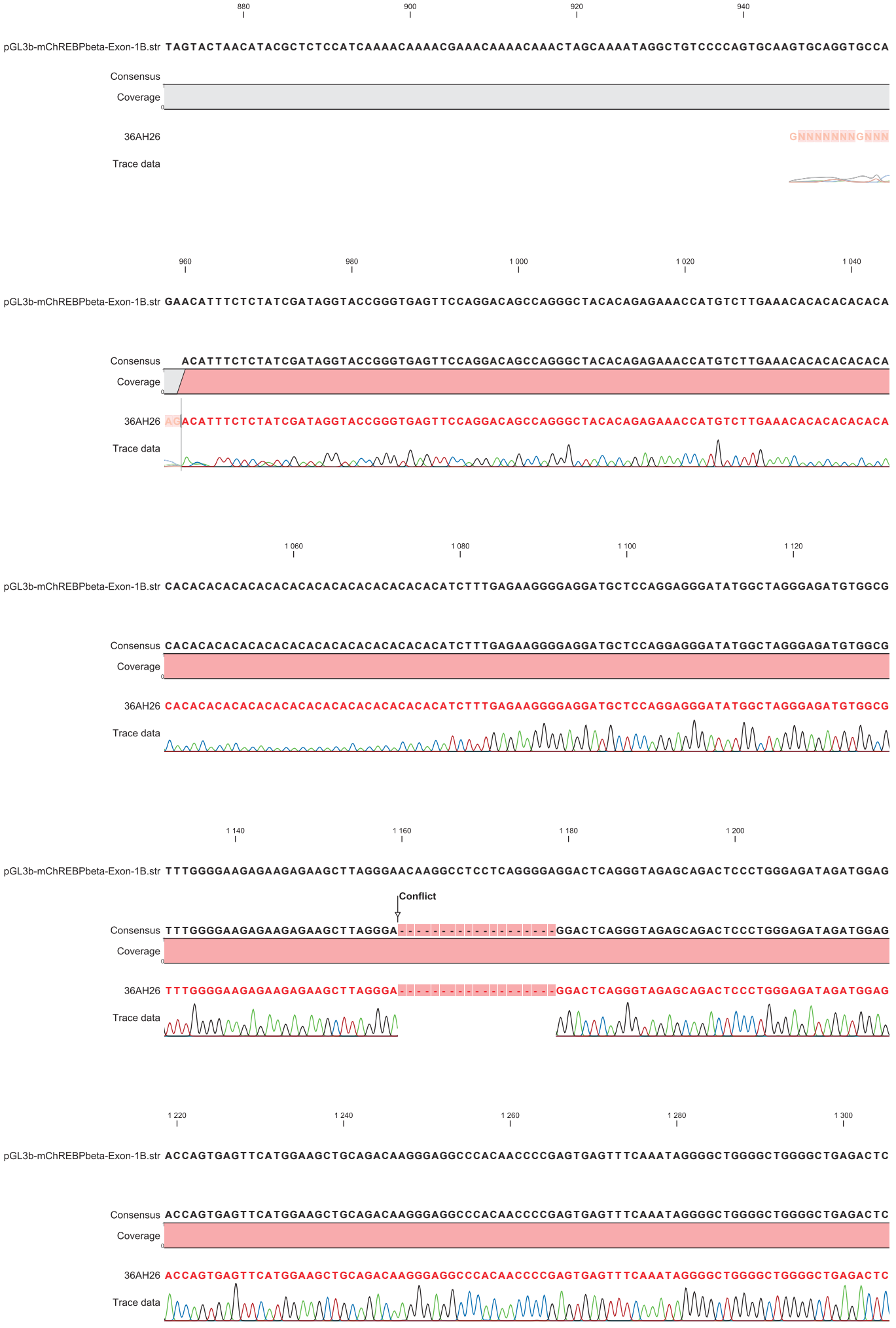

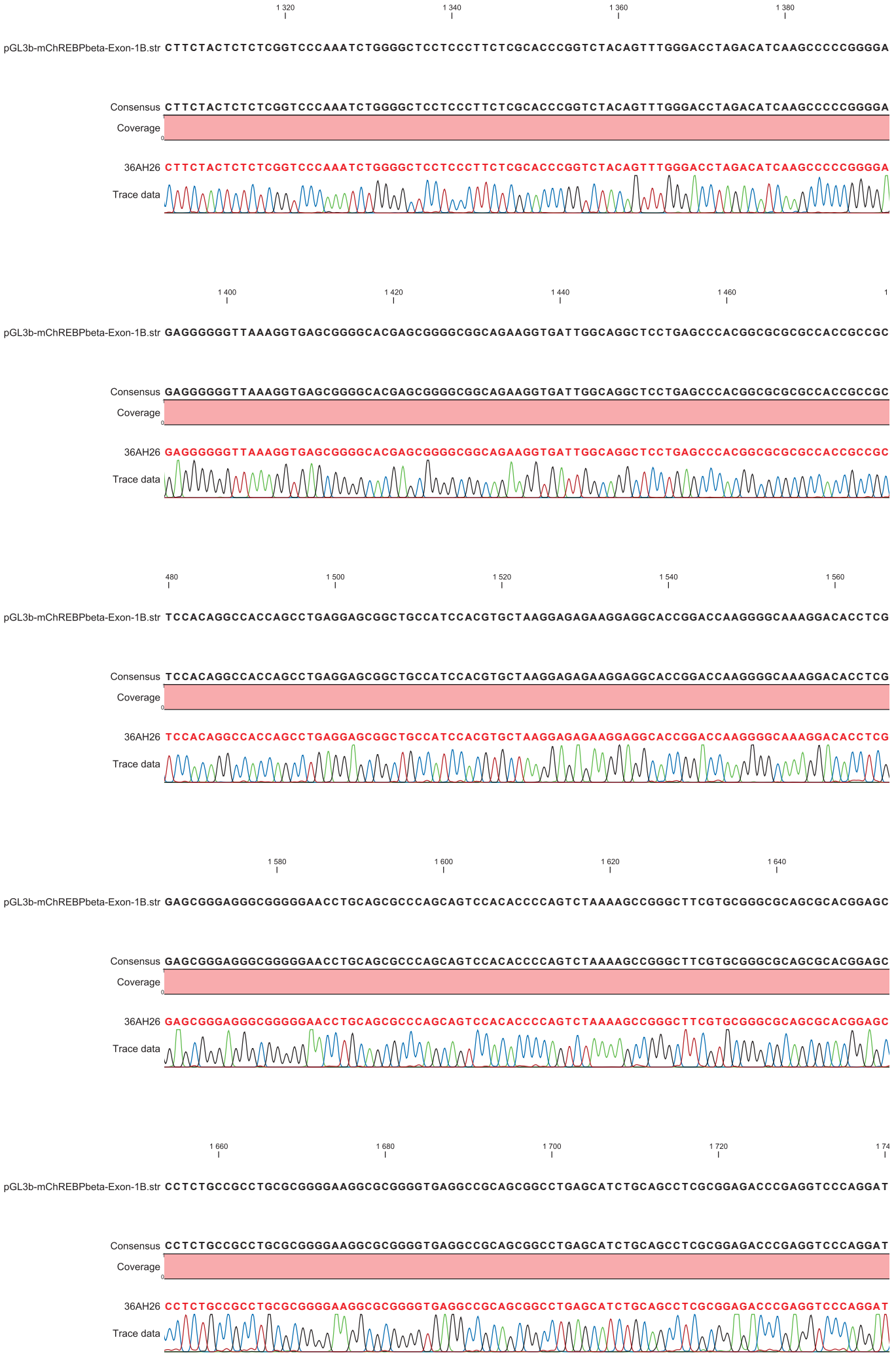
1 320
1 340
1 360
1 380
pGL3b-mChREBPbeta-Exon-1B.str CTTCTACTCTCTCGGTCCCAAATCTGGGGCTCCTCCCTTCTCGCACCCGGTCTACAGTTTGGGACCTAGACATCAAGCCCCCGGGGA
Consensus CTTCTACTCTCTCGGTCCCAAATCTGGGGCTCCTCCCTTCTCGCACCCGGTCTACAGTTTGGGACCTAGACATCAAGCCCCCGGGGA
Coverage
0
36AH26 CTTCTACTCTCTCGGTCCCAAATCTGGGGCTCCTCCCTTCTCGCACCCGGTCTACAGTTTGGGACCTAGACATCAAGCCCCCGGGGA
Trace data
1 400
1 420
1 440
1 460
1
pGL3b-mChREBPbeta-Exon-1B.str GAGGGGGGTTAAAGGTGAGCGGGGCACGAGCGGGGCGGCAGAAGGTGATTGGCAGGCTCCTGAGCCCACGGCGCGCGCCACCGCCGC
Consensus GAGGGGGGTTAAAGGTGAGCGGGGCACGAGCGGGGCGGCAGAAGGTGATTGGCAGGCTCCTGAGCCCACGGCGCGCGCCACCGCCGC
Coverage
0
36AH26 GAGGGGGGTTAAAGGTGAGCGGGGCACGAGCGGGGCGGCAGAAGGTGATTGGCAGGCTCCTGAGCCCACGGCGCGCGCCACCGCCGC
Trace data
480
1 500
1 520
1 540
1 560
pGL3b-mChREBPbeta-Exon-1B.str TCCACAGGCCACCAGCCTGAGGAGCGGCTGCCATCCACGTGCTAAGGAGAGAAGGAGGCACCGGACCAAGGGGCAAAGGACACCTCG
Consensus TCCACAGGCCACCAGCCTGAGGAGCGGCTGCCATCCACGTGCTAAGGAGAGAAGGAGGCACCGGACCAAGGGGCAAAGGACACCTCG
Coverage
0
36AH26 TCCACAGGCCACCAGCCTGAGGAGCGGCTGCCATCCACGTGCTAAGGAGAGAAGGAGGCACCGGACCAAGGGGCAAAGGACACCTCG
Trace data
1 580
1 600
1 620
1 640
pGL3b-mChREBPbeta-Exon-1B.str GAGCGGGAGGGCGGGGGAACCTGCAGCGCCCAGCAGTCCACACCCCAGTCTAAAAGCCGGGCTTCGTGCGGGCGCAGCGCACGGAGC
Consensus GAGCGGGAGGGCGGGGGAACCTGCAGCGCCCAGCAGTCCACACCCCAGTCTAAAAGCCGGGCTTCGTGCGGGCGCAGCGCACGGAGC
Coverage
0
36AH26 GAGCGGGAGGGCGGGGGAACCTGCAGCGCCCAGCAGTCCACACCCCAGTCTAAAAGCCGGGCTTCGTGCGGGCGCAGCGCACGGAGC
Trace data
1 660
1 680
1 700
1 720
1 74
pGL3b-mChREBPbeta-Exon-1B.str CCTCTGCCGCCTGCGCGGGGAAGGCGCGGGGTGAGGCCGCAGCGGCCTGAGCATCTGCAGCCTCGCGGAGACCCGAGGTCCCAGGAT
Consensus CCTCTGCCGCCTGCGCGGGGAAGGCGCGGGGTGAGGCCGCAGCGGCCTGAGCATCTGCAGCCTCGCGGAGACCCGAGGTCCCAGGAT
Coverage
0
36AH26 CCTCTGCCGCCTGCGCGGGGAAGGCGCGGGGTGAGGCCGCAGCGGCCTGAGCATCTGCAGCCTCGCGGAGACCCGAGGTCCCAGGAT
Trace data

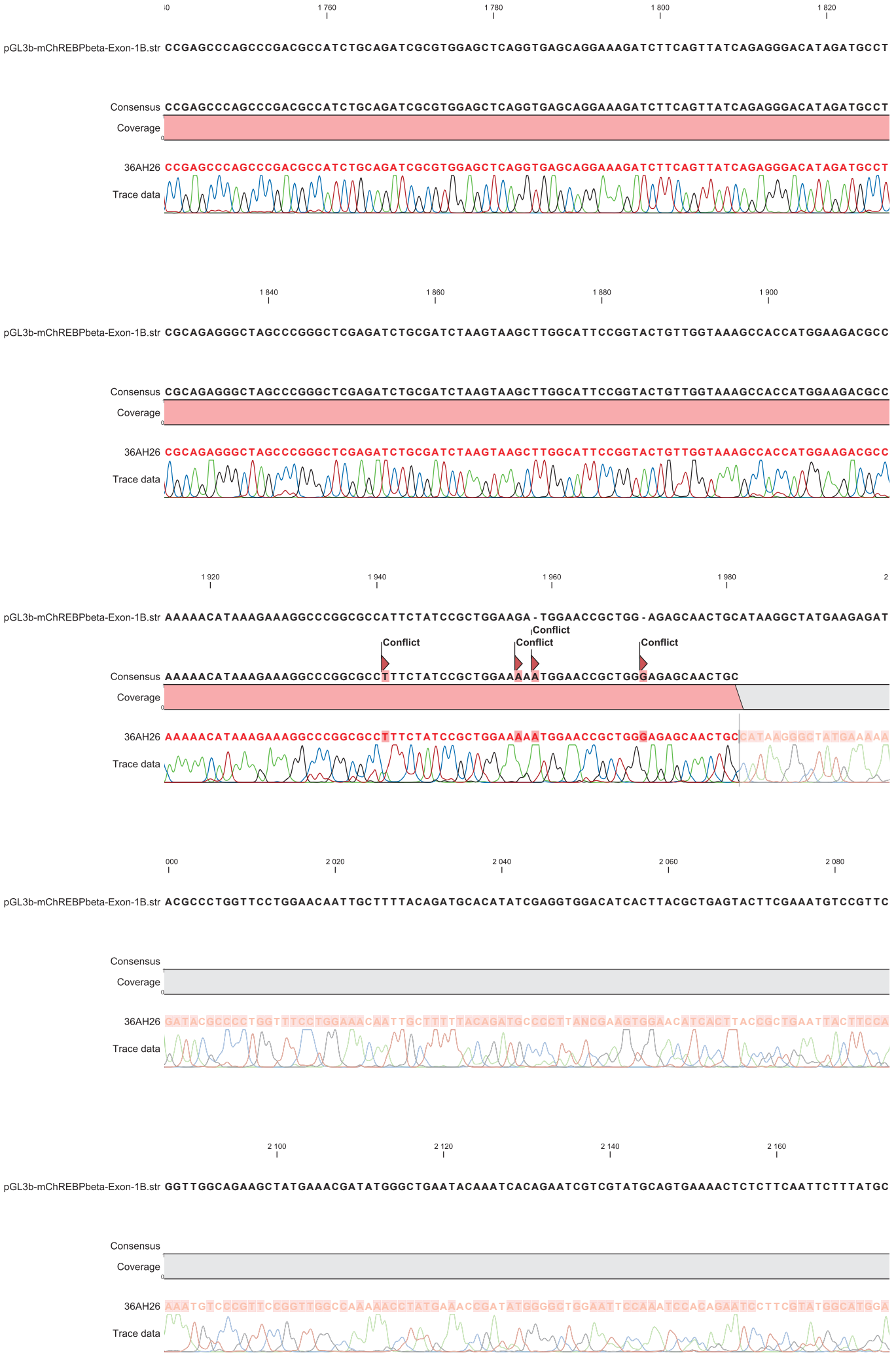
1 760
1 780
1 800
1 820
pGL3b-mChREBPbeta-Exon-1B.str CCGAGCCCAGCCCGACGCCATCTGCAGATCGCGTGGAGCTCAGGTGAGCAGGAAAGATCTTCAGTTATCAGAGGGACATAGATGCCT
Consensus CCGAGCCCAGCCCGACGCCATCTGCAGATCGCGTGGAGCTCAGGTGAGCAGGAAAGATCTTCAGTTATCAGAGGGACATAGATGCCT
Coverage
36AH26 CCGAGCCCAGCCCGACGCCATCTGCAGATCGCGTGGAGCTCAGGTGAGCAGGAAAGATCTTCAGTTATCAGAGGGACATAGATGCCT
Trace data
1 840
1 860
1 880
1 900
pGL3b-mChREBPbeta-Exon-1B.str CGCAGAGGGCTAGCCCGGGCTCGAGATCTGCGATCTAAGTAAGCTTGGCATTCCGGTACTGTTGGTAAAGCCACCATGGAAGACGCC
Consensus CGCAGAGGGCTAGCCCGGGCTCGAGATCTGCGATCTAAGTAAGCTTGGCATTCCGGTACTGTTGGTAAAGCCACCATGGAAGACGCC
Coverage
36AH26 CGCAGAGGGCTAGCCCGGGCTCGAGATCTGCGATCTAAGTAAGCTTGGCATTCCGGTACTGTTGGTAAAGCCACCATGGAAGACGCC
Trace data
1 920
1 940
1 960
1 980
2
pGL3b-mChREBPbeta-Exon-1B.str AAAAACATAAAGAAAGGCCCGGCGCCATTCTATCCGCTGGAAGA - TGGAACCGCTGG - AGAGCAACTGCATAAGGCTATGAAGAGAT
Conflict
Conflict
Conflict
Conflict
Consensus AAAAACATAAAGAAAGGCCCGGCGCCTTTCTATCCGCTGGAAAAATGGAACCGCTGGGAGAGCAACTGC
Coverage
36AH26 AAAAACATAAAGAAAGGCCCGGCGCCTTTCTATCCGCTGGAAAAATGGAACCGCTGGGAGAGCAACTGCCATAAGGGCTATGAAAAA
Trace data
000
2 020
2 040
2 060
2 080
pGL3b-mChREBPbeta-Exon-1B.str ACGCCCTGGTTCCTGGAACAATTGCTTTTACAGATGCACATATCGAGGTGGACATCACTTACGCTGAGTACTTCGAAATGTCCGTTC
Consensus
Coverage
36AH26 GATACGCCCCTGGTTTCCTGGAAACAATTGCTTTTACAGATGCCCCTTANCGAAGTGGAACATCACTTACGCTGAATTACTTCCA
Trace data
2 100
2 120
2 140
2 160
pGL3b-mChREBPbeta-Exon-1B.str GGTTGGCAGAAGCTATGAAACGATATGGGCTGAATACAAATCACAGAATCGTCGTATGCAGTGAAAACTCTCTTCAATTCTTTATGC
Consensus
Coverage
36AH26 AAATGTCCCGTTCCGGTTGGCCAAAAACCTATGAAACCGATATGGGGCTGGAATTCCAAATCCACAGAATCCTTCGTATGGCATGGA
Trace data

Appendix VII: Sequence chromatogram, pGL3b-mChREBPbeta-Exon-1B-Ebox-del

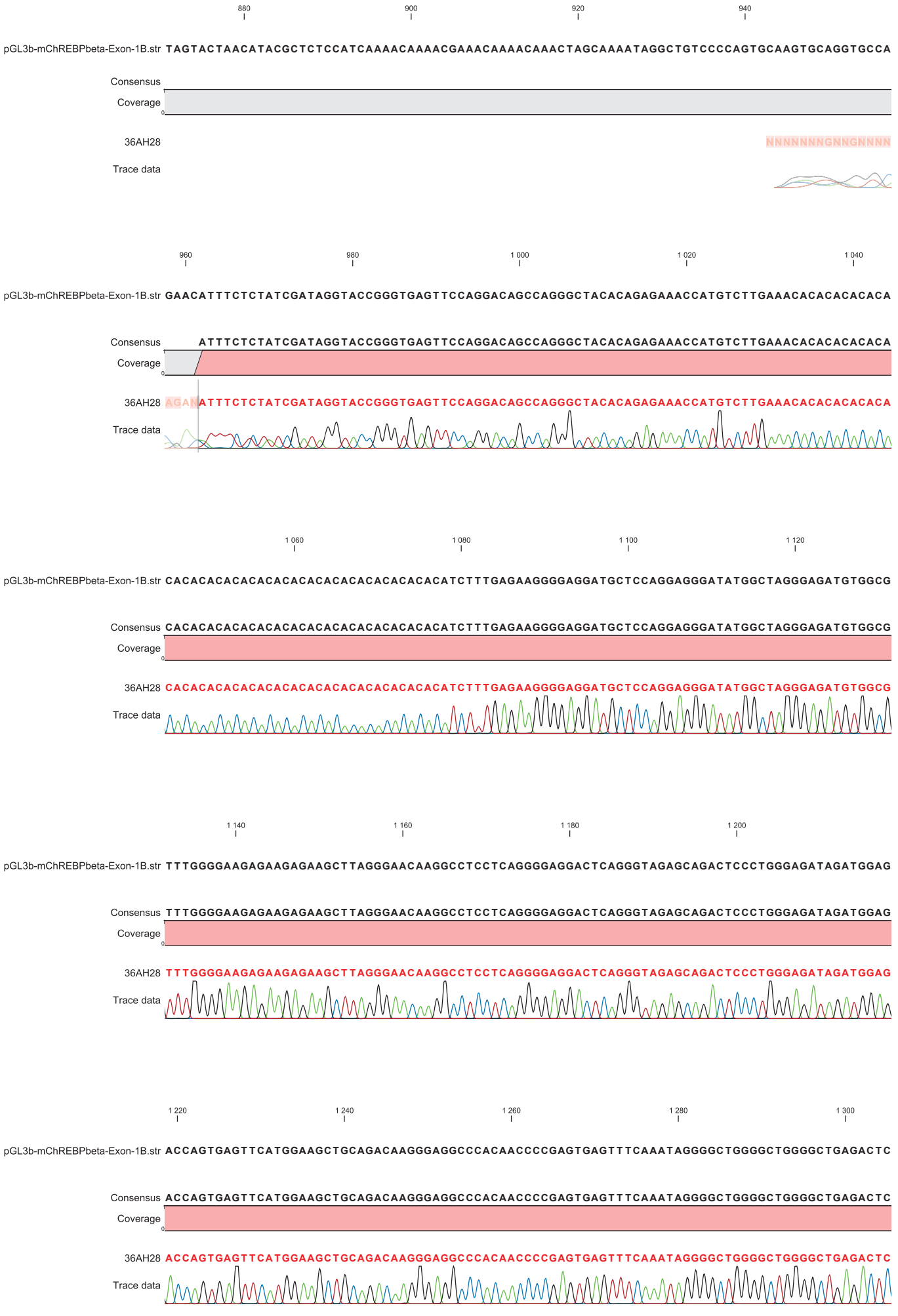

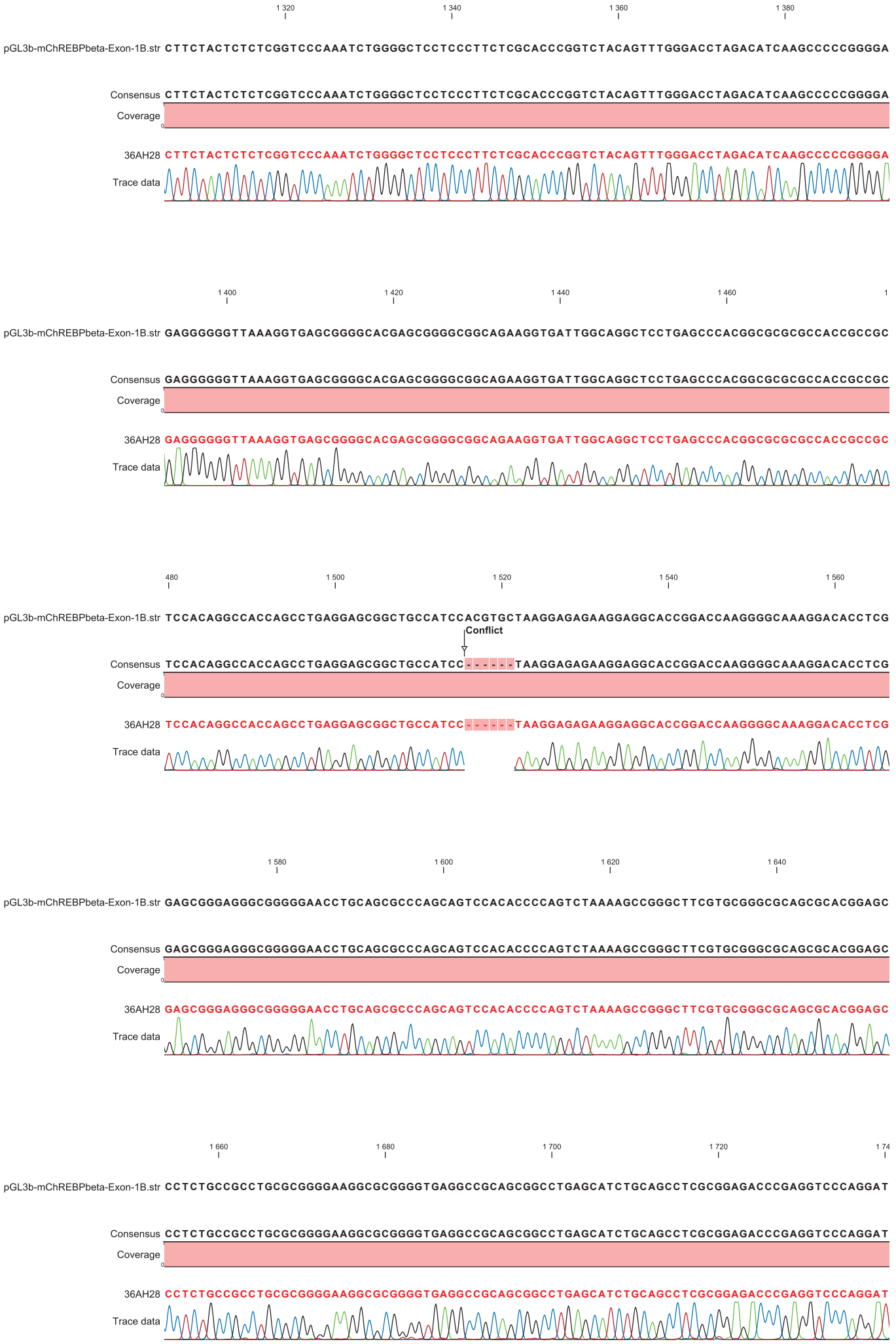
1 320
1 340
1 360
1 380
pGL3b-mChREBPbeta-Exon-1B.str CTTCTACTCTCTCGGTCCCAAATCTGGGGCTCCTCCCTTCTCGCACCCGGTCTACAGTTTGGGACCTAGACATCAAGCCCCCGGGGA
Consensus CTTCTACTCTCTCGGTCCCAAATCTGGGGCTCCTCCCTTCTCGCACCCGGTCTACAGTTTGGGACCTAGACATCAAGCCCCCGGGGA
Coverage
0
36AH28 CTTCTACTCTCTCGGTCCCAAATCTGGGGCTCCTCCCTTCTCGCACCCGGTCTACAGTTTGGGACCTAGACATCAAGCCCCCGGGGA
Trace data
1 400
1 420
1 440
1 460
1
pGL3b-mChREBPbeta-Exon-1B.str GAGGGGGGTTAAAGGTGAGCGGGGCACGAGCGGGGCGGCAGAAGGTGATTGGCAGGCTCCTGAGCCCACGGCGCGCGCCACCGCCGC
Consensus GAGGGGGGTTAAAGGTGAGCGGGGCACGAGCGGGGCGGCAGAAGGTGATTGGCAGGCTCCTGAGCCCACGGCGCGCGCCACCGCCGC
Coverage
0
36AH28 GAGGGGGGTTAAAGGTGAGCGGGGCACGAGCGGGGCGGCAGAAGGTGATTGGCAGGCTCCTGAGCCCACGGCGCGCGCCACCGCCGC
Trace data
480
1 500
1 520
1 540
1 560
pGL3b-mChREBPbeta-Exon-1B.str TCCACAGGCCACCAGCCTGAGGAGCGGCTGCCATCCACGTGCTAAGGAGAGAAGGAGGCACCGGACCAAGGGGCAAAGGACACCTCG
Conflict
Consensus TCCACAGGCCACCAGCCTGAGGAGCGGCTGCCATCC------TAAGGAGAGAAGGAGGCACCGGACCAAGGGGCAAAGGACACCTCG
Coverage
0
36AH28 TCCACAGGCCACCAGCCTGAGGAGCGGCTGCCATCC------TAAGGAGAGAAGGAGGCACCGGACCAAGGGGCAAAGGACACCTCG
Trace data
1 580
1 600
1 620
1 640
pGL3b-mChREBPbeta-Exon-1B.str GAGCGGGAGGGCGGGGGAACCTGCAGCGCCCAGCAGTCCACACCCCAGTCTAAAAGCCGGGCTTCGTGCGGGCGCAGCGCACGGAGC
Consensus GAGCGGGAGGGCGGGGGAACCTGCAGCGCCCAGCAGTCCACACCCCAGTCTAAAAGCCGGGCTTCGTGCGGGCGCAGCGCACGGAGC
Coverage
0
36AH28 GAGCGGGAGGGCGGGGGAACCTGCAGCGCCCAGCAGTCCACACCCCAGTCTAAAAGCCGGGCTTCGTGCGGGCGCAGCGCACGGAGC
Trace data
1 660
1 680
1 700
1 720
1 74
pGL3b-mChREBPbeta-Exon-1B.str CCTCTGCCGCCTGCGCGGGGAAGGCGCGGGGTGAGGCCGCAGCGGCCTGAGCATCTGCAGCCTCGCGGAGACCCGAGGTCCCAGGAT
Consensus CCTCTGCCGCCTGCGCGGGGAAGGCGCGGGGTGAGGCCGCAGCGGCCTGAGCATCTGCAGCCTCGCGGAGACCCGAGGTCCCAGGAT
Coverage
0
36AH28 CCTCTGCCGCCTGCGCGGGGAAGGCGCGGGGTGAGGCCGCAGCGGCCTGAGCATCTGCAGCCTCGCGGAGACCCGAGGTCCCAGGAT
Trace data

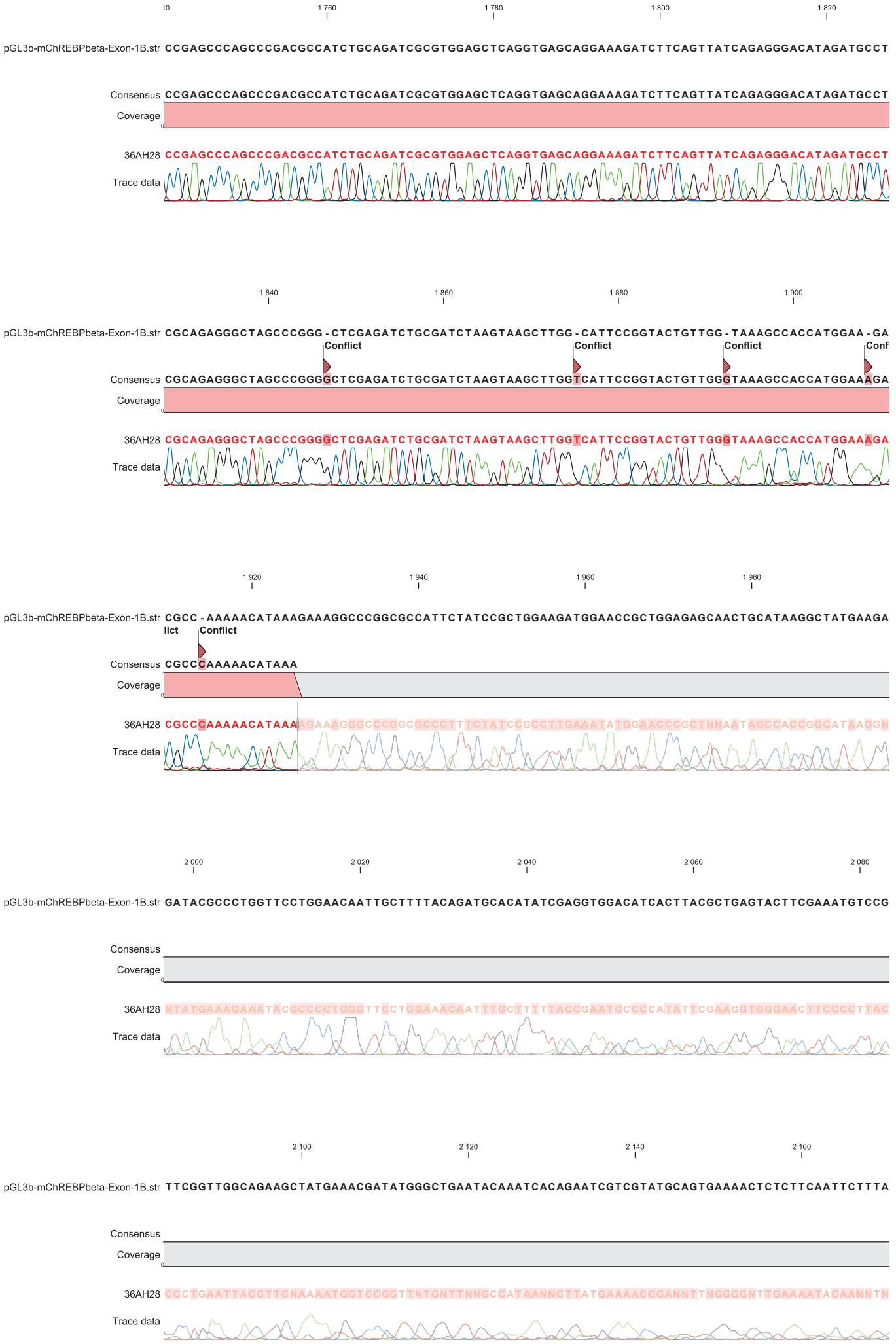
1 760
1 780
1 800
1 820
pGL3b-mChREBPbeta-Exon-1B.str CCGAGCCCAGCCCGACGCCATCTGCAGATCGCGTGGAGCTCAGGTGAGCAGGAAAGATCTTCAGTTATCAGAGGGACATAGATGCCT
Consensus CCGAGCCCAGCCCGACGCCATCTGCAGATCGCGTGGAGCTCAGGTGAGCAGGAAAGATCTTCAGTTATCAGAGGGACATAGATGCCT
Coverage
36AH28 CCGAGCCCAGCCCGACGCCATCTGCAGATCGCGTGGAGCTCAGGTGAGCAGGAAAGATCTTCAGTTATCAGAGGGACATAGATGCCT
Trace data
1 840
1 860
1 880
1 900
pGL3b-mChREBPbeta-Exon-1B.str CGCAGAGGGCTAGCCCGGG - CTCGAGATCTGCGATCTAAGTAAGCTTGG - CATTCCGGTACTGTTGG - TAAAGCCACCATGGAA - GA
Conflict
Conflict
Conflict
Conf
Consensus CGCAGAGGGCTAGCCCGGGGCTCGAGATCTGCGATCTAAGTAAGCTTGGTCATTCCGGTACTGTTGGGTAAAGCCACCATGGAAAGA
Coverage
36AH28 CGCAGAGGGCTAGCCCGGGGCTCGAGATCTGCGATCTAAGTAAGCTTGGTCATTCCGGTACTGTTGGGTAAAGCCACCATGGAAAGA
Trace data
1 920
1 940
1 960
1 980
pGL3b-mChREBPbeta-Exon-1B.str CGCC - AAAAACATAAAGAAAGGCCCGGCGCCATTCTATCCGCTGGAAGATGGAACCGCTGGAGAGCAACTGCATAAGGCTATGAAGA
lict
Conflict
Consensus CGCCCAAAAAACATAAA
Coverage
36AH28 CGCCCAAAAAACATAAAAGAAAGGGCCCGGCGCCCTTTCTATCGCCTTGAAATATGGAACCCGCTNNAATAGCCACCGGCATAAGGN
Trace data
2 000
2 020
2 040
2 060
2 080
pGL3b-mChREBPbeta-Exon-1B.str GATACGCCCTGGTTCCTGGAACAATTGCTTTTACAGATGCACATATCGAGGTGGACATCACTTACGCTGAGTACTTCGAAATGTCCG
Consensus
Coverage
36AH28 NTATGAAAGAAATACGCCCCTGGGTTCCTGGAAACAATTTGCTTTTTACCGAATGCCCCATATTCGAAGGTGGGAACTTCCCCTTAC
Trace data
2 100
2 120
2 140
2 160
pGL3b-mChREBPbeta-Exon-1B.str TTCGGTTGGCAGAAGCTATGAAACGATATGGGCTGAATACAAATCACAGAATCGTCGTATGCAGTGAAAACTCTCTTCAATTCTTTA
Consensus
Coverage
36AH28 CCCTGAATTACCTTCNAAAATGGTCCGGTTNTGNTTNNGCCATAANNCTTATGAAAACCGANNTTNGGGGNTTGAAAATACAANNTN
Trace data

Appendix VIII: Sequence chromatogram, pCMV4-FLAG-mChREBP-LID

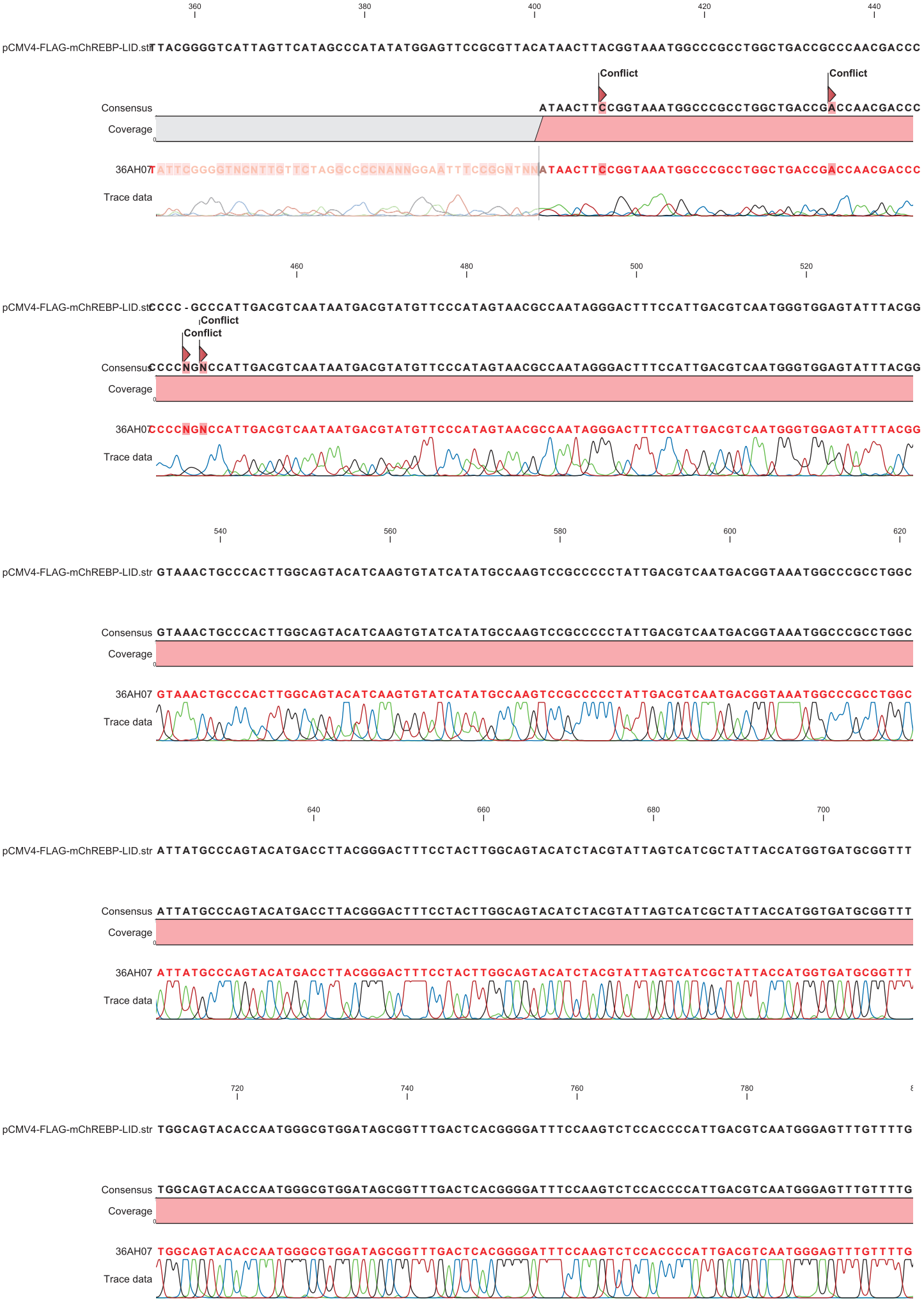

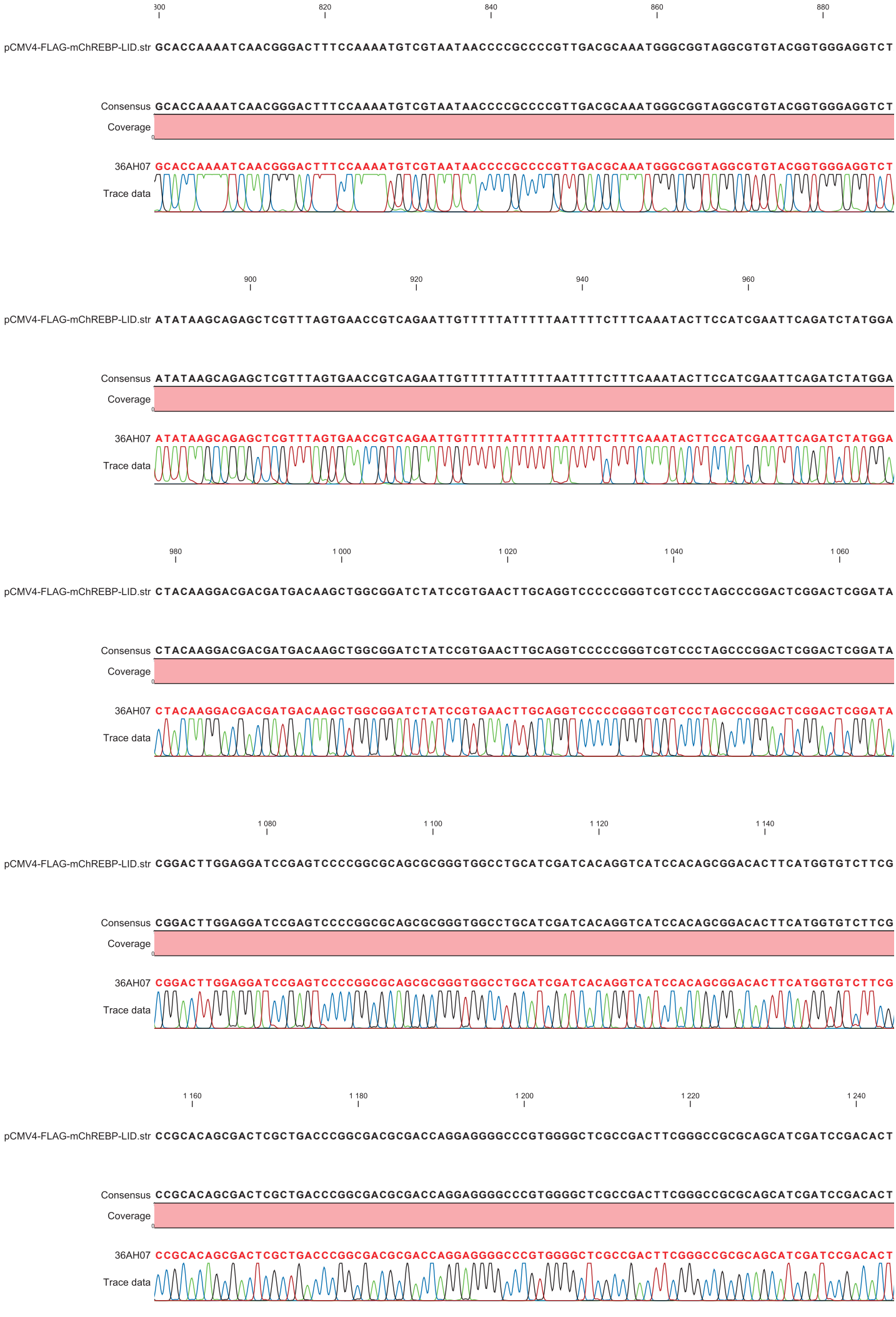
300
820
840
860
880
pCMV4-FLAG-mChREBP-LID.str GCACCAAAATCAACGGGACTTTCCAAAATGTCGTAATAACCCCGCCCCGTTGACGCAAATGGGCGGTAGGCGTGTACGGTGGGAGGTCT
Consensus GCACCAAAATCAACGGGACTTTCCAAAATGTCGTAATAACCCCGCCCCGTTGACGCAAATGGGCGGTAGGCGTGTACGGTGGGAGGTCT
Coverage
0
36AH07 GCACCAAAATCAACGGGACTTTCCAAAATGTCGTAATAACCCCGCCCCGTTGACGCAAATGGGCGGTAGGCGTGTACGGTGGGAGGTCT
Trace data
900
920
940
960
pCMV4-FLAG-mChREBP-LID.str ATATAAGCAGAGCTCGTTTAGTGAACCGTCAGAATTGTTTTTATTTTTAATTTTCTTTCAAATACTTCCATCGAATTCAGATCTATGGA
Consensus ATATAAGCAGAGCTCGTTTAGTGAACCGTCAGAATTGTTTTTATTTTTAATTTTCTTTCAAATACTTCCATCGAATTCAGATCTATGGA
Coverage
0
36AH07 ATATAAGCAGAGCTCGTTTAGTGAACCGTCAGAATTGTTTTTATTTTTAATTTTCTTTCAAATACTTCCATCGAATTCAGATCTATGGA
Trace data
980
1 000
1 020
1 040
1 060
pCMV4-FLAG-mChREBP-LID.str CTACAAGGACGACGATGACAAGCTGGCGGATCTATCCGTGAACTTGCAGGTCCCCCGGGTCGTCCCTAGCCCGGACTCGGACTCGGATA
Consensus CTACAAGGACGACGATGACAAGCTGGCGGATCTATCCGTGAACTTGCAGGTCCCCCGGGTCGTCCCTAGCCCGGACTCGGACTCGGATA
Coverage
0
36AH07 CTACAAGGACGACGATGACAAGCTGGCGGATCTATCCGTGAACTTGCAGGTCCCCCGGGTCGTCCCTAGCCCGGACTCGGACTCGGATA
Trace data
1 080
1 100
1 120
1 140
pCMV4-FLAG-mChREBP-LID.str CGGACTTGGAGGATCCGAGTCCCCGGCGCAGCGCGGGTGGCCTGCATCGATCACAGGTCATCCACAGCGGACACTTCATGGTGTCTTCG
Consensus CGGACTTGGAGGATCCGAGTCCCCGGCGCAGCGCGGGTGGCCTGCATCGATCACAGGTCATCCACAGCGGACACTTCATGGTGTCTTCG
Coverage
0
36AH07 CGGACTTGGAGGATCCGAGTCCCCGGCGCAGCGCGGGTGGCCTGCATCGATCACAGGTCATCCACAGCGGACACTTCATGGTGTCTTCG
Trace data
1 160
1 180
1 200
1 220
1 240
pCMV4-FLAG-mChREBP-LID.str CCGCACAGCGACTCGCTGACCCGGCGACGCGACCAGGAGGGGCCCGTGGGGCTCGCCGACTTCGGGCCGCGCAGCATCGATCCGACACT
Consensus CCGCACAGCGACTCGCTGACCCGGCGACGCGACCAGGAGGGGCCCGTGGGGCTCGCCGACTTCGGGCCGCGCAGCATCGATCCGACACT
Coverage
0
36AH07 CCGCACAGCGACTCGCTGACCCGGCGACGCGACCAGGAGGGGCCCGTGGGGCTCGCCGACTTCGGGCCGCGCAGCATCGATCCGACACT
Trace data

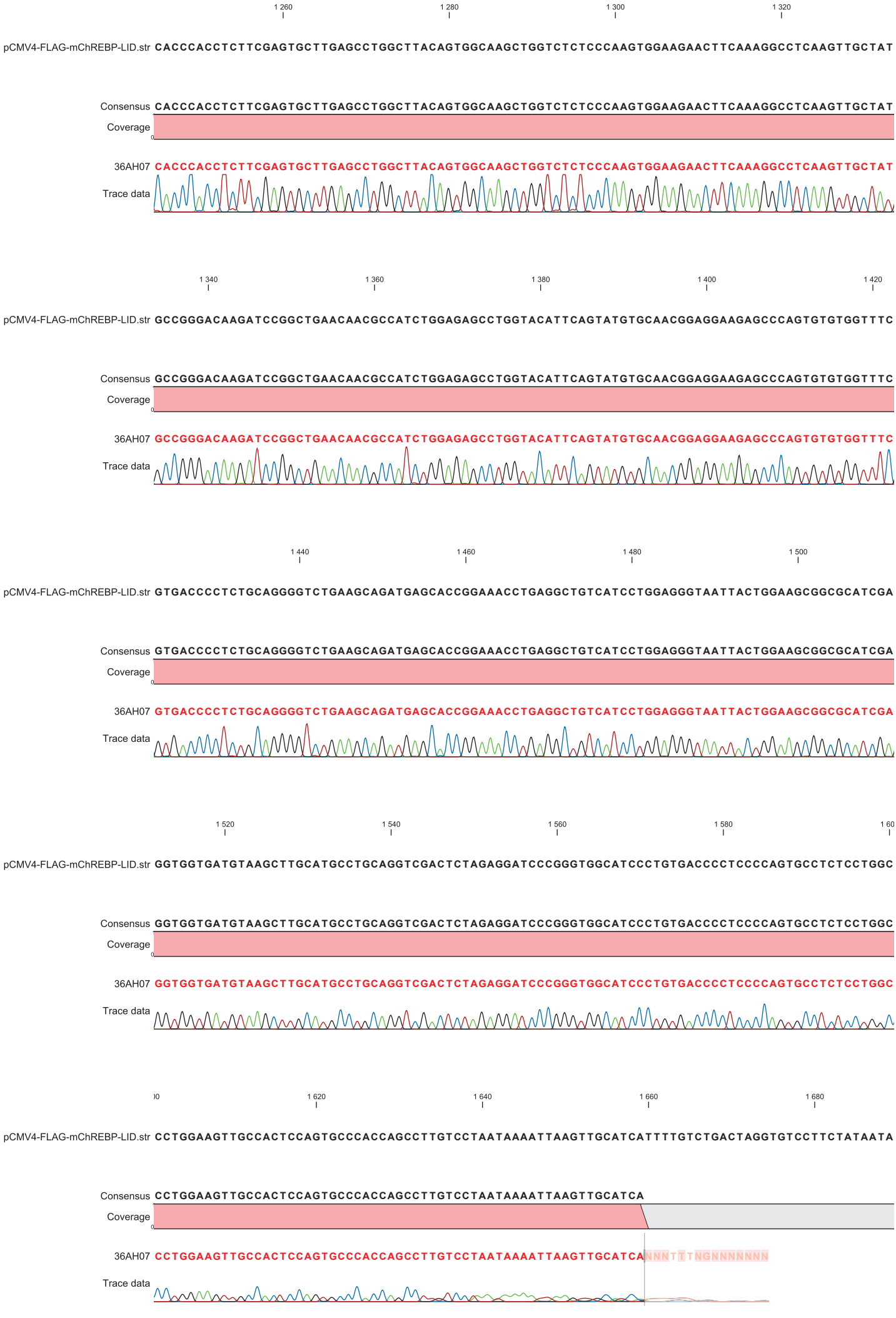
1 260
1 280
1 300
1 320
pCMV4-FLAG-mChREBP-LID.str CACCCACCTCTTCGAGTGCTTGAGCCTGGCTTACAGTGGCAAGCTGGTCTCTCCCAAGTGGAAGAACTTCAAAGGCCTCAAGTTGCTAT
Consensus CACCCACCTCTTCGAGTGCTTGAGCCTGGCTTACAGTGGCAAGCTGGTCTCTCCCAAGTGGAAGAACTTCAAAGGCCTCAAGTTGCTAT
Coverage
36AH07 CACCCACCTCTTCGAGTGCTTGAGCCTGGCTTACAGTGGCAAGCTGGTCTCTCCCAAGTGGAAGAACTTCAAAGGCCTCAAGTTGCTAT
Trace data
1 340
1 360
1 380
1 400
1 420
pCMV4-FLAG-mChREBP-LID.str GCCGGGACAAGATCCGGCTGAACAACGCCATCTGGAGAGCCTGGTACATTCAGTATGTGCAACGGAGGAAGAGCCCAGTGTGTGGTTTC
Consensus GCCGGGACAAGATCCGGCTGAACAACGCCATCTGGAGAGCCTGGTACATTCAGTATGTGCAACGGAGGAAGAGCCCAGTGTGTGGTTTC
Coverage
36AH07 GCCGGGACAAGATCCGGCTGAACAACGCCATCTGGAGAGCCTGGTACATTCAGTATGTGCAACGGAGGAAGAGCCCAGTGTGTGGTTTC
Trace data
1 440
1 460
1 480
1 500
pCMV4-FLAG-mChREBP-LID.str GTGACCCCTCTGCAGGGGTCTGAAGCAGATGAGCACCGGAAACCTGAGGCTGTCATCCTGGAGGGTAATTACTGGAAGCGGCGCATCGA
Consensus GTGACCCCTCTGCAGGGGTCTGAAGCAGATGAGCACCGGAAACCTGAGGCTGTCATCCTGGAGGGTAATTACTGGAAGCGGCGCATCGA
Coverage
36AH07 GTGACCCCTCTGCAGGGGTCTGAAGCAGATGAGCACCGGAAACCTGAGGCTGTCATCCTGGAGGGTAATTACTGGAAGCGGCGCATCGA
Trace data
1 520
1 540
1 560
1 580
1 60
pCMV4-FLAG-mChREBP-LID.str GGTGGTGATGTAAGCTTGCATGCCTGCAGGTCGACTCTAGAGGATCCCGGGTGGCATCCCTGTGACCCCTCCCCAGTGCCTCTCCTGGC
Consensus GGTGGTGATGTAAGCTTGCATGCCTGCAGGTCGACTCTAGAGGATCCCGGGTGGCATCCCTGTGACCCCTCCCCAGTGCCTCTCCTGGC
Coverage
36AH07 GGTGGTGATGTAAGCTTGCATGCCTGCAGGTCGACTCTAGAGGATCCCGGGTGGCATCCCTGTGACCCCTCCCCAGTGCCTCTCCTGGC
Trace data
)0
1 620
1 640
1 660
1 680
pCMV4-FLAG-mChREBP-LID.str CCTGGAAGTTGCCACTCCAGTGCCCACCAGCCTTGTCCTAATAAAATTAAGTTGCATCATTTTGTCTGACTAGGTGTCCTTCTATAATA
Consensus CCTGGAAGTTGCCACTCCAGTGCCCACCAGCCTTGTCCTAATAAAATTAAGTTGCATCA
Coverage
36AH07 CCTGGAAGTTGCCACTCCAGTGCCCACCAGCCTTGTCCTAATAAAATTAAGTTGCATCANNNTTTNGNNNNNNN
Trace data